

## Journal Pre-proofs

New series of isoxazole derivatives targeting EGFR-TK: Synthesis, molecular modeling and antitumor evaluation

Eman T. Warda, Ihsan A. Shehata, Mahmoud B. El-Ashmawy, Nadia S. El-Gohary

PII: S0968-0896(20)30504-6  
DOI: <https://doi.org/10.1016/j.bmc.2020.115674>  
Reference: BMC 115674

To appear in: *Bioorganic & Medicinal Chemistry*

Received Date: 21 May 2020  
Revised Date: 13 July 2020  
Accepted Date: 19 July 2020

Please cite this article as: Warda, E.T., Shehata, I.A., El-Ashmawy, M.B., El-Gohary, N.S., New series of isoxazole derivatives targeting EGFR-TK: Synthesis, molecular modeling and antitumor evaluation, *Bioorganic & Medicinal Chemistry* (2020), doi: <https://doi.org/10.1016/j.bmc.2020.115674>

This is a PDF file of an article that has undergone enhancements after acceptance, such as the addition of a cover page and metadata, and formatting for readability, but it is not yet the definitive version of record. This version will undergo additional copyediting, typesetting and review before it is published in its final form, but we are providing this version to give early visibility of the article. Please note that, during the production process, errors may be discovered which could affect the content, and all legal disclaimers that apply to the journal pertain.

© 2020 Published by Elsevier Ltd.



# New series of isoxazole derivatives targeting EGFR-TK: Synthesis, molecular modeling and antitumor evaluation

Eman T. Warda<sup>a</sup>, Ihsan A. Shehata<sup>a</sup>, Mahmoud B. El-Ashmawy<sup>a</sup>,  
Nadia S. El-Gohary<sup>a,\*</sup>

<sup>a</sup>Department of Medicinal Chemistry, Faculty of Pharmacy, Mansoura University, Mansoura 35516, Egypt

\*Corresponding author: [dr.nadiaelgohary@yahoo.com](mailto:dr.nadiaelgohary@yahoo.com), [nadiaelgohary2005@gmail.com](mailto:nadiaelgohary2005@gmail.com)

**ABSTRACT:** New series of isoxazole derivatives were synthesized and evaluated for *in vitro* antitumor activity against HepG2, MCF-7 and HCT-116 cancer cells. Results showed that **4b** and **25a** are the most active members. Further, **4a**, **8a** and **16b** showed strong activity against the three cancer cells, whereas **6b**, **10a**, **10b** and **16a** exhibited moderate activity against the three cancer cells. Moreover, **25a** showed low cytotoxicity against WISH and WI38 normal cells ( $IC_{50} = 53.19$  and  $38.64 \mu\text{M}$ , respectively), and it might be used as a potent and safe antitumor agent. The nine active compounds **4a**, **4b**, **6b**, **8a**, **10a**, **10b**, **16a**, **16b** and **25a** were studied for EGFR-TK inhibitory activity, where **10a**, **10b** and **25a** showed the highest activity ( $IC_{50} = 0.064$ ,  $0.066$  and  $0.054 \mu\text{M}$ , respectively). Compound **25a** was also assessed against other four target proteins, and it showed promising inhibitory activity against VEGFR-2, CK2 and topoisomerase II $\beta$ , and acceptable inhibitory activity against tubulin polymerization. Cell cycle analysis of cancer cells treated with **25a** proved that it induces cell cycle arrest at G2/M and pre-G1 phases. Furthermore, it was confirmed that **25a** induces cancer cell death through apoptosis, supported by increased caspases 3/9 levels and increased Bax/Bcl-2 ratio in the three cancer cells. In addition, docking studies proved the exact fit of **25a** into the active site of EGFR-TK, VEGFR-2, CK2, topoisomerase II $\beta$  and tubulin. Lipinski's rule and Veber's standards were also analyzed, and results illustrated that **25a** is expected to be well absorbed orally.

**Keywords:** Isoxazoles; Antitumor; EGFR-TK inhibition; Cell cycle analysis; Apoptosis; Computational studies

## 1. Introduction

Epidermal growth factor receptor (EGFR) is a tyrosine kinase (TK) receptor of the ErbB family [1]. It plays a key role in the regulation of various cellular functions that affect **tumorous** growth and progression, including proliferation, differentiation, inhibition of apoptosis, metastasis (through its effects on cell migration, invasiveness, and lack of adhesion dependence), and angiogenesis [2]. Aberrant expression of EGFR-TK has been reported in various human malignancies, including hepatocellular [3], breast [4] and colorectal [5] cancers, and in some studies, EGFR expression was proved to be associated with poor prognosis and resistance to conventional cancer therapies [6,7]. Therefore, inhibitors of EGFR-TK activity by competing with its cognate ligands may potentially constitute an important class of effective drugs in cancer therapy [8,9].

Pursing the different chemical libraries of reported potent antitumor and EGFR-TK inhibitors (EGFR-TKIs) illustrated that several pyrimidine-based small molecules were developed as antitumor EGFR-TKIs such as osimertinib [10], rociletinib [11] and WZ4002 [12] (Fig. 1). In addition, other heterocycles such as isoxazole derivatives were reported as potent antitumor EGFR-TKIs. For example, the isoxazole derivatives **A** exhibited excellent antitumor activity [13], whereas derivative **B** was proved to have good antitumor and EGFR-TK inhibitory activities [14] (Fig. 2). In addition, the isoindoline-1,3-diones **C** were reported to exert outstanding antitumor and EGFR-TK inhibitory activities [15] (Fig. 2). Moreover, lots of bioactive compounds possessing chloroacetamide and chloropropionamide moieties **D** were described as potent antitumor agents with promising EGFR-TK inhibitory activity [16] (Fig. 2). On the other hand, the piperazinyacetamide and piperazinypropionamide derivatives **E** were established as promising antitumor agents [17], whereas the piperazinyacetamide and piperazinypropionamide derivatives **F** were reported to have excellent antitumor and EGFR-TK inhibitory activities [16] (Fig. 2). Besides, several thiazolone derivatives were established as antitumor agents and/or EGFR-TKIs. For example, the thiazolone derivative **G** was described as antitumor agent and EGFR-TKI [18] (Fig. 2). Additionally, lots of arylidenethiazolone derivatives **H** [18] and **I** [19] were reported to possess outstanding antitumor and EGFR-TK inhibitory activities (Fig. 2).

**On the other hand, various anthracene derivatives were proved to exert their anticancer activity through targeting a variety of proteins such as EGFR-TK [20], VEGFR [21], CK2**

[22,23], topoisomerase II [24] and tubulin [25,26] (Fig. 3). Further, the anthracene derivatives were reported to trigger cell cycle arrest and apoptosis in human cancer cells through increasing the levels of caspases 3/9 [27,28], and increasing Bax/Bcl-2 ratio [29,30].

### 1.1. Rational design

The ATP-binding site of EGFR-TK (Fig. 4) has the following features: Adenine binding region which is involved in two key hydrogen bonds formed by the interaction of N1 and N6 of adenine ring with the corresponding amino acids. Many potent inhibitors utilize one of these hydrogen bonds. Sugar pocket which is a hydrophilic region. Hydrophobic binding regions, though not utilized by ATP but they have significant role in binding affinity and inhibitor selectivity. Phosphate region which is largely solvent exposed, and can be utilized for enhancing inhibitor selectivity [31]. The majority of EGFR-TKIs do not exploit the sugar pocket and phosphate region [32]. The core structure of most inhibitors consists of (i) central heteroaromatic ring system that contains at least one hydrogen bond acceptor, and it occupies the adenine binding region [33]. (ii) Terminal hydrophobic head that interacts with the hydrophobic binding region I [34]. (iii) A spacer corresponding to the linker region between the adenine binding region and the hydrophobic binding region I [35]. (iv) Hydrophobic tail which is directly attached to the heteroaromatic ring system, and it occupies the hydrophobic binding region II [36].

The main target of the current research was the synthesis of new isoxazole derivatives carrying the essential pharmacophoric features of the reported and clinically available EGFR-TKIs as osimertinib [10] and rociletinib [11] (Fig. 1) through applying various structural modifications at the four different positions of EGFR-TKIs, including the central heteroaromatic ring system, the hydrophobic head, the spacer and the hydrophobic tail (Fig. 5).

In addition, molecular hybridization is a commonly used strategy in medicinal chemistry to design new effective compounds. It involves the combination of two or more critical entities with relevant biological activities to attain new hybrids with improved potency, selectivity and safety [37,38].

With regard to the reported EGFR-TKIs and adopting the molecular hybridization approach, new series of 4,5,6,7-tetrachloro/tetrabromo-2-(isoxazol-3-yl)-2*H*-isoindoline-1,3-diones **2a,b** and **3a,b** were designed and synthesized through incorporation of isoindoline-1,3-dione scaffold

as a hydrophobic head (occupies the hydrophobic binding region I) to the isoxazole nucleus as a central heteroaromatic ring system (occupies the adenine binding region), in addition to the 5-methyl/*t*-butyl substituent that acts as a hydrophobic tail (occupies the hydrophobic binding region II) (Figs. 5 and 6). Additionally, our chemical diversity was extended to involve the combination of morpholine or substituted piperazines to the *N*-(isoxazol-3-yl)acetamides **4a,b** or propionamides **5a,b** to synthesize new morpholinylacetamide **6a,b**, piperazinylacetamide **7a,b-10a,b**, morpholinylpropionamide **11a,b** and piperazinylpropionamide derivatives **12a,b-15a,b**, whereas the acetamide or propionamide spacers are proposed to occupy the linker region, and the morpholine or substituted piperazine moieties are proposed to occupy the hydrophobic binding region I in the ATP-binding site of EGFR-TK (Figs. 5 and 7). Besides, we found it interesting to incorporate different arylidene moieties to the (isoxazolyl)thiazolone scaffolds **16a,b** to prepare new series of 5-arylidene-2-((5-(methyl/*t*-butyl)isoxazol-3-yl)amino)thiazol-4(*5H*)-ones **17a,b-25a**, whereas the aminothiazolone spacer is proposed to occupy the linker region, and the arylidene moiety is proposed to occupy the hydrophobic binding region I in the ATP-binding site of EGFR-TK (Figs. 5 and 7).

The designed new series of compounds were synthesized and evaluated for *in vitro* antitumor and EGFR-TK inhibitory activities. However, just inhibiting EGFR-TK is not enough for eradication of tumors, that is to say an anticancer agent that direct a single target is not sufficient to improve the symptoms. Due to the limited anticancer activity of therapeutic agents that direct a single target, researchers tried their best to explore other better protocols for cancer therapy, for example, the multitarget-directed drug design strategy, by designing agents which would not only direct a single target but direct multi-targets to trigger various changes in the cellular function, and hence assure high curative effect and delayed resistance development [39]. Multitargeting anticancer remedies exhibit synergistic or at least additive effects in comparison to single-targeted ones, and they gained increased concern in fighting resistant cancer cells [40].

Accordingly, the most active member, [5-((anthracen-9-yl)methylidene)-2-((5-methylisoxazol-3-yl)amino)thiazol-4(*5H*)-one (**25a**)] was further investigated to evaluate its inhibitory activity against other target proteins, including VEGFR-2, CK2, topoisomerase II $\beta$  and tubulin polymerization, as well as its ability to trigger cell cycle arrest and cell apoptosis in HepG2, MCF-7 and HCT-116 cancer cells, and its effects on caspases 3/9 and Bax/Bcl-2 ratio. In addition, the multi-targeting EGFR-TK, VEGFR-2, CK2, topoisomerase II $\beta$  and tubulin polymerization

inhibitory activities of **25a** was supported by molecular docking studies. Elaborate study of structure-activity relationship will expand the future prospects for synthesis and evolution of new more potent members.

## 2. Results and discussion

### 2.1. Chemistry

The 3-amino-5-(methyl/*t*-butyl)isoxazoles **1a,b** were utilized as key starting materials for synthesis of the new compounds **2-25** as delineated in Schemes 1-3. Pointing to Scheme 1, the 4,5,6,7-tetrachloro/tetrabromo-2-(5-(methyl/*t*-butyl)isoxazol-3-yl)-2*H*-isoindoline-1,3-diones **2a,b** and **3a,b** were synthesized through reaction of amines **1a,b** with 4,5,6,7-tetrachloro/tetrabromophthalic anhydride in refluxing glacial acetic acid for 20-30 min. Referring to Scheme 2, the chloroacetamides **4a,b** were synthesized through stirring amines **1a,b** with chloroacetyl chloride in chloroform in presence of triethylamine (TEA) as a catalyst, whereas the chloropropionamides **5a,b** were obtained through stirring amines **1a,b** with chloropropionyl chloride in toluene in presence of anhydrous potassium carbonate as a catalyst. Reaction of chloroacetamides **4a,b** or chloropropionamides **5a,b** with morpholine or substituted piperazines in refluxing toluene in presence of TEA as a catalyst produced the morpholinylacetamides **6a,b**, substituted piperazinylacetamides **7a,b-10a,b**, morpholinylpropionamides **11a,b** and substituted piperazinylpropionamides **12a,b-15a,b**, respectively. With regard to Scheme 3, the thiazolone derivatives **16a,b** were synthesized through heating chloroacetamides **4a,b** with ammonium thiocyanate in refluxing ethanol. Reaction of thiazolone derivatives **16a,b** with aromatic aldehydes in presence of ethanolic solution of sodium hydroxide gave the corresponding 5-arylidene-thiazolone derivatives **17a,b-25a**. The new compounds were characterized by spectral (IR, MS, <sup>1</sup>H NMR and <sup>13</sup>C NMR) and elemental analyses.

## 2.2. Biological screening

### 2.2.1. Cytotoxicity testing

#### 2.2.1.1. *In vitro* antitumor evaluation

The new compounds **2-25** were evaluated for *in vitro* antitumor activity against hepatocellular carcinoma (HepG2), breast carcinoma (MCF-7) and colorectal carcinoma (HCT-116) cells following MTT assay [41-43]. Compounds' concentrations that cause 50% inhibition of cell viability ( $IC_{50}$ ,  $\mu M$ ) were calculated and compared to doxorubicin and erlotinib (standard drugs) (Table 1). The obtained data indicated that compounds **4b** ( $IC_{50} = 9.74 \pm 0.8$ ,  $7.15 \pm 0.6$  and  $9.96 \pm 0.7$   $\mu M$  against HepG2, MCF-7 and HCT-116, respectively) and **25a** ( $IC_{50} = 6.86 \pm 0.5$ ,  $6.38 \pm 0.4$  and  $7.72 \pm 0.5$   $\mu M$  against HepG2, MCF-7 and HCT-116, respectively) have the highest potency against all tested cancer cells. Further, compounds **4a** ( $IC_{50} = 11.10 \pm 1.1$ ,  $10.39 \pm 0.9$  and  $13.07 \pm 1.3$   $\mu M$  against HepG2, MCF-7 and HCT-116, respectively), **8a** ( $IC_{50} = 19.49 \pm 1.6$ ,  $12.62 \pm 1.0$  and  $17.63 \pm 1.4$   $\mu M$  against HepG2, MCF-7 and HCT-116, respectively) and **16b** ( $IC_{50} = 18.27 \pm 1.4$ ,  $9.42 \pm 0.8$  and  $11.48 \pm 1.0$   $\mu M$  against HepG2, MCF-7 and HCT-116, respectively) displayed strong activity against all tested cancer cells, whereas compounds **6b**, **10a**, **10b** and **16a** were evidenced to be strongly active against MCF-7 cells ( $IC_{50} = 19.63 \pm 1.5$ ,  $16.70 \pm 1.3$ ,  $17.16 \pm 1.4$  and  $14.81 \pm 1.2$   $\mu M$ , respectively), and moderately active against HepG2 and HCT-116 cells ( $IC_{50} = 20.81-35.04$   $\mu M$ ). On the other hand, compounds **8b** ( $IC_{50} = 39.14 \pm 2.6$ ,  $27.05 \pm 2.1$  and  $38.38 \pm 2.7$   $\mu M$  against HepG2, MCF-7 and HCT-116, respectively), **15b** ( $IC_{50} = 37.15 \pm 2.6$ ,  $22.96 \pm 1.7$  and  $33.59 \pm 2.4$   $\mu M$  against HepG2, MCF-7 and HCT-116, respectively) and **18a** ( $IC_{50} = 32.83 \pm 2.3$ ,  $24.17 \pm 1.9$  and  $36.60 \pm 2.5$   $\mu M$  against HepG2, MCF-7 and HCT-116, respectively) were proved to be moderately active against the three cancer cells, whereas **15a** and **19b** showed moderate activity against MCF-7 cells ( $IC_{50} = 29.08 \pm 2.3$  and  $39.56 \pm 2.7$   $\mu M$ , respectively). The remaining compounds were found to be of weakly active or inactive against the chosen cancer cells.

### 2.2.1.1.1. Structure-activity relationship

#### Regarding the antitumor activity of compounds **2a,b** and **3a,b**

Presence of substituted 1,3-dioxoisindoline moiety at 3-position of isoxazole ring resulted in weak or no activity against the three tested cancer cells regardless of the type of substituent on both the isoxazole and the isoindoline rings (compounds **2a,b** and **3a,b**).

#### Referring to the activity of chloroacetamides **4a,b** and chloropropionamides **5a,b**

The two chloroacetamides **4a,b** showed higher activity than the corresponding chloropropionamides **5a,b**, and this indicates that increasing the distance between the amide functionality and the halogen led to decreased activity. On the other hand, presence of 5-(*t*-butyl)isoxazol-3-yl moiety in compound **4b** led to mild increase in activity compared to the corresponding 5-methylisoxazol-3-yl counterpart (compound **4a**), the increased activity of **4b** compared to **4a** might be attributed to the higher lipophilicity of **4b** (LogP = 2.27) compared to **4a** (LogP = 0.55). On the opposite side, presence of 5-methylisoxazol-3-yl moiety in **5a** led to higher activity than the corresponding 5-(*t*-butyl)isoxazol-3-yl counterpart (compound **5b**).

#### Taking into account the structures of morpholinylacetamides **6a,b** and piperazinylacetamides **7a,b-10a,b**

The *N*-(5-(*t*-butyl)isoxazol-3-yl)-2-morpholinylacetamide (**6b**) showed strong activity against MCF-7 cells, and moderate activity against HepG2 and HCT-116 cells. Replacing 5-(*t*-butyl)isoxazol-3-yl moiety in **6b** with 5-methylisoxazole counterpart led to weak activity against MCF-7 cells, and no activity against HepG2 and HCT-116 cells, and this might be attributed to decreased lipophilicity of **6a** (LogP = 0.19) compared to **6b** (LogP = 1.91). Further, the 2-(4-ethylpiperazin-1-yl)-*N*-(5-methylisoxazol-3-yl)acetamide (**8a**) exhibited strong activity against the three tested cancer cells, and it is considered to be the most active member amongst the tested piperazinylacetamide derivatives. Replacing 5-methylisoxazol-3-yl moiety in **8a** with 5-(*t*-butyl)isoxazol-3-yl led to decreased activity against all tested cancer cells (compound **8b**). On the other hand, replacing 4-ethylpiperazine moiety in compounds **8a,b** with 4-methylpiperazine led to weak activity against the three tested cancer cells (compounds **7a,b**), and this might be attributed to decreased lipophilicity of **7a,b** (LogP = 0.23 and 1.96, respectively) compared to **8a,b** (LogP = 0.61 and 2.33, respectively). From another point of view, replacing 4-ethylpiperazine moiety in **8a** with 4-phenylpiperazine led to decreased activity against the three tested cancer cells (compound

**10a**), whereas replacing 5-methylisoxazol-3-yl moiety in **10a** with 5-(*t*-butyl)isoxazol-3-yl led to mild increase in activity against HepG2 and HCT-116 cells, and mild decrease in activity against MCF-7 cells (compound **10b**). On contrary, replacing 4-phenylpiperazine moiety in compounds **10a,b** with 4-benzylpiperazine led to decreased activity against the three tested cancer cells (compounds **9a,b** versus **10a,b**), and this might be attributed to decreased lipophilicity of **9a,b** (LogP = 1.63 and 3.36, respectively) compared to **10a,b** (LogP = 1.93 and 3.66, respectively).

*Taking into account the structures of morpholinylpropionamides **11a,b** and piperazinylpropionamides **12a,b-15a,b***

The *N*-(5-methylisoxazol-3-yl)-3-morpholinylpropionamide (**11a**) exhibited weak activity against the three tested cancer cells. Replacing 5-methylisoxazol-3-yl moiety in **11a** with 5-(*t*-butyl)isoxazol-3-yl led to decreased activity against HepG2 and MCF-7 cells, and abolished activity against HCT-116 cells (compound **11b**). On the other hand, the 3-(4-ethylpiperazin-1-yl)-5-(methylisoxazol-3-yl)propionamide (**12a**) showed moderate activity against MCF-7 cells (IC<sub>50</sub> = 44.16±3.0 μM) and weak activity against HepG2 and HCT-116 cells (IC<sub>50</sub> = 56.72±3.5 and 75.81±4.2 μM, respectively). Replacing 5-methylisoxazol-3-yl moiety in **12a** with 5-(*t*-butyl)isoxazol-3-yl led to diminished activity against MCF-7 cells and abolished activity against HepG2 and HCT-116 cells (compound **12b**).

Replacing 4-methylpiperazine moiety in compounds **12a,b** with 4-ethylpiperazine led to increased activity against all tested cancer cells (compounds **13a,b**), and this might be attributed to increased lipophilicity of **13a,b** (LogP = 0.51 and 2.24, respectively) compared to **12a,b** (LogP = 0.14 and 1.86, respectively). On the other hand, replacing 5-methylisoxazol-3-yl moiety in **13a** with 5-(*t*-butyl)isoxazol-3-yl led to decreased activity against the three tested cell lines (compound **13b**). Additionally, replacing 4-ethylpiperazine moiety in **13a,b** with 4-phenylpiperazine led to apparent increase in activity against the three tested cell lines (compounds **15a,b**), and this might be attributed to increased lipophilicity of **15a,b** (LogP = 1.83 and 3.56, respectively) compared to **13a,b** (LogP = 0.51 and 2.24, respectively). On the other hand, replacing 5-methylisoxazol-3-yl moiety in **15a** with 5-(*t*-butyl)isoxazol-3-yl led to increased activity against the three tested cancer cells (compound **15b**). On contrary, replacing 4-phenylpiperazine moiety in **15a,b** with 4-benzylpiperazine led to weak or no activity against the three tested cancer cells (compounds **14a,b**), and this might be attributed to decreased lipophilicity of **14a,b** (LogP = 1.54 and 3.26, respectively) compared to **15a,b** (LogP = 1.83 and 3.56, respectively). Replacing 5-

methylisoxazol-3-yl moiety in **14a** with 5-(*t*-butyl)isoxazol-3-yl led to mild increase in activity against HepG2 and HCT-116 cells, and obvious increase in activity against MCF-7 cells (compound **14b**). Comparing the activity of the piperazinylacetamides **7a,b-10a,b** with that of the piperazinylpropionamides **12a,b-15a,b**, it is evident that the piperazinylacetamide derivatives **7a,b-10a,b** are more active against the three tested cell lines compared to their corresponding piperazinylpropionamide derivatives **12a,b-15a,b**, and this indicates that increasing the distance between the amide functionality and the substituted piperazine moiety is not beneficial for the activity.

*Taking into consideration the structures of compounds 16a,b*

The 2-((5-(*t*-butyl)isoxazol-3-yl)amino)thiazol-4(*5H*)-one (**16b**) showed strong activity against the three tested cancer cells. Replacing 5-(*t*-butyl)isoxazol-3-yl moiety in **16b** with 5-methylisoxazol-3-yl led to mild decrease in activity (compound **16a**), and this might be attributed to decreased lipophilicity of **16a** (LogP = 0.24) compared to **16b** (LogP = 1.97).

*With respect to the 5-arylidene-2-((5-(methyl/*t*-butyl)isoxazol-3-yl)amino)thiazol-4(*5H*)-ones 17a,b-25a*

Presence of (anthracen-9-yl)methylidene moiety at 5-position of thiazole nucleus led to potent activity against all tested cancer cells (compound **25a**), and this might be attributed to the presence of anthracene moiety that is proposed to be involved in hydrophobic interaction with different target proteins (anthracene derivatives were previously reported to exert their antitumor activity through targeting a variety of proteins [20-26]). Replacing anthracen-9-yl moiety in **25a** with either biphenyl-4-yl or naphthalen-2-yl counterparts led to abolished activity against the three tested cancer cells (compounds **23a** and **24a**), and this might be attributed to decreased lipophilicity of **23a** and **24a** (LogP = 4.78 and 4.16, respectively) compared to **25a** (LogP = 5.28). On the opposite side, replacing 5-methylisoxazol-3-yl moiety in **23a** and **24a** with 5-(*t*-butyl)isoxazol-3-yl led to increased activity against the three cancer cells (compounds **23b** and **24b**), and this might be attributed to increased lipophilicity of **23b** and **24b** (LogP = 6.50 and 5.89, respectively) compared to **23a** and **24a** (LogP = 4.78 and 4.16, respectively).

Additionally, replacing (anthracen-9-yl)methylidene moiety in **25a** with (furan-2-yl/5-bromothiophen-2-yl)methylidene or substituted benzylidene moieties led to obvious decrease in activity against all tested cancer cells (compounds **17a-22a**).

On the other hand, the 5-((5-bromothiophen-2-yl)methylidene)-2-((5-methylisoxazol-3-yl)amino)thiazol-4-(5H)-one (**18a**) exhibited moderate activity against the three tested cancer cells. Replacing 5-methylisoxazol-3-yl moiety in **18a** with 5-(*t*-butyl)isoxazol-3-yl led to abolished activity against the three tested cancer cells (compound **18b**). Replacing 5-bromothiophen-2-yl moiety in **18a** with furan-2-yl led to decreased activity against the three cancer cell lines (compound **17a**), whereas exchanging 5-bromothiophen-2-yl moiety in **18b** with furan-2-yl led to increased activity against all tested cancer cells (compound **17b**).

Taking into account the structures of 5-(substituted benzylidene)thiazol-4(5H)-ones **19a,b-22a,b**, it is evident that the activity of these compounds is dependent on the type of substituent on the benzylidene moiety, whereas presence of electron-withdrawing substituents led to higher activity than the electron-donating counterparts, and increasing the number of electron-withdrawing groups led to higher activity, the order of activity is **21a** and **22a** (the benzylidene carrying two electron-withdrawing groups) > **20a** (the benzylidene carrying one electron-withdrawing group) > **19a** (the benzylidene carrying one electron-donating group).

On the other hand, replacing 5-methylisoxazol-3-yl in **19a** and **20a** with 5-(*t*-butyl)isoxazol-3-yl led to obvious increase in activity against the three tested cancer cells (compound **19b** and **20b**), and this might be attributed to increased lipophilicity of **19b** and **20b** (LogP = 5.15 and 5.51, respectively) compared to **19a** and **20a** (LogP = 3.43 and 3.79, respectively). On the opposite side, replacing 5-methylisoxazol-3-yl in **22a** with 5-(*t*-butyl)isoxazol-3-yl led to weak or no activity against the three tested cancer cells (compound **22b**), whereas replacing 5-methylisoxazol-3-yl moiety in **21a** with 5-(*t*-butyl)isoxazol-3-yl led to mild increase in activity against HepG2 and MCF-7 cells, and decreased activity against HCT-116 cells (compound **21b**).

#### 2.2.1.2. *In vitro* cytotoxicity testing of **25a** against normal cells

The potent antitumor compound **25a** was assessed for its cytotoxicity against amnion epithelial (WISH) and lung fibroblast (WI38) normal cells following MTT assay [41-43], and using doxorubicin as a reference drug. IC<sub>50</sub> values (μM) were set, and results revealed that compound **25a** has low cytotoxicity against WISH and WI38 normal cells (IC<sub>50</sub> = 53.19±3.1 and 38.64±2.8 μM, respectively) compared to doxorubicin (IC<sub>50</sub> = 3.18±0.2 and 6.72±0.5 μM, respectively), and hence it was considered to be safe against the selected normal cells at their cytotoxic concentrations against the selected cancer cells.

## 2.2.2. Mechanistic studies

### 2.2.2.1. Enzyme assays

The nine active antitumor compounds **4a**, **4b**, **6b**, **8a**, **10a**, **10b**, **16a**, **16b** and **25a** were subjected to *in vitro* EGFR-TK inhibition assay in order to explore their possible mode of action [44]. Results are presented as percentage inhibition at 10  $\mu\text{M}$  (Fig. 8) and  $\text{IC}_{50}$  ( $\mu\text{M}$ ) (Table 2), and they are compared to erlotinib (standard drug). Compounds **10a**, **10b** and **25a** displayed the highest EGFR-TK inhibitory activity ( $\text{IC}_{50} = 0.064 \pm 0.001$ ,  $0.066 \pm 0.001$  and  $0.054 \pm 0.001$   $\mu\text{M}$ , respectively). Compound **25a** (with potent antitumor and EGFR-TK inhibitory activities) was further assessed for its inhibitory activities against VEGFR-2 [44], CK2 [44], topoisomerase II $\beta$  [45] and tubulin polymerization [46,47]. Results are expressed as % inhibition at 10  $\mu\text{M}$  (Fig. 9) and  $\text{IC}_{50}$  ( $\mu\text{M}$ ) (Table 3), and compared to sorafenib (standard VEGFR-2 inhibitor), quinalizarin (standard CK2 inhibitor), doxorubicin (standard topoisomerase II $\beta$  inhibitor) and colchicine (standard tubulin polymerization inhibitor). Compound **25a** displayed promising inhibitory activity against VEGFR-2 ( $\text{IC}_{50} = 0.087 \pm 0.003$   $\mu\text{M}$ ) compared to sorafenib ( $\text{IC}_{50} = 0.08 \pm 0.002$   $\mu\text{M}$ ), CK2 ( $\text{IC}_{50} = 0.171 \pm 0.005$   $\mu\text{M}$ ) compared to quinalizarin ( $\text{IC}_{50} = 0.11 \pm 0.003$   $\mu\text{M}$ ) and topoisomerase II $\beta$  ( $\text{IC}_{50} = 0.13 \pm 0.001$   $\mu\text{M}$ ) compared to doxorubicin ( $\text{IC}_{50} = 0.727 \pm 0.005$   $\mu\text{M}$ ). On the other hand, its tubulin polymerization inhibitory activity ( $\text{IC}_{50} = 3.61 \pm 0.06$   $\mu\text{M}$ ) was found to be 3 times lower than that of colchicine ( $\text{IC}_{50} = 1.28 \pm 0.03$   $\mu\text{M}$ ). These results referred that EGFR-TK might be a good target for the new active isoxazole derivatives. Additionally, VEGFR-2, CK2 and topoisomerase II $\beta$  were proved to be other good targets for compound **25a**.

#### 2.2.2.1.1. Structure-activity relationship

Referring to results of EGFR-TK inhibitory activity, the 5-((anthracen-9-yl)methylidene)-2-((5-methylisoxazol-3-yl)amino)thiazol-4(5H)-one (**25a**) showed the highest EGFR-TK inhibitory activity ( $\text{IC}_{50} = 0.054 \pm 0.001$   $\mu\text{M}$ ), the high inhibitory activity of **25a** might be attributed to the presence of the 5-((anthracen-9-yl)methylidene)thiazolone moiety that offers an additional site for hydrophobic interaction, as well as two additional hydrogen bond acceptor sites. Replacing the 5-((anthracen-9-yl)methylidene)thiazolone moiety in **25a** with 5-unsubstituted thiazolone counterpart led to decreased activity (compound **16a**,  $\text{IC}_{50} = 0.081 \pm 0.002$   $\mu\text{M}$ ), and this ensures the importance of anthracene moiety for the enzymatic inhibitory activity. Replacing the 5-

methylisoxazolyl moiety in **16a** with 5-*t*-butylisoxazolyl counterpart led to decreased activity (compound **16b**,  $IC_{50} = 0.15 \pm 0.003 \mu\text{M}$ ), the decreased activity of **16b** compared to **16a** might be attributed to the steric hindrance induced by the *t*-butyl substituent that hindered the exact fit of **16b** with ATP-binding site of EGFR-TK. Interestingly, the *N*-(5-(methyl/*t*-butyl)isoxazol-3-yl)-2-(4-phenylpiperazin-1-yl)acetamides **10a** and **10b** displayed promising EGFR-TK inhibitory activity ( $IC_{50} = 0.064 \pm 0.001$  and  $0.066 \pm 0.001 \mu\text{M}$ , respectively), the promising activity of **10a** and **10b** might be attributed to the presence of the phenylpiperazine moiety that offers an additional site for hydrophobic interaction as well as two additional hydrogen bond acceptor sites. Replacing the phenylpiperazine moiety in **10a** with ethylpiperazine led to mild decrease in activity (compound **8a**,  $IC_{50} = 0.081 \pm 0.002 \mu\text{M}$ ), the decreased activity of **8a** might be attributed to its decreased lipophilicity ( $\text{LogP} = 0.61$ ) compared to **10a** ( $\text{LogP} = 1.93$ ). On the other hand, replacing the phenylpiperazine moiety in **10b** with morpholine led to decreased activity (compound **6b**,  $IC_{50} = 0.144 \pm 0.003 \mu\text{M}$ ), the decreased activity of **6b** compared to **10b** might be attributed to the absence of the phenyl moiety as a site for hydrophobic interaction in **6b**. In addition, replacing the 2-(4-phenylpiperazinyl)acetamide moiety in **10a** and **10b** with chloroacetamide led to decreased EGFR-TK inhibitory activity (compounds **4a** and **4b**,  $IC_{50} = 0.106 \pm 0.002$  and  $0.124 \pm 0.004 \mu\text{M}$ , respectively), the decreased activity of **4a** and **4b** compared to **10a** and **10b** might be attributed to the absence of the phenyl moiety as a site for hydrophobic interaction as well as the absence of the two additional hydrogen bond acceptor sites in **4a** and **4b**.

#### 2.2.2.2. Cell cycle analysis

Diverse studies proved that EGFR-TKIs trigger cell cycle arrest and cell apoptosis [48-50]. For further understanding of the mechanism of antitumor activity of the most potent compound **25a**, its effects on cell cycle distribution in HepG2, MCF-7 and HCT-116 cancer cells were studied following the flow cytometry assay [51-53]. Analysis of cell cycle arrest in the three cancer cells treated with compound **25a** (at the  $IC_{50}$  of the corresponding cell line) are illustrated in Figs. 10 and 11, and compared to that of the untreated cells. Results of cell cycle arrest in HepG2 revealed that compound **25a** decreased % cells at G0/G1 phase (from 51.88% to 38.11%) and S phase (from 34.03% to 24.96%), and increased % cells at G2/M phase (from 14.09% to 36.93%) and pre-G1 phase (from 1.44% to 13.29%) (Figs. 10 and 11). With regard to results of cell cycle arrest in

MCF-7, compound **25a** decreased % cells at G0/G1 phase (from 56.14% to 44.29%) and S phase (from 32.91% to 26.41%), and increased % cells at G2/M phase (from 10.95% to 29.30%) and pre-G1 phase (from 1.78% to 16.41%) (Figs. 10 and 11). Similarly, compound **25a** decreased HCT-116 cells in G0/G1 phase (from 48.52% to 29.67%) and S phase (from 35.61% to 27.44%), and increased HCT-116 cells at G2/M phase (from 15.87% to 42.89%) and pre-G1 phase (from 1.19% to 22.69%) (Figs. 10 and 11). The above results indicated that **25a** exhibited significant increase in cell population of the three cancer cells at G2/M and pre-G1 phases.

#### 2.2.2.3. Cell apoptosis

Compound **25a** was studied for its ability to trigger cell apoptosis in the three tested cancer cell lines applying the annexin V/PI double staining flow cytometry assay [51-53]. The dot plot flow cytometry data of the pigmented cells with propidium iodide (PI) and annexin V-FITC are displayed in Fig. 12. Results revealed that after 24 h of exposure, compound **25a** (at the IC<sub>50</sub> of the corresponding cell line) triggered early and late apoptosis in the three cancer cells in comparison to the control untreated cells. The proportion of total apoptosis in HCT-116 cells treated with 10  $\mu$ M of compound **25a** was more than that of HepG2 and MCF-7 cells (Figs. 12 and 13). On the other hand, compound **25a** triggered weak necrosis in the three cancer cells (Figs. 12 and 13) confirming that cancer cell death triggered by **25a** occurs mostly through apoptosis.

#### 2.2.2.4. Effects on caspases 3/9

However multiple genes have been involved in apoptosis, caspases are the key mediators of this process. Caspases are a family of cysteine-aspartic proteases that have fundamental role in programmed cell death [54]. Caspases are divided into two main groups, initiator caspases like caspase-9 that are involved in mitochondrial intrinsic pathway and effector caspases like caspase-3 that are included in extrinsic death receptor pathway as well as intrinsic mitochondrial pathway [55]. The up-regulation of caspases in cancer cells is a prime determinant of the efficacy of anticancer agents [56]; thus, drugs that up-regulate the levels of caspases are capable of inducing apoptosis [56]. Caspase-3 is mostly expressed in HepG2 and HCT-116 cancer cells [57,58], whereas MCF-7 cells do not express this caspase type [59,60], and instead they express caspase-9 [61,62]. Accordingly, compound **25a** was screened for its capability to elevate the levels of caspase-3 in HepG2 and HCT-116 [63], and caspase-9 in MCF-7 cells [63]. Results (Fig. 14A)

disclosed that **25a** elevated the level of caspase-3 in HepG2 and HCT-116 cells by 5.4 and 14.2 folds, respectively in comparison to the corresponding untreated cells. On the other hand, **25a** elevated the level of caspase-9 in MCF-7 cells by 4.7 folds in comparison to the untreated cells (Fig. 14B).

#### 2.2.2.5. Effects on Bax and Bcl-2 proteins

Bcl-2 is an example of antiapoptotic proteins that protect cells against apoptosis. This protein inhibits the opening of mitochondrial permeability transition pores and significantly prevents mitochondrial membrane permeability, and in turn prevents the liberation of the apoptogenic factors to cytosol [64,65]. On contrary, Bax is an apoptotic protein, and elevated level of Bax protein permits increased mitochondrial membrane permeability and allows liberation of the apoptogenic factors to cytosol [66,67]. To ensure that compound **25a** triggers apoptosis through affecting the mitochondrial mediated pathway, we extended our investigation to measure the levels of Bax and Bcl-2 proteins in HepG2, MCF-7 and HCT-116 cells [68]. Results (Fig. 15A) revealed that compound **25a** caused 4.1, 7.0 and 6.9 folds increase in the level of Bax protein in HepG2, MCF-7 and HCT-116 cells, respectively in comparison to the control untreated cells. On contrary, it decreased the level of Bcl-2 protein by 0.56, 0.62 and 0.64 folds in HepG2, MCF-7 and HCT-116 cells, respectively in comparison to the control untreated cells (Fig. 15B). These results confirmed that compound **25a** might trigger apoptosis through increasing Bax/Bcl-2 ratio, and in turn through affecting the mitochondrial mediated pathway.

### 3. Computational studies

#### 3.1. Molecular docking

Molecular docking studies were conducted in order to better understand the binding interactions of the potent antitumor agent **25a** with EGFR-TK, VEGFR-2, CK2, topoisomerase II $\beta$  and tubulin aiming to explain its promising inhibitory activities. Further, docking studies will help to identify the key structural features essential for inhibition of each target, and hence it will offer some insights into the extra structural modifications that will help in the development of new more potent multi-targeting antitumor agents.

In the current research, molecular docking studies relied on the crystal structure of EGFR in complex with erlotinib (PDB ID: 1M17) [69], crystal structure of VEGFR-2 in complex with sorafenib (PDB ID: 4ASD) [70], crystal structure of human CK2 $\alpha$  subunit in complex with quinalizarin (PDB ID: 3FL5) [71], crystal structure of topoisomerase II $\beta$  in complex with DNA and etoposide (PDB ID: 3QX3) [72] and crystal structure of tubulin-(DAMA-colchicine) complex (PDB code: 4O2B) [73] were implemented applying “molecular operating environment (MOE) version 2015.10” Chemical Computing Group Inc. software [74] in order to attain an idea about the binding mode of **25a** to EGFR-TK, VEGFR-2, CK2, topoisomerase II $\beta$  and tubulin.

In order to explore the binding mode of **25a** to EGFR-TK, first, the molecular docking setup was validated by performing re-docking of erlotinib with the active site of EGFR-TK. The re-docking validation step reproduced the experimental binding mode of the co-crystallized ligand efficiently indicating the proportionality of the utilized setup for the purposed docking study, and this is proved by the small root-mean-square deviation (RMSD) of 0.80 Å (<2 Å) between the docked pose and the co-crystallized ligand, and by the capability of the docking poses to reproduce the key interactions shown by the co-crystallized ligand with the hot spot amino acids in the active site, including two H-bonding interactions, one formed between N1 atom of erlotinib and Met769 residue, and the second one is a water mediated H-bonding formed between N3 atom of erlotinib and Thr766 residue, as well as arene-cation interaction between the phenyl ring of the anilino moiety in erlotinib and Lys721 residue (Fig. 16).

Analysis of docking results illustrated that compound **25a** can interact with the hot key amino acids in the active site of EGFR-TK (docking energy score ( $\Delta G$ ) = -10.80 kcal/mol) in a manner similar to the interactions of the co-crystalized ligand (erlotinib) (docking energy score ( $\Delta G$ ) = -10.70 kcal/mol) (Fig. 17). Compound **25a** displayed two key H-bonding interactions, one formed between N atom of thiazolone and Met769 residue, and the second one is a water mediated H-bonding formed between O atom of the carbonyl and Thr766 residue, as well as arene-cation interaction between the anthracene moiety and Lys721 residue (Fig. 17).

Also, superimposition of the co-crystallized ligand (erlotinib) and the docking pose of compound **25a** into the active site of EGFR-TK showed the overlap of anthracene ring in **25a** with phenyl of anilino moiety in erlotinib, as well as the overlap of thiazolone ring in **25a** with quinazoline ring in erlotinib (Fig. 18). The obtained results proved that **25a** can bind to the active

site of EGFR-TK to a good extent, and it occupied the active site similarly to erlotinib (Fig. 17); thus, it might exert its anticancer activity *via* EGFR-TK inhibition.

In order to rationalize the promising VEGFR-2 inhibitory activity of compound **25a**, and to get an idea about its binding mode to VEGFR-2, molecular docking of **25a** into the active site of VEGFR-2 was carried out. The co-crystallized ligand (sorafenib) is involved in eight H-bonding interactions with Glu885, Asp1046, Cys919, Cys1045 and Leu840 residues (Fig. 19 A). Analysis of docking results of the binding interactions of **25a** with VEGFR-2 illustrated that **25a** fits well into the active site of VEGFR-2 with docking energy score ( $\Delta G$ ) = -13.73 Kcal/mol close to that of sorafenib with docking energy score ( $\Delta G$ ) = -15.10 Kcal/mol, and it is proved to be involved in the formation of three key H-bonding interactions, one formed between N atom of thiazolone and Asp1046 residue, the second one formed between S atom of thiazolone and Glu885 residue, and the third one is a water mediated H-bonding formed between NH and Glu885 residue similarly to sorafenib. In addition, it displayed arene-H interaction between the anthracene moiety and Ile892 residue (Fig. 19 B and C).

A molecular docking study based on the crystal structure of human CK2 $\alpha$  subunit (PDB ID: 3FL5) [71] was performed. The co-crystallized ligand (quinalizarin) is involved in two H-bonding interactions formed between the two hydroxy groups at 1- & 2-positions of anthracene moiety and Lys68 residue, as well as arene-H interaction between the anthracene moiety and Ile174 residue (Fig. 20A). The structure model of **25a** and CK2 $\alpha$  complex showed that compound **25a** fits well into the active site of CK2 $\alpha$  with docking energy score ( $\Delta G$ ) = -6.21 Kcal/mol close to that of quinalizarin with docking energy score ( $\Delta G$ ) = -6.71 Kcal/mol, and it is involved in two key H-bonding interactions, one formed between NH and Asn161 residue, and the second one formed between O atom of the carbonyl and Lys68 residue, as well as arene-H interaction between the anthracene moiety and Ile66 residue, and arene-arene interaction between the anthracene moiety and Phe113 residue (Fig. 20B and C).

In addition, docking analysis was carried out to assess the docking energy score and binding mode of **25a** to topoisomerase II $\beta$  using the crystal structure of topoisomerase II $\beta$  in complex with DNA and etoposide (PDB ID: 3QX3) [72]. Binding mode of doxorubicin to the active site of topoisomerase II $\beta$  revealed five key H-bonding interactions with Lys739, Asn786, Asn867 and Lys814 residues (Fig. 21A). The detailed analysis of the binding interactions of **25a** to topoisomerase II $\beta$  showed that it occupied the active site of topoisomerase II $\beta$  with good docking

energy score ( $\Delta G$ ) = -5.86 Kcal/mol close to that of doxorubicin with docking energy score ( $\Delta G$ ) = -6.51 Kcal/mol, and it displayed three key H-bonding interactions, one formed between NH and Met782 residue, the second one formed between S atom of thiazolone and Met782 residue, and the third one formed between O atom of the carbonyl and Lys814 residue, as well as arene-cation interaction between the anthracene moiety and Lys814 residue (Fig. 21B and C).

In order to explore the binding mode of compound **25a** with tubulin, docking was done in the colchicine-binding site of tubulin using the crystal structure of tubulin-(DAMA-colchicine) complex (PDB ID: 4O2B) [73]. The co-crystallized ligand (DAMA-colchicine) is involved in two H-bonding interactions with ValA181 and AlaA180 residues, as well as a hydrophobic interaction with MetB259 (Fig. 22A). Binding interactions of **25a** with the colchicine-binding site of tubulin are displayed in Fig. 22B and C, and revealed that **25a** showed a consistent binding mode (docking energy score ( $\Delta G$ ) = -7.35 kcal/mol) close to that of the co-crystallized ligand (DAMA-colchicine) (docking energy score ( $\Delta G$ ) = -8.09 kcal/mol), and it is involved in two key H-bonding interactions, one formed between O atom of the carbonyl and LysB254 residue, and the second one formed between S atom of thiazolone and GluA183 residue, as well as two arene-H interactions, one between the anthracene moiety and SerA140 residue, and the second one between the isoxazole moiety and Leu248 residue.

Summary of residues involved in arene-cation, arene-H and arene-arene interactions, number of hydrogen bonds, residues involved in hydrogen bonding interaction and docking energy score (kcal/mol) of compound **25a** with EGFR-TK, VEGFR-2, CK2, topoisomerase II $\beta$  and tubulin is presented in Table 4.

Generally speaking, docking results proved the exact fit of **25a** into the active site of the five target proteins (EGFR-TK, VEGFR-2, CK2, topoisomerase II $\beta$  and tubulin), and that the anthracene and thiazolone moieties are the essential pharmacophoric features for binding interactions with the five targets. Moreover, the NH group is an additional moiety essential for H-bonding interaction with the active site of VEGFR-2, CK2 and topoisomerase II $\beta$ . On the other hand, the isoxazole moiety is an additional pharmacophoric moiety essential for arene-H interaction with the active site of tubulin. The identification of the pharmacophoric features of **25a** would enable the design of new more potent multi-targeting inhibitors as prospective antitumor agents.

### 3.2. Molinspiration calculations

*In silico* studies are considered to be valuable tools in drug discovery, since they are beneficial in prediction of physicochemical properties, pharmacokinetics and toxicity of drugs [75]. The new compounds were analyzed for prediction of Lipinski's rule [76] and Veber's standards [77] applying Molinspiration software [78].

Lipinski's rule is important in prognosis of oral absorption of drugs [76], and it is dependent on the compound's physicochemical properties. Similarly, topological polar surface area (TPSA) and number of rotatable bonds (Nrotb) have great effect on the rate at which drugs are orally absorbed [77]. Molinspiration software [78] was adopted for assessment of Lipinski's rule and Veber's standards of the new members. Results (Table 5) suggested that most of the investigated compounds are in harmony with the accepted standards of Lipinski's rule, TPSA and Nrotb. It is noted that all of the new compounds (except **3b**) have zero or one violation of Lipinski's rule, and they are anticipated to be well absorbed orally. Molecules violating more than one might have poor oral absorption [76].

## 4. Conclusion

Results of *in vitro* antitumor screening revealed that **4b** and **25a** have the highest antitumor activity against the three tested cancer cells ( $IC_{50} = 6.38-9.96 \mu M$ ). In addition, **25a** showed low cytotoxicity against WISH and WI38 normal cells ( $IC_{50} = 53.19$  and  $38.64 \mu M$ , respectively), and it might be used as a potent and safe antitumor agent. Attempts of studying the possible mode of action of the active compounds in the current research revealed that they have potent EGFR-TK inhibitory activity ( $IC_{50} = 0.054-0.15 \mu M$ ), and it could be the possible target for the new active compounds. Further, compound **25a** (the potent antitumor EGFR-TKI) showed promising VEGFR-2, CK2 and topoisomerase II $\beta$  inhibitory activities, and acceptable tubulin polymerization inhibitory activity, hence it is considered to be a promising multi-targeting antitumor agent. Results of cell cycle analysis disclosed that **25a** triggers cell cycle arrest at G2/M and pre-G1 phases in the three cancer cell lines. Additionally, cancer cell death was proved to occur mostly through apoptosis (supported by increased levels of caspases 3/9, and increased Bax/Bcl-2 ratio). Further, docking studies confirmed the exact binding interactions of **25a** with the active site of EGFR-TK, VEGFR-2, CK2, topoisomerase II $\beta$  and tubulin. Moreover, Molinspiration calculations assured

that **25a** is expected to have good oral absorption. Taking together, compound **25a** is considered to be a promising lead for design and discovery of new more potent multi-targeting inhibitors as prospective antitumor agents.

## 5. Experimental

### 5.1. Chemistry

Melting points (°C) were measured on Stuart melting point (SMP30) apparatus. IR spectral analyses (KBr disc) were achieved on Mattson 5000 FT IR spectrometer ( $\nu$  in  $\text{cm}^{-1}$ ), Mansoura University, Egypt. Bruker 400 (100) MHz and Joel 500 (125) MHz spectrometers were utilized for analysis of  $^1\text{H}$ ,  $^{13}\text{C}$  and  $^{15}\text{N}$  NMR spectra in  $\text{CDCl}_3$  or  $\text{DMSO-}d_6$  (chemical shifts in  $\delta$  units, ppm) using tetramethylsilane as a standard, Mansoura University, Egypt. Mass spectral analyses were achieved on direct probe controller inlet part to single quadropole mass analyzer in (thermo scientific GC-MS) model (ISQ LT) using thermo x-caliber software at the Regional Center of Mycology and Biotechnology (RCMB), Al-Azhar University, Nasr City, Egypt. Elemental microanalyses (% C, H, N) were carried out, and they agreed with the proposed structures within  $\pm 0.4\%$  of the calculated values, Microanalytical Center, Cairo University, Egypt. TLC sheets (silica gel 60 F254) were used for the control of reaction times. Petroleum ether/ethyl acetate (8:2) was used for elution, and UV (366 nm) was used for spot visualization. Compounds **1a,b** were purchased from Sigma Aldrich Chemicals Co., USA. Compounds **4a** [79-81], **4b** [82,83] and **16a** [81] were prepared according to the reported procedures. Compound **10a** was previously mentioned in literature [84]. Compounds **8a** and **13a** are commercially available but no available data were reported for them in literature.

#### 5.1.1. Synthesis of 4,5,6,7-tetrachloro/tetrabromo-*N*-(5-(methyl/*t*-butyl)isoxazol-3-yl)-2*H*-isoindoline-1,3-diones **2a,b** and **3a,b**

A mixture of 3-aminoisoxazole **1a-b** (0.003 mol) and substituted phthalic anhydride (0.003 mol) in glacial acetic acid (10 mL) was heated at 100 °C for 20-30 min. The solution was concentrated under vacuum, and the formed precipitate was filtered and crystallized from ethanol/water (2:1) to give compounds **2a,b** and **3a,b**.

**5.1.1.1. 4,5,6,7-Tetrachloro-N-(5-methylisoxazol-3-yl)isoindoline-1,3-dione (2a)**

Yield 65%, m.p. 215-217 °C. IR: 1706, 1619 (2C=O). <sup>1</sup>H NMR (400 MHz, DMSO-*d*<sub>6</sub>): δ 2.43 (s, 3H, CH<sub>3</sub>), 6.71 (s, 1H, Isoxazole-H). <sup>13</sup>C NMR: δ 12.6, 96.8, 129.3, 133.9, 135.1, 157.9, 165.0, 170.8. MS *m/z* (%): 370 (1.82, M<sup>+</sup>+4), 368 (62.01, M<sup>+</sup>+2), 366 (100.00, M<sup>+</sup>). Anal. Calcd. (Found) for C<sub>12</sub>H<sub>4</sub>Cl<sub>4</sub>N<sub>2</sub>O<sub>3</sub> (365.98): C, 39.38 (39.21); H, 1.10 (1.30); N, 7.65 (7.82) %.

**5.1.1.2. N-(5-(*t*-Butyl)isoxazol-3-yl)-4,5,6,7-tetrachloroisoindoline-1,3-dione (2b)**

Yield 62%, m.p. 245-247 °C. IR: 1793, 1737 (2C=O). <sup>1</sup>H NMR (400 MHz, DMSO-*d*<sub>6</sub>): δ 1.38 (s, 9H, C(CH<sub>3</sub>)<sub>3</sub>), 6.56 (s, 1H, Isoxazole -H). <sup>13</sup>C NMR: δ 28.8, 33.3, 96.8, 128.7, 129.1, 139.3, 153.1, 161.1, 182.7. MS *m/z* (%): 412 (10.34, M<sup>+</sup>+4), 410 (48.30, M<sup>+</sup>+2), 408 (68.60, M<sup>+</sup>), 393 (100.00). Anal. Calcd. (Found) for C<sub>15</sub>H<sub>10</sub>Cl<sub>4</sub>N<sub>2</sub>O<sub>3</sub> (408.06): C, 44.15 (43.99); H, 2.47 (2.15); N, 6.87 (6.65) %.

**5.1.1.3. 4,5,6,7-Tetrabromo-N-(5-methylisoxazol-3-yl)isoindoline-1,3-dione (3a)**

Yield 42%, m.p. 249-251 °C. IR: 1782, 1726 (2C=O). <sup>1</sup>H NMR (400 MHz, CDCl<sub>3</sub>): δ 2.53 (s, 3H, CH<sub>3</sub>), 6.46 (s, 1H, Isoxazole-H). <sup>13</sup>C NMR: δ 12.9, 98.2, 122.6, 129.8, 138.9, 147.7, 160.5, 171.5. MS *m/z* (%): 548 (14.00, M<sup>+</sup>+4), 546 (65.49, M<sup>+</sup>+2), 544 (100.00, M<sup>+</sup>). Anal. Calcd. (Found) for C<sub>12</sub>H<sub>4</sub>Br<sub>4</sub>N<sub>2</sub>O<sub>3</sub> (543.79): C, 26.50 (26.23); H, 0.74 (0.57); N, 5.15 (4.85) %.

**5.1.1.4. 4,5,6,7-Tetrabromo-N-(5-(*t*-butyl)isoxazol-3-yl)isoindoline-1,3-dione (3b)**

Yield 45%, m.p. 270-272 °C. IR: 1740, 1705 (2C=O). <sup>1</sup>H NMR (400 MHz, DMSO-*d*<sub>6</sub>): δ 1.38 (s, 9H, C(CH<sub>3</sub>)<sub>3</sub>), 6.55 (s, 1H, Isoxazole-H). <sup>13</sup>C NMR: δ 28.8, 33.3, 96.9, 121.7, 131.4, 137.6, 153.3, 161.5, 182.6. MS *m/z* (%): 590 (5.72, M<sup>+</sup>+4), 588 (34.23, M<sup>+</sup>+2), 586 (57.66, M<sup>+</sup>), 571 (100.00). Anal. Calcd. (Found) for C<sub>15</sub>H<sub>10</sub>Br<sub>4</sub>N<sub>2</sub>O<sub>3</sub> (585.87): C, 30.75 (30.91); H, 1.72 (1.89); N, 4.78 (4.62) %.

**5.1.2. Synthesis of 2-chloro-N-(5-(methyl/*t*-butyl)isoxazol-3-yl)acetamides 4a,b**

A mixture of amine **1a,b** (0.003 mol) and chloroacetyl chloride (0.67 g, 0.006 mol) in chloroform (10 mL) in presence of TEA (0.1 mL) was stirred at room temperature for 2-4 h. The solution was concentrated under vacuum, and then poured onto ice-water. The precipitated solid was filtered and crystallized from chloroform to produce the desired compounds **4a,b**.

**5.1.2.1. 2-Chloro-*N*-(5-methylisoxazol-3-yl)acetamide (4a) [79-81]**

Yield 65%, m.p. 189-191 °C [79]. <sup>1</sup>H NMR (500 MHz, DMSO-*d*<sub>6</sub>): δ 2.37 (s, 3H, CH<sub>3</sub>), 4.28 (s, 2H, COCH<sub>2</sub>), 6.62 (s, 1H, Isoxazole-H), 11.27 (s, 1H, NH). Anal. Calcd. (Found) for C<sub>6</sub>H<sub>7</sub>ClN<sub>2</sub>O<sub>2</sub> (174.58): C, 41.28 (41.00); H, 4.04 (3.87); N, 16.05 (15.75) %.

**5.1.2.2. *N*-(5-(*t*-Butyl)isoxazol-3-yl)-2-chloroacetamide (4b) [82,83]**

Yield 60%, m.p. 93-95 °C. <sup>1</sup>H NMR (400 MHz, CDCl<sub>3</sub>): δ 1.27 (s, 9H, C(CH<sub>3</sub>)<sub>3</sub>), 4.14 (s, 2H, COCH<sub>2</sub>), 6.62 (s, 1H, Isoxazole-H), 9.63 (s, 1H, NH). Anal. Calcd. (Found) for C<sub>9</sub>H<sub>13</sub>ClN<sub>2</sub>O<sub>2</sub> (216.07): C, 49.89 (50.17); H, 6.05 (6.21); N, 12.93 (13.15) %.

**5.1.3. Synthesis of 3-chloro-*N*-(5-(methyl/*t*-butyl)isoxazol-3-yl)propionamides 5a,b**

A mixture of amine **1a,b** (0.003 mol) and chloropropionyl chloride (0.76 g, 0.006 mol) in toluene (10 mL) in presence of anhydrous potassium carbonate (0.82 g, 0.006 mol) was stirred at room temperature for 2-4 h. The solution was concentrated under vacuum, and then poured onto ice-water. The precipitated solid was filtered and crystallized from toluene to produce the desired compounds **5a,b**.

**5.1.3.1. 3-Chloro-*N*-(5-methylisoxazol-3-yl)propionamide (5a)**

Yield 65%, m.p. 120-122 °C. IR: 3222 (NH), 1704 (C=O). <sup>1</sup>H NMR (500 MHz, CDCl<sub>3</sub>): δ 2.43 (s, 3H, CH<sub>3</sub>), 2.93 (t, 2H, COCH<sub>2</sub>CH<sub>2</sub>, *J* = 13.0 Hz), 3.88 (t, 2H, COCH<sub>2</sub>CH<sub>2</sub>, *J* = 13.0 Hz), 6.78 (s, 1H, Isoxazole-H), 10.16 (s, 1H, NH). <sup>13</sup>C NMR: δ 12.6, 39.1, 39.5, 96.7, 158.2, 168.2, 170.2. MS *m/z* (%): 191 (1.85, M<sup>+</sup>+2), 189 (5.28, M<sup>+</sup>), 188 (10.37, M<sup>+</sup>-1), 63 (100.00). Anal. Calcd. (Found) for C<sub>7</sub>H<sub>9</sub>ClN<sub>2</sub>O<sub>2</sub> (188.61): C, 44.58 (44.30); H, 4.81 (4.66); N, 14.85 (14.53) %.

**5.1.3.2. *N*-(5-(*t*-Butyl)isoxazol-3-yl)-3-chloropropionamide (5b)**

Yield 60%, m.p. 84-86 °C. IR: 3257 (NH), 1716 (C=O). <sup>1</sup>H NMR (400 MHz, CDCl<sub>3</sub>): δ 1.28 (s, 9H, C(CH<sub>3</sub>)<sub>3</sub>), 2.87 (t, 2H, COCH<sub>2</sub>CH<sub>2</sub>, *J* = 13.0 Hz), 3.81 (t, 2H, COCH<sub>2</sub>CH<sub>2</sub>, *J* = 13.0 Hz), 6.68 (s, 1H, Isoxazole-H), 10.21 (s, 1H, NH). <sup>13</sup>C NMR: δ 28.6, 33.1, 39.2, 39.8, 93.6, 157.8, 168.2, 182.0. MS *m/z* (%): 233 (1.68, M<sup>+</sup>+2), 232 (6.61, M<sup>+</sup>+1), 231 (13.92, M<sup>+</sup>), 63 (100.00). Anal. Calcd. (Found) for C<sub>10</sub>H<sub>15</sub>ClN<sub>2</sub>O<sub>2</sub> (230.69): C, 44.58 (44.32); H, 4.81 (4.54); N, 14.85 (14.60) %.

#### 5.1.4. Synthesis of 2-morpholinyl/2-(4-substituted piperazin-1-yl)acetamides **6a,b-10a,b** and 2-morpholinyl/2-(4-substituted piperazin-1-yl)propionamides **11a,b-15a,b**

A mixture of acetamide **4a,b** or propionamide **5a,b** (0.002 mol), morpholine (0.17 g, 0.002 mol) or substituted piperazine (0.002 mol) and TEA (0.2 mL) in toluene (10 mL) was heated under reflux for 15-24 h. The solvent was removed under vacuum, and the remained residue was taken onto ice-water. The precipitated solid was filtered and crystallized from toluene to produce the desired compounds **6a,b-10a,b** and **11a,b-15a,b**, respectively.

##### 5.1.4.1. *N*-(5-Methylisoxazol-3-yl)-2-morpholinylacetamide (**6a**)

Yield 50%, m.p. 99-101 °C. IR: 3483 (NH), 1704 (C=O). <sup>1</sup>H NMR (400 MHz, CDCl<sub>3</sub>): δ 2.33 (s, 3H, CH<sub>3</sub>), 2.60 (s, 4H, Morpholine-2CH<sub>2</sub>), 3.18 (s, 2H, COCH<sub>2</sub>), 3.71 (t, 4H, Morpholine-2CH<sub>2</sub>, *J* = 9.0 Hz), 6.63 (s, 1H, Isoxazole-H), 9.63 (s, 1H, NH). <sup>13</sup>C NMR: δ 12.7, 53.7, 61.9, 66.6, 96.2, 157.3, 168.1, 170.2. MS *m/z* (%): 225 (7.38, M<sup>+</sup>), 42 (100.00). Anal. Calcd. (Found) for C<sub>10</sub>H<sub>15</sub>N<sub>3</sub>O<sub>3</sub> (225.25): C, 53.32 (53.20); H, 6.71 (6.46); N, 18.66 (18.37) %.

##### 5.1.4.2. *N*-(5-(*t*-Butyl)isoxazol-3-yl)-2-morpholinylacetamide (**6b**)

Yield 55%, m.p. 94-96 °C. IR: 3449 (NH), 1690 (C=O). <sup>1</sup>H NMR (500 MHz, CDCl<sub>3</sub>): δ 1.34 (s, 9H, C(CH<sub>3</sub>)<sub>3</sub>), 2.60 (t, 4H, Morpholine-2CH<sub>2</sub>, *J* = 9.0 Hz), 3.16 (s, 2H, COCH<sub>2</sub>), 3.76 (t, 4H, Morpholine-2CH<sub>2</sub>, *J* = 9.0 Hz), 6.69 (s, 1H, Isoxazole-H), 9.53 (s, 1H, NH). <sup>13</sup>C NMR: δ 28.6, 33.0, 53.8, 62.2, 66.8, 92.9, 156.9, 168.3, 181.9. MS *m/z* (%): 268 (8.79, M<sup>+</sup>+1), 267 (12.79, M<sup>+</sup>), 100 (100.00). Anal. Calcd. (Found) for C<sub>13</sub>H<sub>21</sub>N<sub>3</sub>O<sub>3</sub> (267.33): C, 58.41 (58.69); H, 7.92 (8.08); N, 15.72 (15.97) %.

##### 5.1.4.3. *N*-(5-Methylisoxazol-3-yl)-2-(4-methylpiperazin-1-yl)acetamide (**7a**)

Yield 49%, m.p. 76-78 °C. IR: 3424 (NH), 1704 (C=O). <sup>1</sup>H NMR (400 MHz, CDCl<sub>3</sub>): δ 2.33 (s, 3H, CH<sub>3</sub>), 2.41 (s, 3H, CH<sub>3</sub>), 2.52 (s, 4H, Piperazine-2CH<sub>2</sub>), 2.65 (s, 4H, Piperazine-2CH<sub>2</sub>), 3.16 (s, 2H, COCH<sub>2</sub>), 6.73 (s, 1H, Isoxazole-H), 9.60 (s, 1H, NH). <sup>13</sup>C NMR: δ 12.7, 45.8, 53.3, 54.9, 61.5, 96.1, 157.4, 168.7, 170.1. MS *m/z* (%): 239 (9.74, M<sup>+</sup>+1), 238 (21.08, M<sup>+</sup>), 79 (100.00). Anal. Calcd. (Found) for C<sub>11</sub>H<sub>18</sub>N<sub>4</sub>O<sub>2</sub> (238.29): C, 55.45 (55.17); H, 7.61 (7.44); N, 23.51 (23.19) %.

##### 5.1.4.4. *N*-(5-(*t*-Butyl)isoxazol-3-yl)-2-(4-methylpiperazin-1-yl)acetamide (**7b**)

Yield 46%, m.p. 92-94 °C. IR: 3450 (NH), 1656 (C=O). <sup>1</sup>H NMR (500 MHz, CDCl<sub>3</sub>): δ 1.34 (s, 9H, C(CH<sub>3</sub>)<sub>3</sub>), 2.33 (s, 3H, CH<sub>3</sub>), 2.52-2.64 (m, 8H, Piperazine-4CH<sub>2</sub>), 3.16 (s, 2H, COCH<sub>2</sub>), 6.69 (s, 1H, Isoxazole-H), 9.57 (s, 1H, NH). <sup>13</sup>C NMR: δ 28.6, 33.0, 45.0, 52.1, 54.4, 61.3, 92.9, 156.9, 168.1,

181.9. MS  $m/z$  (%): 281 (1.59,  $M^{+1}$ ), 280 (3.58,  $M^{+}$ ), 42 (100.00). Anal. Calcd. (Found) for  $C_{14}H_{24}N_4O_2$  (280.37): C, 59.98 (59.86); H, 8.63 (8.38); N, 19.98 (19.64) %.

**5.1.4.5. 2-(4-Ethylpiperazin-1-yl)-N-(5-methylisoxazol-3-yl)acetamide (8a)**

Yield 40%, m.p. 53-55 °C.  $^1H$  NMR (400 MHz,  $CDCl_3$ ):  $\delta$  1.03 (t, 3H,  $CH_2CH_3$ ,  $J=13.0$  Hz), 2.33-2.57 (m, 13H,  $CH_3$ ,  $CH_2CH_3$ , Piperazine-4 $CH_2$ ), 3.09 (s, 2H,  $COCH_2$ ), 6.65 (s, 1H, Isoxazole-H), 9.54 (s, 1H, NH).  $^{13}C$  NMR:  $\delta$  11.9, 12.7, 52.2, 52.6, 53.4, 61.6, 96.1, 157.4, 168.8, 170.1. Anal. Calcd. (Found) for  $C_{12}H_{20}N_4O_2$  (252.32): C, 57.12 (56.86); H, 7.99 (7.67); N, 22.21 (21.99) %.

**5.1.4.6. N-(5-(*t*-Butyl)isoxazol-3-yl)-2-(4-ethylpiperazin-1-yl)acetamide (8b)**

Yield 45%, m.p. 75-77 °C. IR: 3234 (NH), 1701 (C=O).  $^1H$  NMR (500 MHz,  $CDCl_3$ ):  $\delta$  1.09 (t, 3H,  $CH_2CH_3$ ,  $J=15.0$  Hz), 1.33 (s, 9H,  $C(CH_3)_3$ ), 2.43-2.64 (m, 10H,  $CH_2CH_3$ , Piperazine-4 $CH_2$ ), 3.15 (s, 2H,  $COCH_2$ ), 6.68 (s, 1H, Isoxazole-H), 9.59 (s, 1H, NH).  $^{13}C$  NMR:  $\delta$  11.5, 28.6, 32.9, 52.1, 52.4, 53.0, 61.5, 92.9, 156.9, 168.6, 181.8. MS  $m/z$  (%): 294 (20.22,  $M^{+}$ ), 46 (100.00). Anal. Calcd. (Found) for  $C_{15}H_{26}N_4O_2$  (294.40): C, 61.20 (61.04); H, 8.90 (8.63); N, 19.03 (18.78) %.

**5.1.4.7. 2-(4-Benzylpiperazin-1-yl)-N-(5-methylisoxazol-3-yl)acetamide (9a)**

Yield 70%, m.p. 110-112 °C. IR: 3453 (NH), 1719 (C=O).  $^1H$  NMR (400 MHz,  $CDCl_3$ ):  $\delta$  2.41 (s, 3H,  $CH_3$ ), 2.53 (s, 4H, Piperazine-2 $CH_2$ ), 2.63 (s, 4H, Piperazine-2 $CH_2$ ), 3.15 (s, 2H,  $COCH_2$ ), 3.54 (s, 2H, Phenyl- $CH_2$ ), 6.73 (s, 1H, Isoxazole-H), 7.27-7.33 (m, 5H, Ar-H), 9.62 (s, 1H, NH).  $^{13}C$  NMR:  $\delta$  12.6, 52.7, 53.2, 61.5, 62.6, 96.1, 127.4, 128.3, 129.3, 136.9, 157.3, 168.7, 170.1. MS  $m/z$  (%): 315 (100.00,  $M^{+1}$ ), 314 (57.68,  $M^{+}$ ), 313 (28.54,  $M^{+1}$ ). Anal. Calcd. (Found) for  $C_{17}H_{22}N_4O_2$  (314.39): C, 64.95 (65.23); H, 7.05 (7.22); N, 17.82 (18.12) %.

**5.1.4.8. 2-(4-Benzylpiperazin-1-yl)-N-(5-(*t*-butyl)isoxazol-3-yl)acetamide (9b)**

Yield 75%, m.p. 64-66 °C. IR: 3390 (NH), 1705 (C=O).  $^1H$  NMR (500 MHz,  $CDCl_3$ ):  $\delta$  1.34 (s, 9H,  $C(CH_3)_3$ ), 2.52 (s, 4H, Piperazine-2 $CH_2$ ), 2.62 (s, 4H, Piperazine-2 $CH_2$ ), 3.14 (s, 2H,  $COCH_2$ ), 3.53 (s, 2H, Phenyl- $CH_2$ ), 6.69 (s, 1H, Isoxazole-H), 7.26-7.32 (m, 5H, Ar-H), 9.61 (s, 1H, NH).  $^{13}C$  NMR:  $\delta$  28.6, 32.9, 52.8, 53.4, 61.6, 62.8, 92.8, 127.1, 128.2, 129.1, 137.6, 156.9, 168.8, 181.8. MS  $m/z$  (%): 357 (54.82,  $M^{+1}$ ), 356 (100.00,  $M^{+}$ ). Anal. Calcd. (Found) for  $C_{20}H_{28}N_4O_2$  (356.47): C, 67.39 (67.55); H, 7.92 (8.19); N, 15.72 (15.97) %.

**5.1.4.9. N-(5-Methylisoxazol-3-yl)-2-(4-phenylpiperazin-1-yl)acetamide (10a) [84]**

Yield 60%, m.p. 118-120 °C.  $^1H$  NMR (400 MHz,  $CDCl_3$ ):  $\delta$  2.34 (s, 3H,  $CH_3$ ), 2.69 (t, 4H, Piperazine-2 $CH_2$ ,  $J = 9.6$  Hz), 3.15 (s, 2H,  $COCH_2$ ), 3.18 (t, 4H, Piperazine-2 $CH_2$ ,  $J = 9.6$  Hz), 6.66 (s, 1H, Isoxazole-H), 6.80-6.87 (m, 3H, Ar-H), 7.20 (t, 2H, Ar-H,  $J = 16.0$  Hz), 9.55 (s, 1H,

NH).  $^{13}\text{C}$  NMR:  $\delta$  12.7, 49.4, 53.6, 61.8, 96.2, 116.4, 120.2, 129.3, 150.9, 157.4, 168.6, 170.2. Anal. Calcd. (Found) for  $\text{C}_{16}\text{H}_{20}\text{N}_4\text{O}_2$  (300.36): C, 63.98 (63.73); H, 6.71 (6.42); N, 18.65 (18.31) %.

**5.1.4.10. *N*-(5-(*t*-Butyl)isoxazol-3-yl)-2-(4-phenylpiperazin-1-yl)acetamide (10b)**

Yield 65%, m.p. 136-138 °C. IR: 3267 (NH), 1713 (C=O).  $^1\text{H}$  NMR (400 MHz,  $\text{CDCl}_3$ ):  $\delta$  1.35 (s, 9H,  $\text{C}(\text{CH}_3)_3$ ), 2.76 (t, 4H, Piperazine-2 $\text{CH}_2$ ,  $J = 9.6$  Hz), 3.23-3.26 (m, 6H,  $\text{COCH}_2$ , Piperazine-2 $\text{CH}_2$ ), 6.71 (s, 1H, Isoxazole-H), 6.87-6.94 (m, 4H, Ar-H), 7.28 (t, 1H, Ar-H,  $J = 14.8$  Hz), 9.62 (s, 1H, NH).  $^{13}\text{C}$  NMR:  $\delta$  28.7, 33.1, 49.3, 53.6, 61.6, 92.9, 116.4, 120.2, 129.3, 150.9, 157.1, 168.6, 181.9. MS  $m/z$  (%): 243 (45.37,  $\text{M}^{+1}$ ), 342 (100.00,  $\text{M}^+$ ). Anal. Calcd. (Found) for  $\text{C}_{19}\text{H}_{26}\text{N}_4\text{O}_2$  (342.44): C, 66.64 (66.51); H, 7.65 (7.48); N, 16.36 (16.10) %.

**5.1.4.11. *N*-(5-Methylisoxazol-3-yl)-3-morpholinylpropionamide (11a)**

Yield 50%, m.p. 94-96 °C. IR: 3216 (NH), 1705 (C=O).  $^1\text{H}$  NMR (500 MHz,  $\text{CDCl}_3$ ):  $\delta$  2.39 (s, 3H,  $\text{CH}_3$ ), 2.55 (t, 2H,  $\text{COCH}_2\text{CH}_2$ ,  $J = 12.0$  Hz), 2.60 (s, 4H, Morpholine-2 $\text{CH}_2$ ), 2.72 (t, 2H,  $\text{COCH}_2\text{CH}_2$ ,  $J = 12.0$  Hz), 3.82 (t, 4H, Morpholine-2 $\text{CH}_2$ ,  $J = 9.0$  Hz), 6.65 (s, 1H, Isoxazole-H), 11.45 (s, 1H, NH).  $^{13}\text{C}$  NMR:  $\delta$  12.6, 31.8, 52.7, 53.6, 66.8, 96.5, 157.9, 169.7, 170.3. MS  $m/z$  (%): 239 (5.60,  $\text{M}^+$ ), 43 (100.00). Anal. Calcd. (Found) for  $\text{C}_{11}\text{H}_{17}\text{N}_3\text{O}_3$  (239.27): C, 55.22 (55.08); H, 7.16 (6.97); N, 17.56 (17.33) %.

**5.1.4.12. *N*-(5-(*t*-Butyl)isoxazol-3-yl)-3-morpholinylpropionamide (11b)**

Yield 55%, m.p. 102-104 °C. IR: 3256 (NH), 1709 (C=O).  $^1\text{H}$  NMR (400 MHz,  $\text{CDCl}_3$ ):  $\delta$  1.27 (s, 9H,  $\text{C}(\text{CH}_3)_3$ ), 2.51 (t, 2H,  $\text{COCH}_2\text{CH}_2$ ,  $J = 11.6$  Hz), 2.56 (s, 4H, Morpholine-2 $\text{CH}_2$ ), 2.68 (t, 2H,  $\text{COCH}_2\text{CH}_2$ ,  $J = 11.6$  Hz), 3.76 (t, 4H, Morpholine-2 $\text{CH}_2$ ,  $J = 8.8$  Hz), 6.56 (s, 1H, Isoxazole-H), 11.48 (s, 1H, NH).  $^{13}\text{C}$  NMR:  $\delta$  28.7, 31.9, 33.0, 52.8, 53.7, 66.8, 93.3, 157.8, 170.3, 181.6. MS  $m/z$  (%): 282 (100.00,  $\text{M}^{+1}$ ), 281 (14.37,  $\text{M}^+$ ). Anal. Calcd. (Found) for  $\text{C}_{14}\text{H}_{23}\text{N}_3\text{O}_3$  (281.36): C, 59.77 (59.62); H, 8.24 (8.11); N, 14.94 (14.77) %.

**5.1.4.13. *N*-(5-Methylisoxazol-3-yl)-3-(4-methylpiperazin-1-yl)propionamide (12a)**

Yield 45%, m.p. 82-84 °C. IR: 3194 (NH), 1699 (C=O).  $^1\text{H}$  NMR (500 MHz,  $\text{CDCl}_3$ ):  $\delta$  2.33 (s, 3H,  $\text{CH}_3$ ), 2.37 (s, 3H,  $\text{CH}_3$ ), 2.50-2.72 (m, 12H,  $\text{COCH}_2\text{CH}_2$ , Piperazine-4 $\text{CH}_2$ ), 6.64 (s, 1H, Isoxazole-H), 11.63 (s, 1H, NH).  $^{13}\text{C}$  NMR:  $\delta$  12.6, 32.1, 45.5, 51.9, 53.0, 54.7, 96.5, 158.0, 169.6, 170.5.  $^{15}\text{N}$  NMR:  $\delta$  -6.9, 213.6, 336.1. MS  $m/z$  (%): 252 (5.74,  $\text{M}^+$ ), 56 (100.00). Anal. Calcd. (Found) for  $\text{C}_{12}\text{H}_{20}\text{N}_4\text{O}_2$  (252.32): C, 57.12 (57.37); H, 7.99 (8.22); N, 22.21 (22.48) %.

**5.1.4.14. *N*-(5-(*t*-Butyl)isoxazol-3-yl)-3-(4-methylpiperazin-1-yl)propionamide (12b)**

Yield 49%, m.p. 72-74 °C. IR: 3181 (NH), 1698 (C=O). <sup>1</sup>H NMR (500 MHz, CDCl<sub>3</sub>): δ 1.33 (s, 9H, C(CH<sub>3</sub>)<sub>3</sub>), 2.36 (s, 3H, CH<sub>3</sub>), 2.51-2.74 (m, 12H, COCH<sub>2</sub>CH<sub>2</sub>, Piperazine-4CH<sub>2</sub>), 6.63 (s, 1H, Isoxazole-H), 11.70 (s, 1H, NH). <sup>13</sup>C NMR: δ 28.6, 32.1, 32.9, 45.5, 51.8, 53.0, 54.7, 93.3, 157.8, 170.4, 181.4. <sup>15</sup>N NMR: δ -12.8, 199.9, 406.9. MS *m/z* (%): 294 (19.32, M<sup>+</sup>), 70 (100.00). Anal. Calcd. (Found) for C<sub>15</sub>H<sub>26</sub>N<sub>4</sub>O<sub>2</sub> (294.40): C, 61.20 (61.08); H, 8.90 (8.66); N, 19.03 (18.76) %.

**5.1.4.15. 3-(4-Ethylpiperazin-1-yl)-*N*-(5-methylisoxazol-3-yl)propionamide (13a)**

Yield 50%, m.p. 74-76 °C. <sup>1</sup>H NMR (400 MHz, CDCl<sub>3</sub>): δ 1.11 (t, 3H, CH<sub>2</sub>CH<sub>3</sub>, *J* = 14.40 Hz), 2.39-2.73 (m, 17H, CH<sub>3</sub>, CH<sub>2</sub>CH<sub>3</sub>, COCH<sub>2</sub>CH<sub>2</sub>, Piperazine-4CH<sub>2</sub>), 6.66 (s, 1H, Isoxazole-H), 11.71 (s, 1H, NH). <sup>13</sup>C NMR: δ 11.9, 12.6, 32.1, 52.1, 52.2, 52.7, 53.1, 96.6, 158.1, 169.6, 170.6. Anal. Calcd. (Found) for C<sub>13</sub>H<sub>22</sub>N<sub>4</sub>O<sub>2</sub> (266.35): C, 58.62 (58.90); H, 8.33 (8.59); N, 21.04 (21.26) %.

**5.1.4.16. *N*-(5-(*t*-Butyl)isoxazol-3-yl)-3-(4-ethylpiperazin-1-yl)propionamide (13b)**

Yield 55%, m.p. 89-91 °C. IR: 3182 (NH), 1697 (C=O). <sup>1</sup>H NMR (400 MHz, CDCl<sub>3</sub>): δ 1.13 (t, 3H, CH<sub>2</sub>CH<sub>3</sub>, *J* = 14.40 Hz), 1.34 (s, 9H, C(CH<sub>3</sub>)<sub>3</sub>), 2.48-2.75 (m, 14H, CH<sub>2</sub>CH<sub>3</sub>, COCH<sub>2</sub>CH<sub>2</sub>, Piperazine-4CH<sub>2</sub>), 6.63 (s, 1H, Isoxazole-H), 11.79 (s, 1H, NH). <sup>13</sup>C NMR: δ 11.9, 28.6, 32.1, 32.9, 52.1, 52.2, 52.6, 53.1, 93.3, 157.8, 170.6, 181.4. <sup>15</sup>N NMR: δ 34.2, 89.7, 199.9. MS *m/z* (%): 309 (5.23, M<sup>+</sup>+1), 308 (8.60, M<sup>+</sup>), 57 (100.00). Anal. Calcd. (Found) for C<sub>16</sub>H<sub>28</sub>N<sub>4</sub>O<sub>2</sub> (308.43): C, 62.31 (62.20); H, 9.15 (9.03); N, 18.17 (17.89) %.

**5.1.4.17. 3-(4-Benzylpiperazin-1-yl)-*N*-(5-methylisoxazol-3-yl)propionamide (14a)**

Yield 60%, m.p. 74-76 °C. IR: 3194 (NH), 1698 (C=O). <sup>1</sup>H NMR (500 MHz, CDCl<sub>3</sub>): δ 2.39 (s, 3H, CH<sub>3</sub>), 2.51-2.73 (m, 12H, COCH<sub>2</sub>CH<sub>2</sub>, Piperazine-4CH<sub>2</sub>), 3.55 (s, 2H, Phenyl-CH<sub>2</sub>), 6.65 (s, 1H, Isoxazole-H), 7.26-7.33 (m, 5H, Ar-H), 11.72 (s, 1H, NH). <sup>13</sup>C NMR: δ 12.6, 32.0, 52.1, 52.8, 53.0, 62.6, 96.5, 127.2, 128.2, 129.2, 137.6, 158.0, 169.6, 170.5. MS *m/z* (%): 329 (100.00, M<sup>+</sup>+1), 328 (73.38, M<sup>+</sup>), 327 (29.90, M<sup>+</sup>-1). Anal. Calcd. (Found) for C<sub>18</sub>H<sub>24</sub>N<sub>4</sub>O<sub>2</sub> (328.42): C, 65.83 (65.67); H, 7.37 (7.05); N, 17.06 (16.84) %.

**5.1.4.18. 3-(4-Benzylpiperazin-1-yl)-*N*-(5-(*t*-butyl)isoxazol-3-yl)propionamide (14b)**

Yield 65%, m.p. 113-115 °C. IR: 3448 (NH), 1695 (C=O). <sup>1</sup>H NMR (500 MHz, CDCl<sub>3</sub>): δ 1.33 (s, 9H, C(CH<sub>3</sub>)<sub>3</sub>), 2.56-2.76 (m, 12H, COCH<sub>2</sub>CH<sub>2</sub>, Piperazine-4CH<sub>2</sub>), 3.59 (s, 2H, Phenyl-CH<sub>2</sub>), 6.63 (s, 1H, Isoxazole-H), 7.26-7.35 (m, 5H, Ar-H), 11.69 (s, 1H, NH). <sup>13</sup>C NMR: δ 28.6, 32.0, 32.9, 51.9, 52.7, 52.9, 62.5, 93.3, 127.4, 128.3, 129.3, 137.0, 157.8, 170.4, 181.4. MS *m/z* (%): 371

(100.00,  $M^{+1}$ ), 370 (68.54,  $M^{+}$ ), 369 (10.26,  $M^{+1}$ ). Anal. Calcd. (Found) for  $C_{21}H_{30}N_4O_2$  (370.50): C, 68.08 (67.77); H, 8.16 (7.94); N, 15.12 (14.83) %.

#### 5.1.4.19. *N*-(5-Methylisoxazol-3-yl)-3-(4-phenylpiperazin-1-yl)propionamide (15a)

Yield 52%, m.p. 134-136 °C. IR: 3223 (NH), 1698 (C=O).  $^1H$  NMR (500 MHz,  $CDCl_3$ ):  $\delta$  2.39 (s, 3H,  $CH_3$ ), 2.60 (t, 2H,  $COCH_2CH_2$ ,  $J = 11.5$  Hz), 2.82 (s, 6H, Piperazine-3 $CH_2$ ), 3.32-3.34 (m, 4H,  $COCH_2CH_2$ , Piperazine- $CH_2$ ), 6.65 (s, 1H, Isoxazole-H), 6.87-7.29 (m, 5H, Ar-H), 11.50 (s, 1H, NH).  $^{13}C$  NMR:  $\delta$  12.6, 32.1, 49.2, 52.4, 53.2, 96.5, 116.4, 120.2, 129.1, 150.8, 157.9, 169.7, 170.4. MS  $m/z$  (%): 315 (34.80,  $M^{+1}$ ), 314 (100.00,  $M^{+}$ ). Anal. Calcd. (Found) for  $C_{17}H_{22}N_4O_2$  (314.39): C, 64.95 (64.72); H, 7.05 (6.86); N, 17.82 (17.53) %.

#### 5.1.4.20. *N*-(5-(*t*-Butyl)isoxazol-3-yl)-3-(4-phenylpiperazin-1-yl)propionamide (15b)

Yield 58%, m.p. 123-125 °C. IR: 3240 (NH), 1704 (C=O).  $^1H$  NMR (500 MHz,  $CDCl_3$ ):  $\delta$  1.33 (s, 9H,  $C(CH_3)_3$ ), 2.59 (t, 2H,  $COCH_2CH_2$ ,  $J = 11.5$  Hz), 2.81 (s, 6H, Piperazine-3 $CH_2$ ), 3.32-3.34 (m, 4H,  $COCH_2CH_2$ , Piperazine- $CH_2$ ), 6.62 (s, 1H, Isoxazole-H), 6.87-7.27 (m, 5H, Ar-H), 11.62 (s, 1H, NH).  $^{13}C$  NMR:  $\delta$  28.6, 32.1, 32.9, 49.2, 52.3, 53.2, 93.3, 116.4, 120.2, 129.1, 150.9, 157.7, 170.7, 181.5. MS  $m/z$  (%): 357 (18.84,  $M^{+1}$ ), 356 (100.00,  $M^{+}$ ). Anal. Calcd. (Found) for  $C_{20}H_{28}N_4O_2$  (356.47): C, 67.39 (67.50); H, 7.92 (8.14); N, 15.72 (15.83) %.

### 5.1.5. Synthesis of 2-((5-(methyl/*t*-butyl)isoxazol-3-yl)amino)thiazol-4(5H)-ones 16a,b

A mixture of 2-chloroacetamide **4a,b** (0.002 mol) and ammonium thiocyanate (0.30 g, 0.004 mol) in absolute ethanol (10 mL) was heated under reflux for 3-5 h. The reaction mixture was concentrated under vacuum, and the precipitate formed was filtered, washed with water and crystallized from ethanol to produce the desired compounds **16a,b**.

#### 5.1.5.1. 2-((5-Methylisoxazol-3-yl)amino)thiazol-4(5H)-one (16a) [81]

Yield 60%, m.p. 204-206 °C [81].  $^1H$  NMR (400 MHz,  $DMSO-d_6$ ):  $\delta$  2.49 (s, 3H,  $CH_3$ ), 4.13 (s, 2H, Thiazole-H), 6.64 (s, 1H, Isoxazole-H), 11.38 (s, 1H, NH).  $^{13}C$  NMR:  $\delta$  12.6, 37.1, 96.6, 158.1, 165.1, 170.6, 174.7. Anal. Calcd. (Found) for  $C_7H_7N_3O_2S$  (197.21): C, 42.63 (42.37); H, 3.58 (3.35); N, 21.31 (21.02) %.

#### 5.1.5.2. 2-((5-(*t*-Butyl)isoxazol-3-yl)amino)thiazol-4(5H)-one (16b)

Yield 75%, m.p. 240-242 °C. IR: 3447 (NH), 1732 (C=O).  $^1H$  NMR (400 MHz,  $DMSO-d_6$ ):  $\delta$  1.30 (s, 9H,  $C(CH_3)_3$ ), 4.04 (s, 2H, Thiazole-H), 6.08 (s, 1H, Isoxazole-H).  $^{13}C$  NMR:  $\delta$  28.9, 32.9, 35.9,

96.5, 163.6, 165.2, 175.0, 181.6. MS  $m/z$  (%): 239 (19.71,  $M^+$ ), 102 (100.00). Anal. Calcd. (Found) for  $C_{10}H_{13}N_3O_2S$  (239.29): C, 50.19 (50.04); H, 5.48 (5.19); N, 17.56 (17.35) %.

### 5.1.6. Synthesis of 5-arylidene-2-((5-(methyl/*t*-butyl)isoxazol-3-yl)amino)thiazol-4(5*H*)-ones 17a,b-25a

A mixture of compound **16a,b** (0.001 mol) and the appropriate araldehyde (0.001 mol) in absolute ethanol (10 mL) was stirred at room temperature for 10 min, then an aqueous solution of 10% NaOH (10 mL) was added dropwise. The mixture was stirred at room temperature for 24 h, then neutralized with 1*N* HCl. The precipitated solid was filtered, washed with water and crystallized from ethanol to give the desired compounds **17a,b-25a**.

#### 5.1.6.1. 5-((Furan-2-yl)methylidene)-2-((5-methylisoxazol-3-yl)amino)thiazol-4(5*H*)-one (17a)

Yield 50%, m.p. 80-82 °C. IR: 3425 (NH), 1699 (C=O).  $^1H$  NMR (500 MHz, DMSO- $d_6$ ):  $\delta$  2.29 (s, 3H,  $CH_3$ ), 6.55-6.60 (m, 3H, Isoxazole-H, Furan-2H), 7.06 (s, 1H, Furan-H), 7.82 (s, 1H, C=CH).  $^{13}C$  NMR:  $\delta$  12.3, 99.3, 109.9, 112.6, 132.9, 144.0, 151.7, 166.8, 167.6, 168.4, 172.4, 180.2. MS  $m/z$  (%): 275 (32.33,  $M^+$ ), 168 (100.00). Anal. Calcd. (Found) for  $C_{12}H_9N_3O_3S$  (275.28): C, 52.36 (52.11); H, 3.30 (3.12); N, 15.26 (15.04) %.

#### 5.1.6.2. 2-((5-(*t*-Butyl)isoxazol-3-yl)amino)-5-((furan-2-yl)methylidene)thiazol-4(5*H*)-one (17b)

Yield 55%, m.p. 216-218 °C. IR: 3450 (NH), 1708 (C=O).  $^1H$  NMR (500 MHz, DMSO- $d_6$ ):  $\delta$  1.30 (s, 9H,  $C(CH_3)_3$ ), 6.17 (s, 1H, Isoxazole-H), 6.74 (t, 1H, Furan-H,  $J = 3.5$  Hz), 7.05 (d, 1H, Furan-H), 7.49 (s, 1H, Furan-H), 8.07 (s, 1H, C=CH), 12.50 (s, 1H, NH).  $^{13}C$  NMR:  $\delta$  28.4, 32.6, 96.7, 113.5, 117.5, 132.0, 147.3, 149.6, 164.6, 164.7, 167.5, 167.6, 181.5. MS  $m/z$  (%): 318 (22.23,  $M^+ + 1$ ), 317 (100.00,  $M^+$ ). Anal. Calcd. (Found) for  $C_{15}H_{15}N_3O_3S$  (317.36): C, 56.77 (56.92); H, 4.76 (4.95); N, 13.24 (13.45) %.

#### 5.1.6.3. 5-((5-Bromothiophen-2-yl)methylidene)-2-((5-methylisoxazol-3-yl)amino)thiazol-4(5*H*)-one (18a)

Yield 65%, m.p. 259-261 °C. IR: 3449 (NH), 1710 (C=O).  $^1H$  NMR (500 MHz, DMSO- $d_6$ ):  $\delta$  2.29 (s, 3H,  $CH_3$ ), 6.54 (s, 1H, Isoxazole-H), 7.18 (d, 1H, Thiophene-H,  $J = 3.5$  Hz), 7.27 (d, 1H, Thiophene-H,  $J = 3.5$  Hz), 7.41 (s, 1H, C=CH).  $^{13}C$  NMR:  $\delta$  12.8, 99.6, 115.4, 130.8, 132.0, 134.9, 143.6, 167.5, 167.9, 169.1, 171.6, 180.4. MS  $m/z$  (%): 372 (1.28,  $M^+ + 2$ ), 370 (4.98,  $M^+$ ), 95 (100.00). Anal. Calcd. (Found) for  $C_{12}H_8BrN_3O_2S_2$  (370.24): C, 38.93 (38.71); H, 2.18 (2.43); N, 11.35 (11.12) %.

**5.1.6.4. 5-((5-Bromothiophen-2-yl)methylidene)-2-((5-(*t*-butyl)isoxazol-3-yl)amino)thiazol-4(5H)-one (18b)**

Yield 68%, m.p. 243-245 °C. IR: 3451 (NH), 1706 (C=O). <sup>1</sup>H NMR (400 MHz, DMSO-*d*<sub>6</sub>): δ 1.33 (s, 9H, C(CH<sub>3</sub>)<sub>3</sub>), 6.24 (s, 1H, Isoxazole-H), 7.45 (d, 1H, Thiophene-H, *J* = 4.0 Hz), 7.52 (d, 1H, Thiophene-H, *J* = 4.0 Hz), 7.92 (s, 1H, C=CH), 12.82 (s, 1H, NH). <sup>13</sup>C NMR: δ 28.9, 33.1, 97.2, 118.9, 132.8, 134.4, 135.2, 139.6, 162.2, 164.8, 167.5, 167.7, 182.2. MS *m/z* (%): 414 (3.38, M<sup>+</sup>+2), 412 (10.15, M<sup>+</sup>), 57 (100.00). Anal. Calcd. (Found) for C<sub>15</sub>H<sub>14</sub>BrN<sub>3</sub>O<sub>2</sub>S<sub>2</sub> (412.32): C, 43.70 (43.91); H, 3.42 (3.67); N, 10.19 (10.37) %.

**5.1.6.5. 2-((5-Methylisoxazol-3-yl)amino)-5-((4-methylphenyl)methylidene)thiazol-4(5H)-one (19a)**

Yield 50%, m.p. 242-244 °C. IR: 3450 (NH), 1711 (C=O). <sup>1</sup>H NMR (400 MHz, DMSO-*d*<sub>6</sub>): δ 2.37 (s, 3H, CH<sub>3</sub>), 2.42 (s, 3H, CH<sub>3</sub>), 6.24 (s, 1H, Isoxazole-H), 7.38 (d, 2H, Ar-H, *J* = 8.0 Hz), 7.52 (d, 2H, Ar-H, *J* = 8.0 Hz), 7.69 (s, 1H, C=CH), 12.68 (s, 1H, NH). <sup>13</sup>C NMR: δ 12.7, 21.6, 99.8, 129.6, 129.8, 130.5, 130.9, 141.0, 143.3, 165.5, 167.8, 167.9, 171.2. MS *m/z* (%): 300 (10.21, M<sup>+</sup>+1), 299 (47.98, M<sup>+</sup>), 43 (100.00). Anal. Calcd. (Found) for C<sub>15</sub>H<sub>13</sub>N<sub>3</sub>O<sub>2</sub>S (299.35): C, 60.18 (60.05); H, 4.38 (4.21); N, 14.04 (13.83) %.

**5.1.6.6. 2-((5-(*t*-Butyl)isoxazol-3-yl)amino)-5-((4-methylphenyl)methylidene)thiazol-4(5H)-one (19b)**

Yield 53%, m.p. 246-248 °C. IR: 3451 (NH), 1711 (C=O). <sup>1</sup>H NMR (500 MHz, DMSO-*d*<sub>6</sub>): δ 1.30 (s, 9H, C(CH<sub>3</sub>)<sub>3</sub>), 2.35 (s, 3H, CH<sub>3</sub>), 6.19 (s, 1H, Isoxazole-H), 7.36 (d, 2H, Ar-H, *J* = 8.0 Hz), 7.51 (d, 2H, Ar-H, *J* = 8.0 Hz), 7.66 (s, 1H, C=CH), 12.62 (s, 1H, NH). <sup>13</sup>C NMR: δ 21.6, 28.9, 33.1, 97.2, 130.6, 130.9, 131.7, 137.8, 140.9, 164.9, 166.6, 168.0, 168.2, 182.1. MS *m/z* (%): 342 (23.08, M<sup>+</sup>+1), 341 (92.93, M<sup>+</sup>), 148 (100.00). Anal. Calcd. (Found) for C<sub>18</sub>H<sub>19</sub>N<sub>3</sub>O<sub>2</sub>S (341.43): C, 63.32 (63.13); H, 5.61 (5.30); N, 12.31 (12.09) %.

**5.1.6.7. 5-((4-Bromophenyl)methylidene)-2-((5-methylisoxazol-3-yl)amino)thiazol-4(5H)-one (20a)**

Yield 70%, m.p. 248-250 °C. IR: 3451 (NH), 1715 (C=O). <sup>1</sup>H NMR (500 MHz, DMSO-*d*<sub>6</sub>): δ 2.29 (s, 3H, CH<sub>3</sub>), 6.57 (s, 1H, Isoxazole-H), 7.25 (s, 1H, C=CH), 7.46 (d, 2H, Ar-H, *J* = 8.0 Hz), 7.64 (d, 2H, Ar-H, *J* = 8.0 Hz). <sup>13</sup>C NMR: δ 12.8, 99.7, 121.2, 131.3, 132.3, 135.6, 135.9, 167.5, 167.9, 169.0, 172.5, 180.9. MS *m/z* (%): 366 (2.18, M<sup>+</sup>+2), 364 (4.52, M<sup>+</sup>), 89 (100.00). Anal. Calcd. (Found) for C<sub>14</sub>H<sub>10</sub>BrN<sub>3</sub>O<sub>2</sub>S (364.22): C, 46.17 (46.43); H, 2.77 (2.56); N, 11.54 (11.24) %.

**5.1.6.8. 5-((4-Bromophenyl)methylidene)-2-((5-(*t*-butyl)isoxazol-3-yl)amino)thiazol-4(5H)-one (20b)**

Yield 76%, m.p. 258-260 °C. IR: 3450 (NH), 1718 (C=O). <sup>1</sup>H NMR (400 MHz, DMSO-*d*<sub>6</sub>): δ 1.33 (s, 9H, C(CH<sub>3</sub>)<sub>3</sub>), 6.23 (s, 1H, Isoxazole-H), 7.58 (d, 2H, Ar-H, *J* = 8.0 Hz), 7.69 (s, 1H, C=CH), 7.78 (d, 2H, Ar-H, *J* = 8.0 Hz), 12.75 (s, 1H, NH). <sup>13</sup>C NMR: δ 28.9, 33.1, 97.2, 124.2, 125.4, 130.4, 132.3, 132.8, 132.9, 156.9, 164.9, 167.6, 182.2. MS *m/z* (%): 408 (35.17, M<sup>+</sup>+2), 406 (100.00, M<sup>+</sup>). Anal. Calcd. (Found) for C<sub>17</sub>H<sub>16</sub>BrN<sub>3</sub>O<sub>2</sub>S (406.30): C, 50.26 (50.14); H, 3.97 (3.73); N, 10.34 (10.11) %.

**5.1.6.9. 5-((3,4-Dichlorophenyl)methylidene)-2-((5-methylisoxazol-3-yl)amino)thiazol-4(5H)-one (21a)**

Yield 80%, m.p. 223-225 °C. IR: 3451 (NH), 1721 (C=O). <sup>1</sup>H NMR (500 MHz, DMSO-*d*<sub>6</sub>): δ 2.29 (s, 3H, CH<sub>3</sub>), 6.57 (s, 1H, Isoxazole-H), 7.26 (s, 1H, C=CH), 7.50 (s, 1H, NH), 7.68-7.77 (m, 3H, Ar-H). <sup>13</sup>C NMR: δ 12.8, 99.7, 128.7, 129.5, 130.2, 131.5, 131.9, 135.0, 137.3, 167.3, 167.9, 169.0, 169.3, 172.0. MS *m/z* (%): 358 (1.10, M<sup>+</sup>+4), 356 (4.87, M<sup>+</sup>+2), 354 (14.06, M<sup>+</sup>), 124 (100.00). Anal. Calcd. (Found) for C<sub>14</sub>H<sub>9</sub>Cl<sub>2</sub>N<sub>3</sub>O<sub>2</sub>S (354.20): C, 47.47 (47.31); H, 2.56 (2.24); N, 11.86 (11.65) %.

**5.1.6.10. 2-((5-(*t*-Butyl)isoxazol-3-yl)amino)-5-((3,4-dichlorophenyl)methylidene)thiazol-4(5H)-one (21b)**

Yield 85%, m.p. 226-228 °C. IR: 3449 (NH), 1719 (C=O). <sup>1</sup>H NMR (400 MHz, DMSO-*d*<sub>6</sub>): δ 1.32 (s, 9H, C(CH<sub>3</sub>)<sub>3</sub>), 6.24 (s, 1H, Isoxazole-H), 7.58 (d, 1H, Ar-H, *J* = 8.0 Hz), 7.69 (s, 1H, C=CH), 7.83 (d, 1H, Ar-H, *J* = 8.0 Hz), 7.92 (s, 1H, Ar-H), 12.87 (s, 1H, NH). <sup>13</sup>C NMR: δ 28.8, 33.1, 97.2, 128.9, 129.4, 131.5, 132.5, 132.9, 134.5, 136.3, 164.7, 165.9, 167.6, 167.9, 182.2. MS *m/z* (%): 400 (5.23, M<sup>+</sup>+4), 398 (15.65, M<sup>+</sup>+2), 397 (100.00, M<sup>+</sup>+1), 396 (20.71, M<sup>+</sup>). Anal. Calcd. (Found) for C<sub>17</sub>H<sub>15</sub>Cl<sub>2</sub>N<sub>3</sub>O<sub>2</sub>S (396.29): C, 51.53 (51.65); H, 3.82 (3.96); N, 10.60 (10.83) %.

**5.1.6.11. 5-(2-Chloro-6-fluorophenyl)methylidene)-2-((5-methylisoxazol-3-yl)amino)thiazol-4(5H)-one (22a)**

Yield 82%, m.p. 245-247 °C. IR: 3450 (NH), 1722 (C=O). <sup>1</sup>H NMR (400 MHz, DMSO-*d*<sub>6</sub>): δ 2.39 (s, 3H, CH<sub>3</sub>), 6.22 (s, 1H, Isoxazole-H), 7.42 (t, 1H, Ar-H, *J* = 18.0 Hz), 7.51 (d, 1H, Ar-H, *J* = 8.0 Hz), 7.57 (t, 1H, Ar-H, *J* = 14.0 Hz), 7.61 (s, 1H, C=CH), 12.84 (s, 1H, NH). <sup>13</sup>C NMR: δ 12.7, 99.8, 115.8, 122.8, 122.9, 125.8, 126.6, 132.4, 132.9, 134.3, 159.8, 160.6, 160.9, 164.8, 165.2, 171.4. MS

$m/z$  (%): 340 (1.02,  $M^{+2}$ ), 338 (2.28,  $M^{+}$ ), 337 (5.60,  $M^{+1}$ ), 43 (100.00). Anal. Calcd. (Found) for  $C_{14}H_9ClFN_3O_2S$  (337.75): C, 49.79 (49.47); H, 2.69 (2.54); N, 12.44 (12.23) %.

**5.1.6.12. 2-((5-(*t*-Butyl)isoxazol-3-yl)amino)-5-(2-chloro-6-fluorophenyl)methylidene)thiazol-4(5H)-one (22b)**

Yield 89%, m.p. 214-216 °C. IR: 3449 (NH), 1714 (C=O).  $^1H$  NMR (400 MHz, DMSO- $d_6$ ):  $\delta$  1.29 (s, 9H, C(CH<sub>3</sub>)<sub>3</sub>), 6.21 (s, 1H, Isoxazole-H), 7.42 (t, 1H, Ar-H,  $J$  = 18.0 Hz), 7.51 (d, 1H, Ar-H,  $J$  = 8.0 Hz), 7.59 (t, 1H, Ar-H,  $J$  = 14.0 Hz), 7.61 (s, 1H, C=CH), 12.82 (s, 1H, NH).  $^{13}C$  NMR:  $\delta$  28.8, 33.1, 97.2, 115.7, 120.9, 121.2, 122.9, 126.6, 132.5, 133.0, 134.4, 156.0, 158.2, 160.7, 164.8, 166.7, 182.2. MS  $m/z$  (%): 381 (5.15,  $M^{+2}$ ), 379 (6.88,  $M^{+}$ ), 57 (100.00). Anal. Calcd. (Found) for  $C_{17}H_{15}ClFN_3O_2S$  (379.83): C, 53.76 (53.45); H, 3.98 (3.76); N, 11.06 (10.82) %.

**5.1.6.13. 2-((5-Methylisoxazol-3-yl)amino)-5-((1,1-biphenyl-4-yl)methylidene)thiazol-4(5H)-one (23a)**

Yield 85%, m.p. 267-269 °C. IR: 3449 (NH), 1712 (C=O).  $^1H$  NMR (400 MHz, DMSO- $d_6$ ):  $\delta$  2.43 (s, 3H, CH<sub>3</sub>), 6.26 (s, 1H, Isoxazole-H), 7.43 (t, 1H, Ar-H,  $J$  = 14.4 Hz), 7.52 (t, 2H, Ar-H,  $J$  = 14.4 Hz), 7.72-7.78 (m, 5H, Ar-H, C=CH), 7.89 (d, 2H, Ar-H,  $J$  = 8.0 Hz), 12.72 (s, 1H, NH).  $^{13}C$  NMR:  $\delta$  12.7, 99.9, 126.8, 127.3, 127.9, 128.7, 129.6, 131.2, 132.5, 139.0, 142.0, 153.0, 153.7, 156.9, 157.2, 171.3. MS  $m/z$  (%): 362 (28.98,  $M^{+1}$ ), 361 (100.00,  $M^{+}$ ). Anal. Calcd. (Found) for  $C_{20}H_{15}N_3O_2S$  (361.42): C, 66.47 (66.26); H, 4.18 (3.88); N, 11.63 (11.51) %.

**5.1.6.14. 2-((5-(*t*-Butyl)isoxazol-3-yl)amino)-5-((1,1-biphenyl-4-yl)methylidene)thiazol-4(5H)-one (23b)**

Yield 90%, m.p. 255-257 °C. IR: 3450 (NH), 1711 (C=O).  $^1H$  NMR (400 MHz, DMSO- $d_6$ ):  $\delta$  1.33 (s, 9H, C(CH<sub>3</sub>)<sub>3</sub>), 6.25 (s, 1H, Isoxazole-H), 7.43 (t, 1H, Ar-H,  $J$  = 14.4 Hz), 7.52 (t, 2H, Ar-H,  $J$  = 14.4 Hz), 7.73-7.77 (m, 5H, Ar-H, C=CH), 7.89 (d, 2H, Ar-H,  $J$  = 8.0 Hz), 12.72 (s, 1H, NH).  $^{13}C$  NMR:  $\delta$  28.9, 33.1, 97.2, 125.5, 127.3, 127.9, 128.7, 129.6, 131.2, 132.8, 139.4, 142.1, 153.0, 159.1, 164.4, 173.5, 182.2. MS  $m/z$  (%): 404 (30.07,  $M^{+1}$ ), 403 (100.00,  $M^{+}$ ). Anal. Calcd. (Found) for  $C_{23}H_{21}N_3O_2S$  (403.50): C, 68.46 (68.25); H, 5.25 (4.94); N, 10.41 (10.26) %.

**5.1.6.15. 2-((5-Methylisoxazol-3-yl)amino)-5-((naphthalen-2-yl)methylidene)thiazol-4(5H)-one (24a)**

Yield 92%, m.p. 249-251 °C. IR: 3450 (NH), 1716 (C=O).  $^1H$  NMR (400 MHz, DMSO- $d_6$ ):  $\delta$  2.44 (s, 3H, CH<sub>3</sub>), 6.27 (s, 1H, Isoxazole-H), 7.63 (s, 2H, Ar-H), 7.73 (d, 1H, Ar-H,  $J$  = 7.6 Hz), 7.88 (s, 1H, Ar-H), 7.99-8.09 (m, 3H, Ar-H), 8.22 (s, 1H, C=CH), 12.73 (s, 1H, NH).  $^{13}C$  NMR:  $\delta$  12.8, 99.8,

126.3, 127.6, 128.2, 128.4, 129.2, 129.5, 131.3, 131.5, 131.6, 133.2, 133.6, 150.2, 159.4, 165.4, 168.0, 171.2. MS  $m/z$  (%): 336 (14.00,  $M^{+1}$ ), 335 (76.00,  $M^{+}$ ), 43 (100.00). Anal. Calcd. (Found) for  $C_{18}H_{13}N_3O_2S$  (335.38): C, 64.46 (64.16); H, 3.91 (3.66); N, 12.53 (12.40) %.

**5.1.6.16. 2-((5-(*t*-Butyl)isoxazol-3-yl)amino)-5-((naphthalen-2-yl-methylidene)thiazol-4(5H)-one (24b)**

Yield 85%, m.p. 239-241 °C. IR: 3450 (NH), 1716 (C=O).  $^1H$  NMR (400 MHz, DMSO- $d_6$ ):  $\delta$  1.34 (s, 9H, C(CH<sub>3</sub>)<sub>3</sub>), 6.25 (s, 1H, Isoxazole-H), 7.62-7.63 (m, 2H, Ar-H), 7.73 (d, 1H, Ar-H,  $J = 7.6$  Hz), 7.87 (s, 1H, Ar-H), 7.98-8.10 (m, 3H, Ar-H), 8.22 (s, 1H, C=CH), 12.77 (s, 1H, NH).  $^{13}C$  NMR:  $\delta$  28.9, 33.1, 97.2, 126.3, 127.7, 128.2, 128.4, 129.1, 129.5, 131.5, 131.8, 133.6, 141.2, 154.9, 159.4, 162.2, 164.8, 172.6, 182.2. MS  $m/z$  (%): 378 (23.28,  $M^{+1}$ ), 377 (100.00,  $M^{+}$ ). Anal. Calcd. (Found) for  $C_{21}H_{19}N_3O_2S$  (377.46): C, 66.82 (66.61); H, 5.07 (4.85); N, 11.13 (10.89) %.

**5.1.6.17. 5-((Anthracen-9-yl)methylidene)-2-((5-methylisoxazol-3-yl)amino)thiazol-4(5H)-one (25a)**

Yield 90%, m.p. 293-295 °C. IR: 3447 (NH), 1709 (C=O).  $^1H$  NMR (400 MHz, DMSO- $d_6$ ):  $\delta$  2.26 (s, 3H, CH<sub>3</sub>), 6.09 (s, 1H, Isoxazole-H), 7.60-7.62 (m, 4H, Ar-H), 8.03 (d, 2H, Ar-H,  $J = 8.8$  Hz), 8.12-8.21 (m, 2H, Ar-H), 8.53 (s, 1H, C=CH), 8.77 (s, 1H, Ar-H), 12.72 (s, 1H, NH).  $^{13}C$  NMR:  $\delta$  12.6, 99.7, 125.6, 125.9, 126.3, 126.6, 127.5, 128.4, 129.5, 129.7, 131.2, 133.3, 156.5, 166.1, 166.8, 171.1. MS  $m/z$  (%): 386 (25.36,  $M^{+1}$ ), 385 (100.00,  $M^{+}$ ). Anal. Calcd. (Found) for  $C_{22}H_{15}N_3O_2S$  (385.44): C, 68.56 (68.34); H, 3.92 (3.69); N, 10.90 (10.63) %.

## 5.2. Biological evaluation

The detailed procedures of biological assays are described in the [supplementary file](#).

## 5.3. Molecular docking studies

The detailed procedure of molecular docking studies is described in the [supplementary file](#).

## Acknowledgments

Deepest gratitude to Holding company for biological products and vaccines (VACSERA), Egypt for carrying out the biological screening assays.

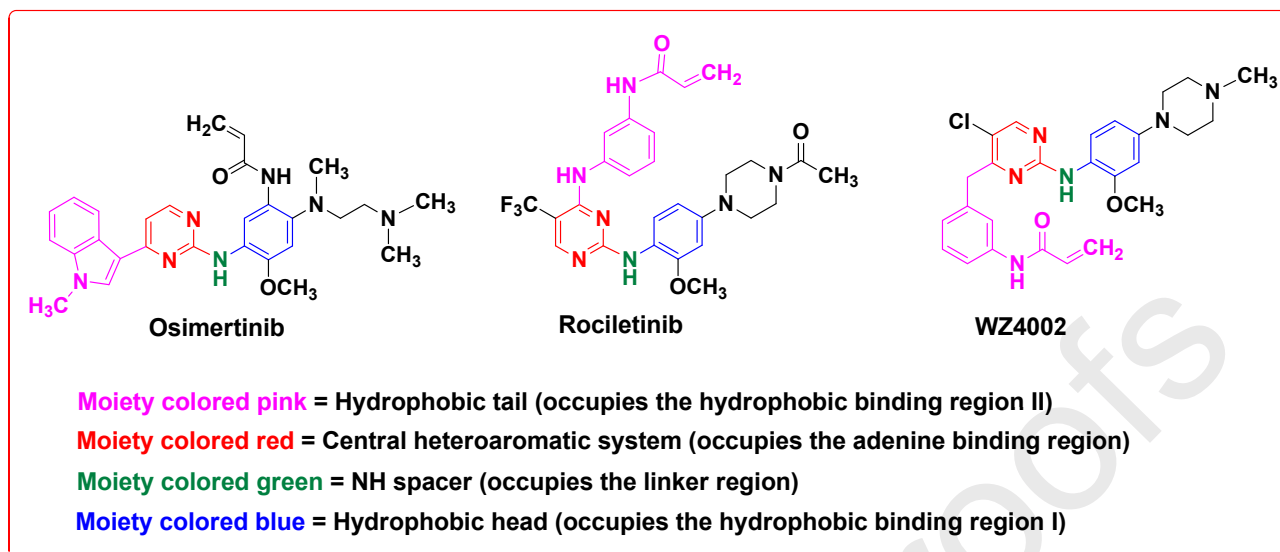
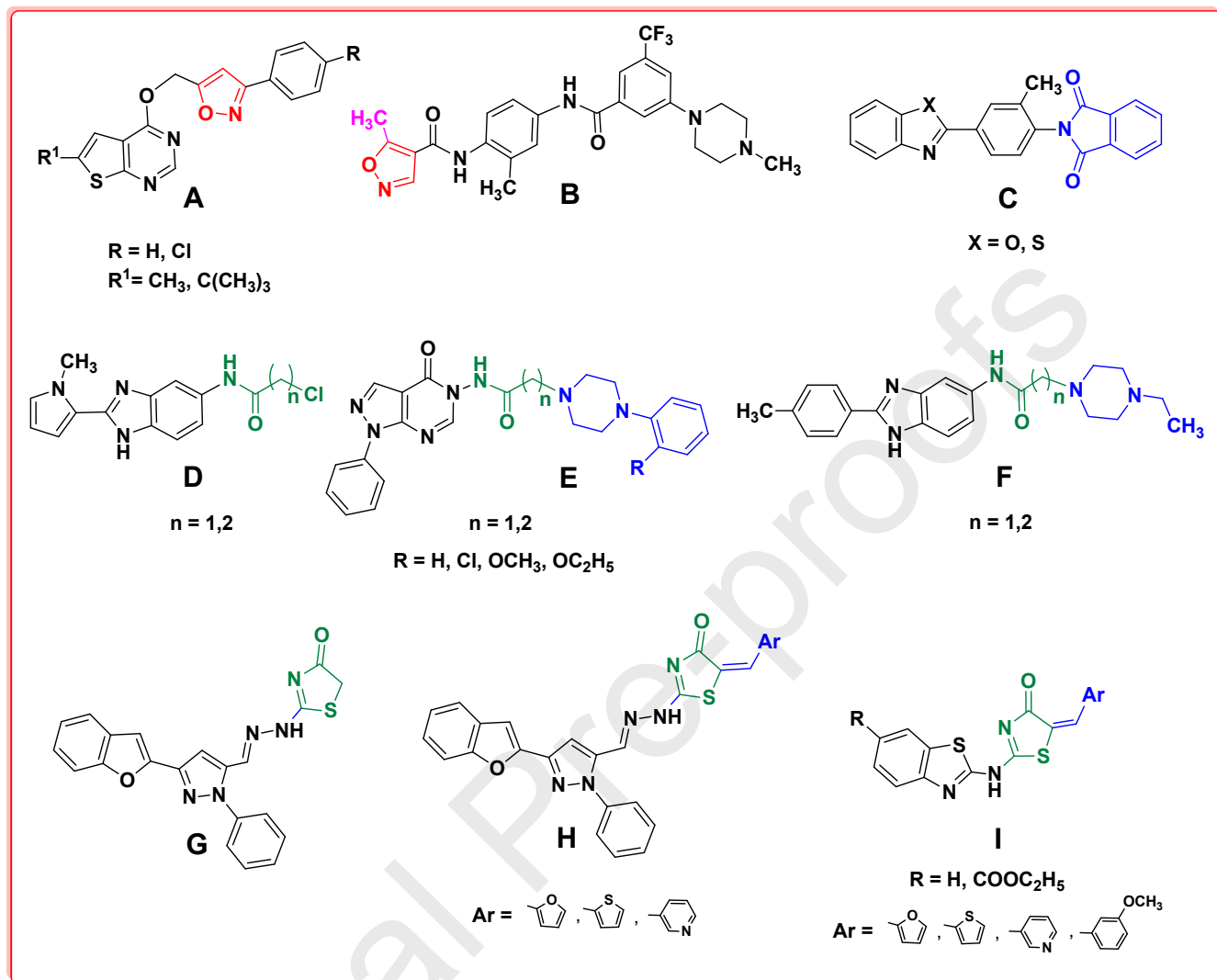
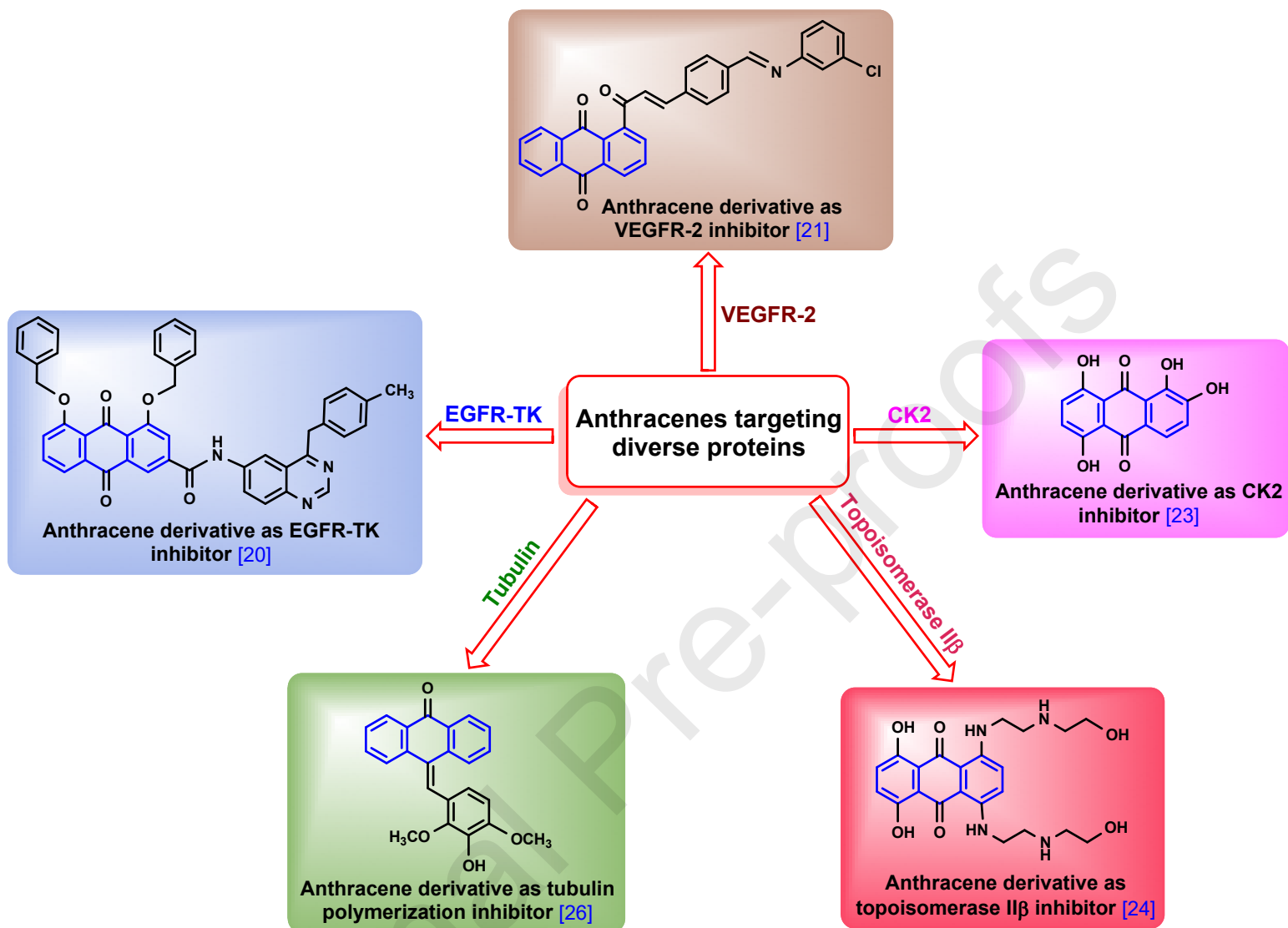


Fig. 1. Reported pyrimidine-based EGFR-TK inhibitors.



**Fig. 2.** Examples of isoxazoles **A,B**, isoindoline-1,3-diones **C**, chloroacetamides and chloropropionamides **D**, piperazinyloxyacetamides and piperazinyloxypropionamides **E,F**, thiazolone **G** and arylidene-thiazolones **H,I** with reported antitumor and EGFR-TK inhibitory activities.



**Fig. 3.** Examples of anthracene derivatives with reported EGFR-TK, VEGFR-2, CK2, topoisomerase II $\beta$  and tubulin polymerization inhibitory activities.

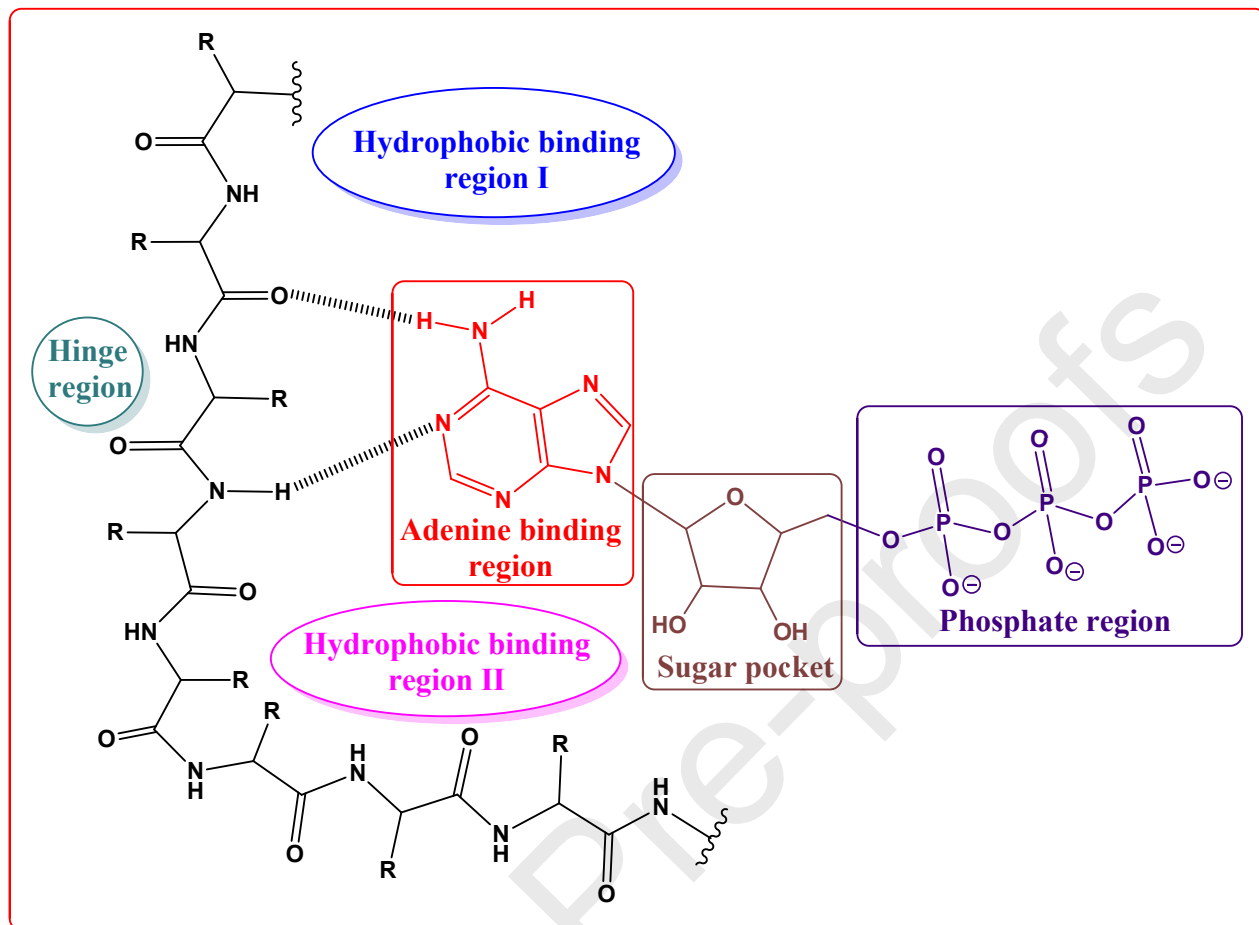


**Fig. 4.** The pharmacophore model of the ATP-binding site of EGFR-TK.

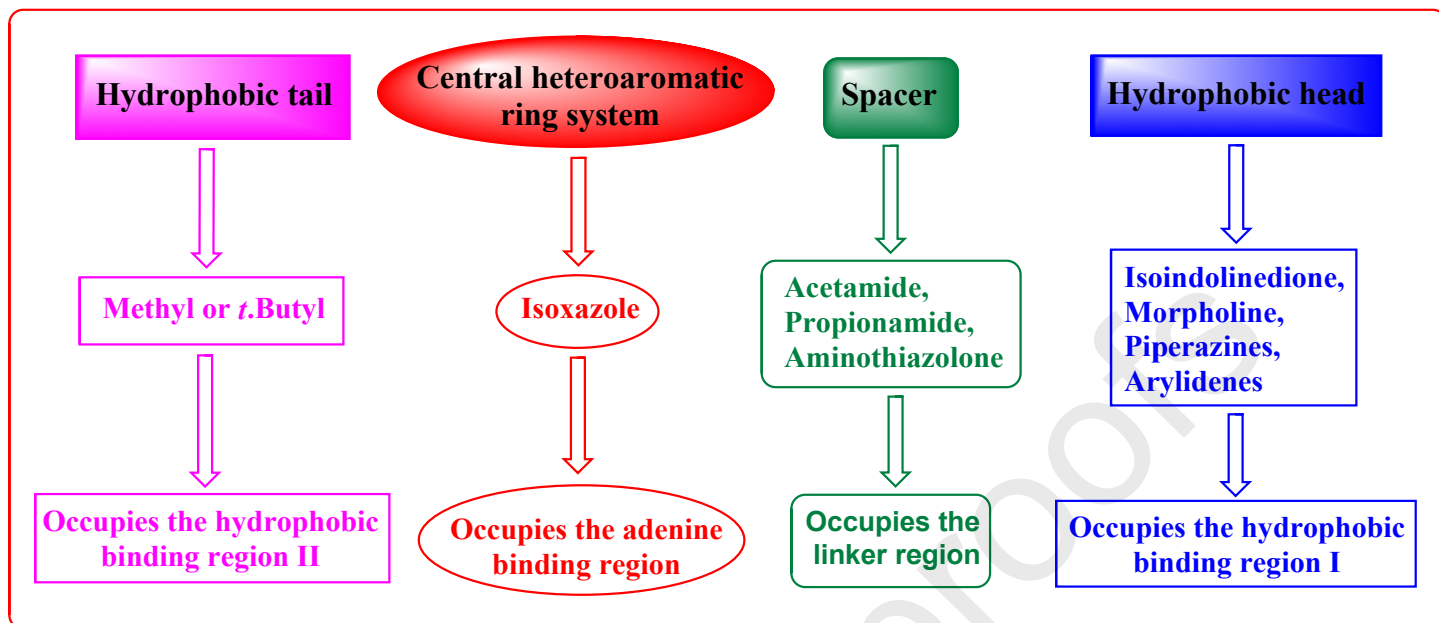


**Fig. 5.** Summary of the possible modifications carried out for design of the new compounds with expected EGFR-TK inhibitory activity.

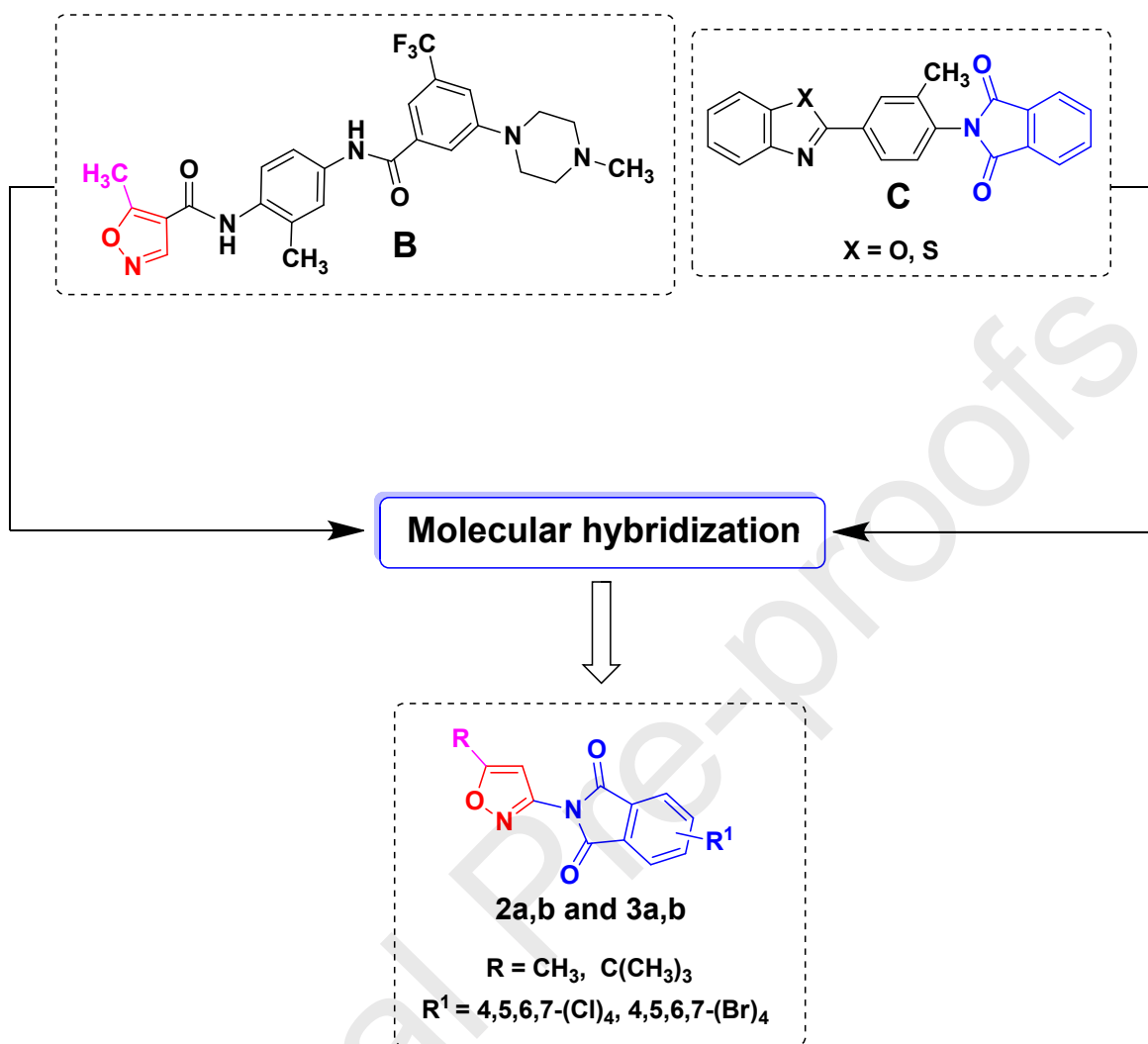


Fig. 6. The designed new hybrids **2a,b** and **3a,b** as potential antitumor agents and EGFR-TKIs.

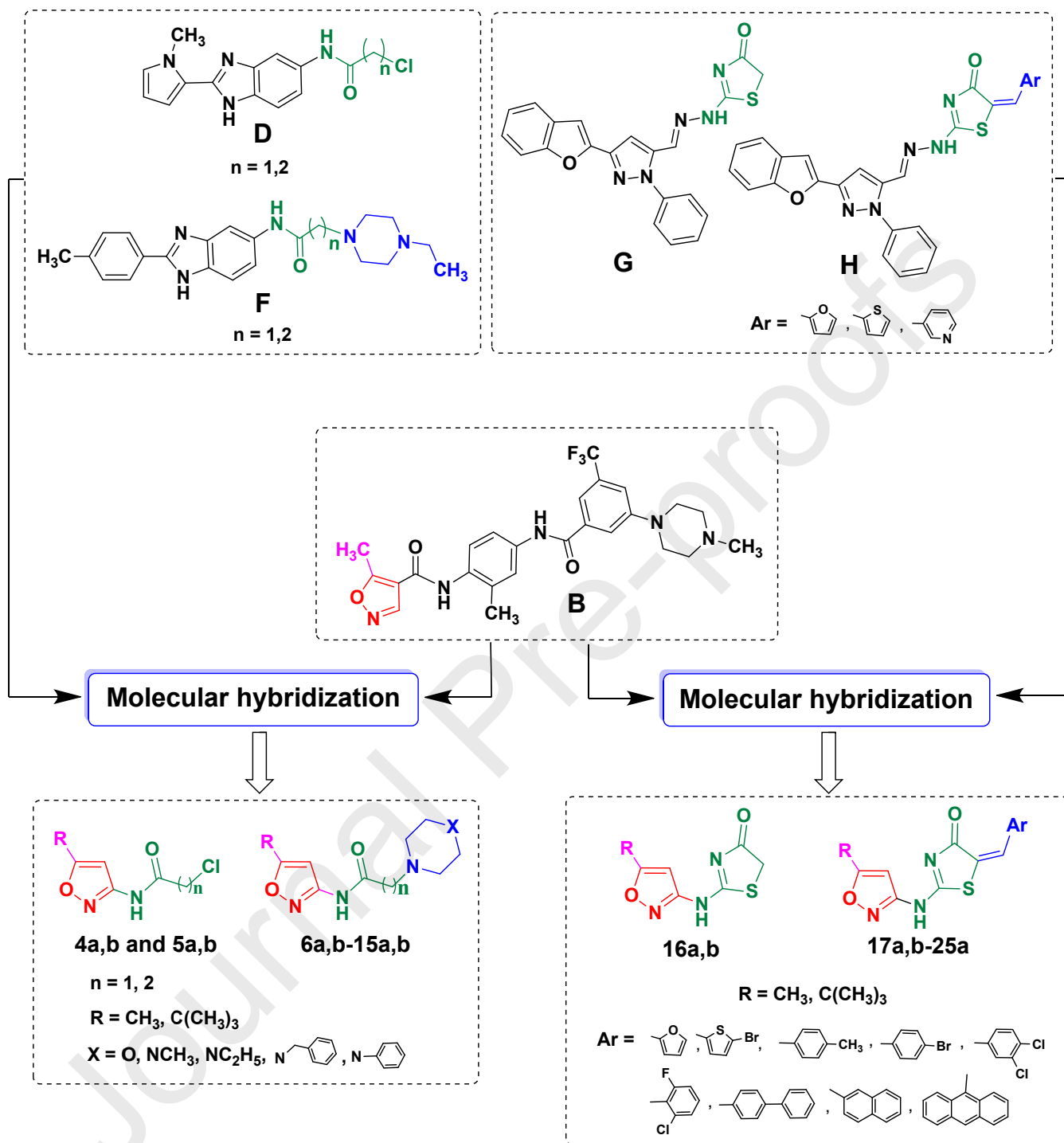
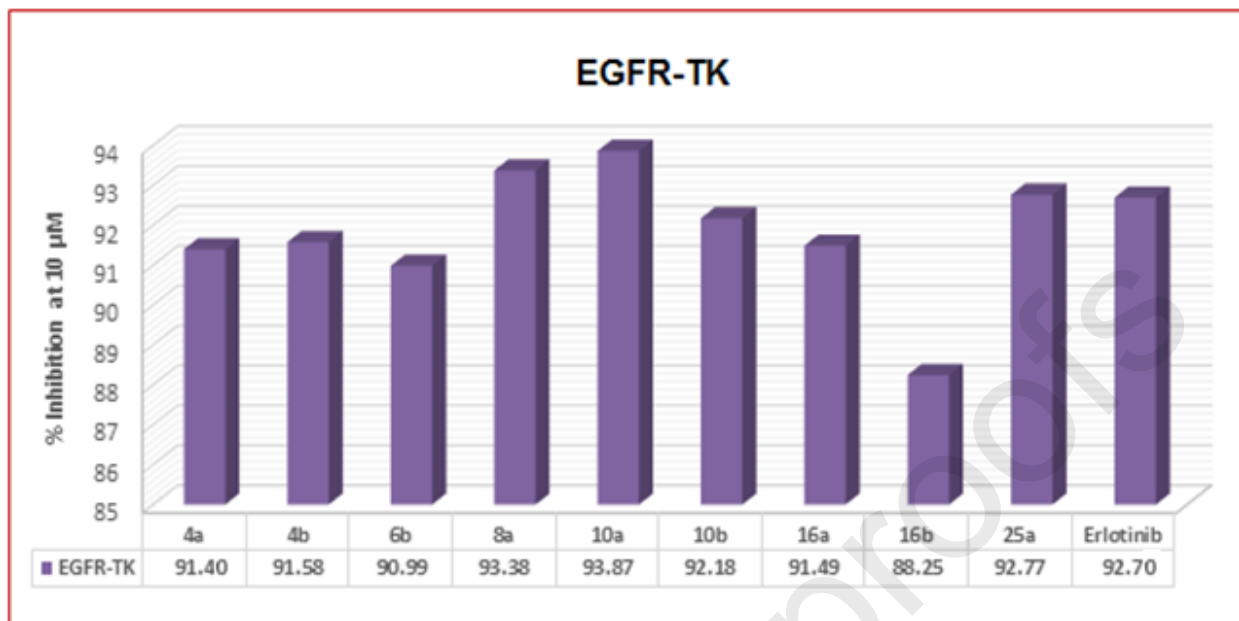
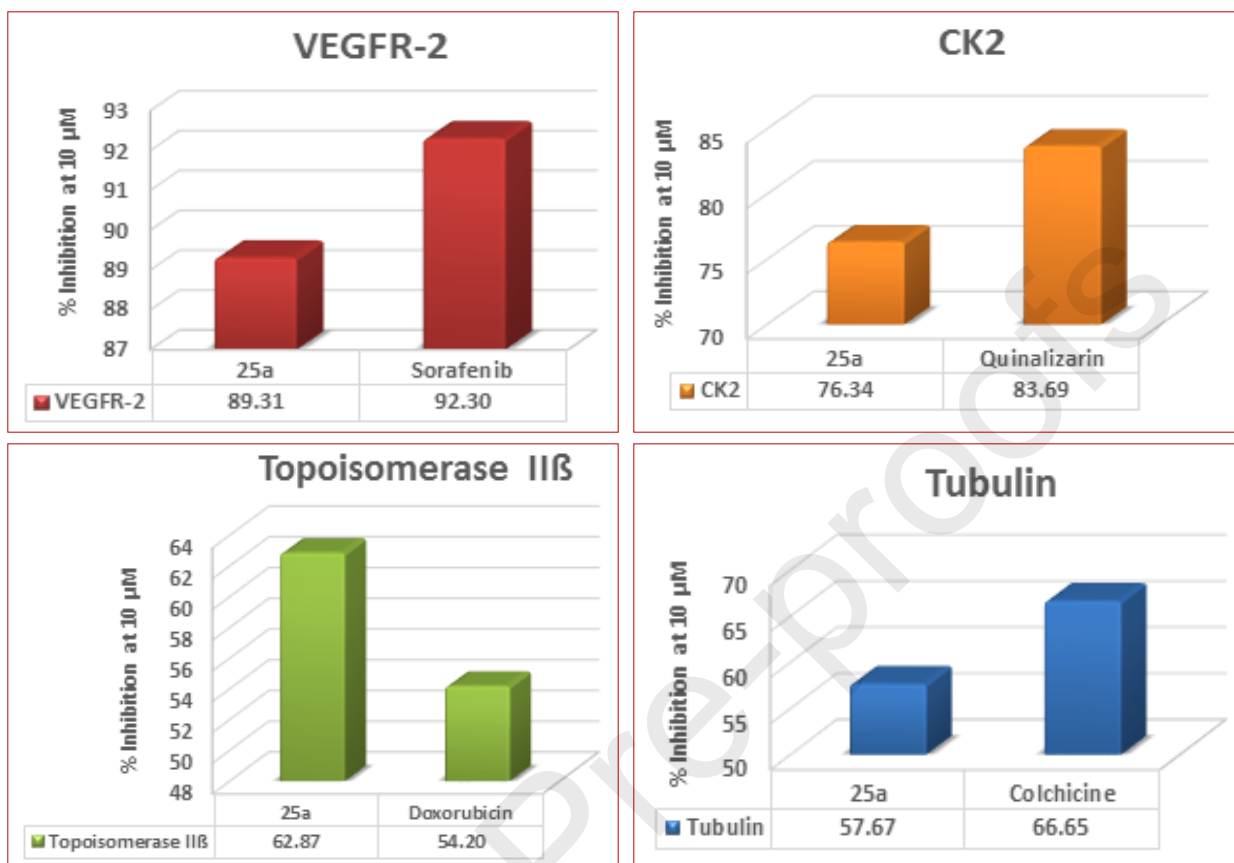


Fig. 7. The designed new hybrids **4a,b**, **5a,b**, **6a,b-15a,b**, **16a,b** and **17a,b-25a** as potential antitumor agents and EGFR-TKIs.



**Fig. 8.** Percentage inhibition of EGFR-TK by compounds **4a**, **4b**, **6b**, **8a**, **10a**, **10b**, **16a**, **16b** and **25a** at concentration of **10 µM**.



**Fig. 9.** Percentage inhibition of VEGFR-2, CK2, topoisomerase II $\beta$  and tubulin polymerization by compound 25a at concentration of 10  $\mu$ M.

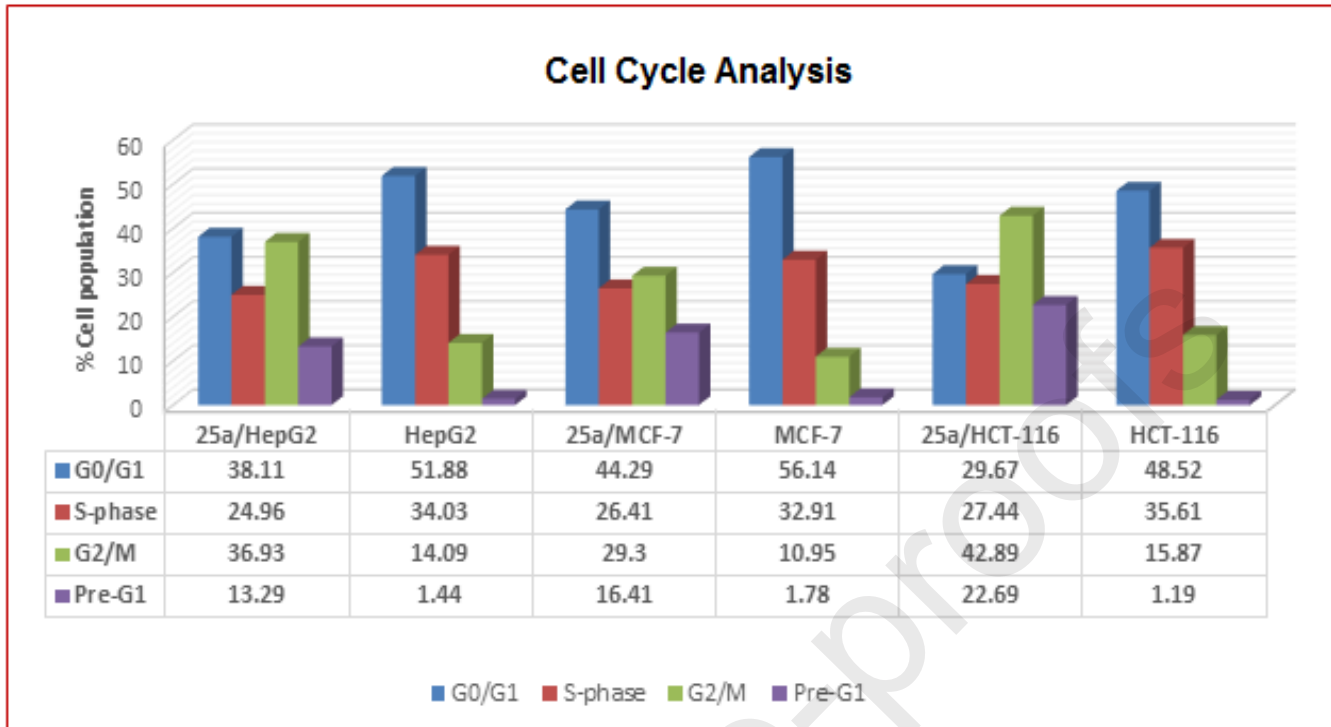


**Fig. 10.** Cell cycle distribution for HepG2, MCF-7 and HCT-116 cells treated with vehicle control and **25a** (at the  $IC_{50}$  of the corresponding cell line) for 24 h.

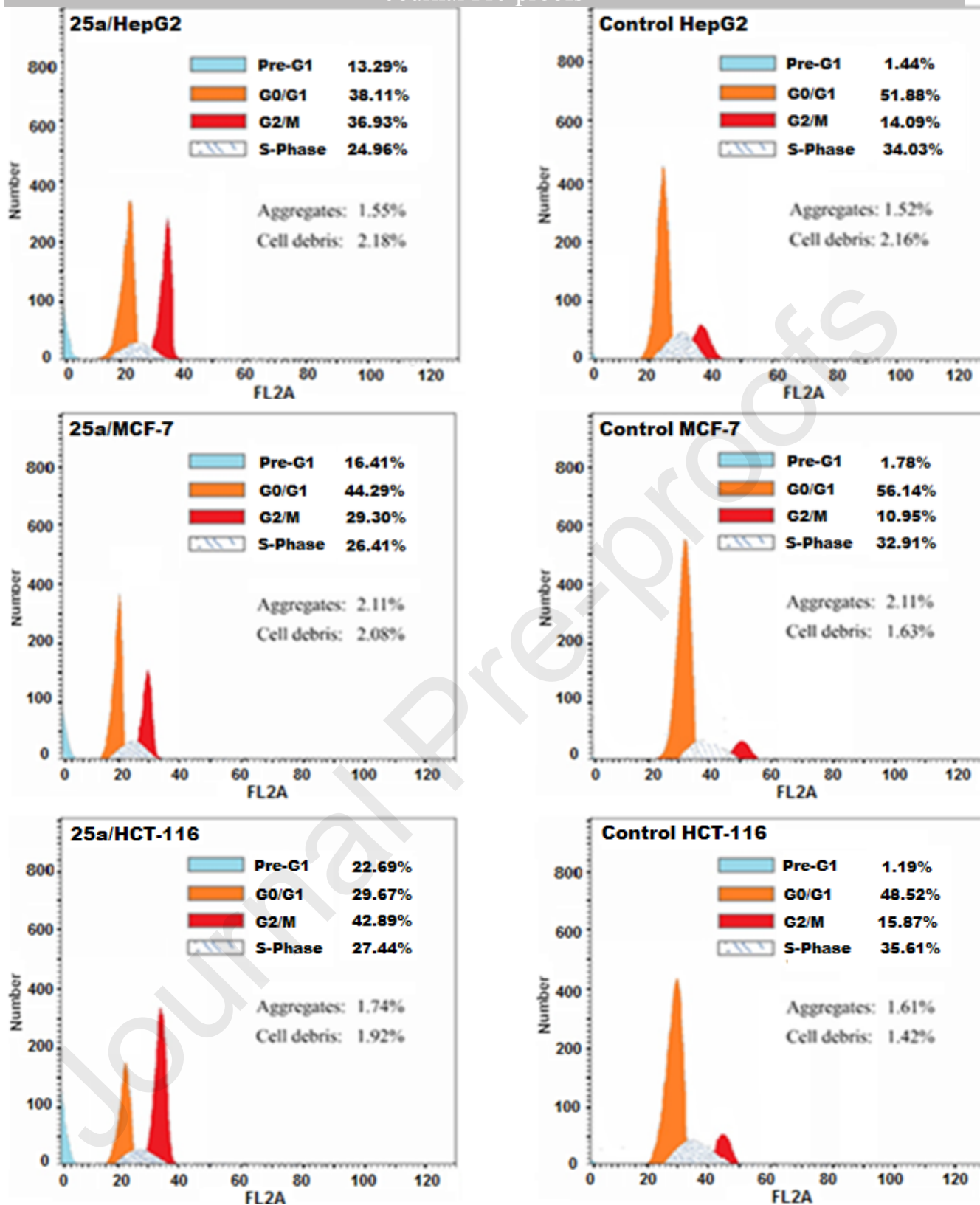


**Fig. 11.** Flow cytometry analysis of cell cycle distribution in HepG2, MCF-7 and HCT-116 cells after treatment with 25a (at the  $IC_{50}$  of the corresponding cell line) for 24 h.

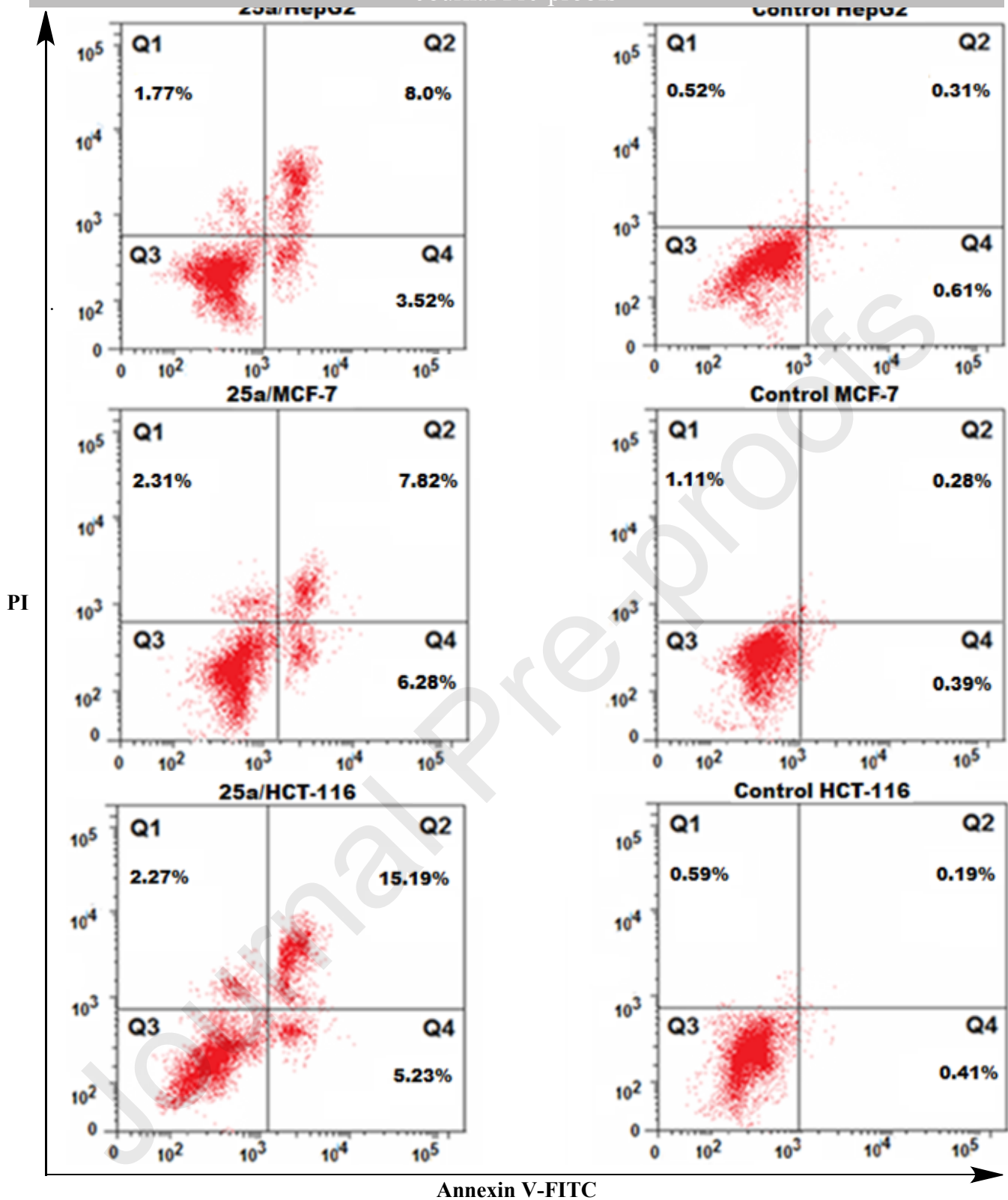


**Fig. 12.** Annexin V-FITC/PI double staining for analysis of apoptosis in HepG2, MCF-7 and HCT-116 cells after treatment with 25a (at the  $IC_{50}$  of the corresponding cell line) for 24 h. Q1 quadrant refers to necrotic cells; Q2 quadrant refers to late apoptosis; Q3 quadrant refers to live cells; Q4 quadrant refers to early apoptosis. Total apoptosis is the summation of early and late apoptosis.

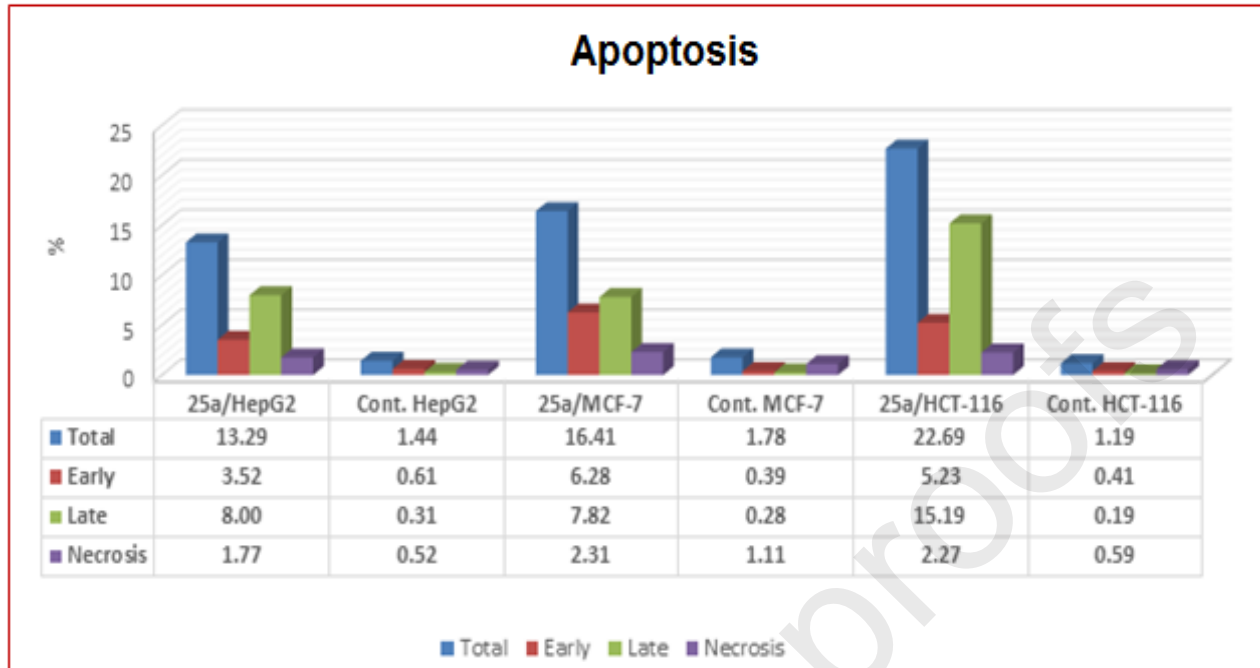


**Fig. 13.** Percentage apoptosis in HepG2, MCF-7 and HCT-116 cells after treatment with vehicle control and **25a** (at the  $IC_{50}$  of the corresponding cell line) for 24 h.

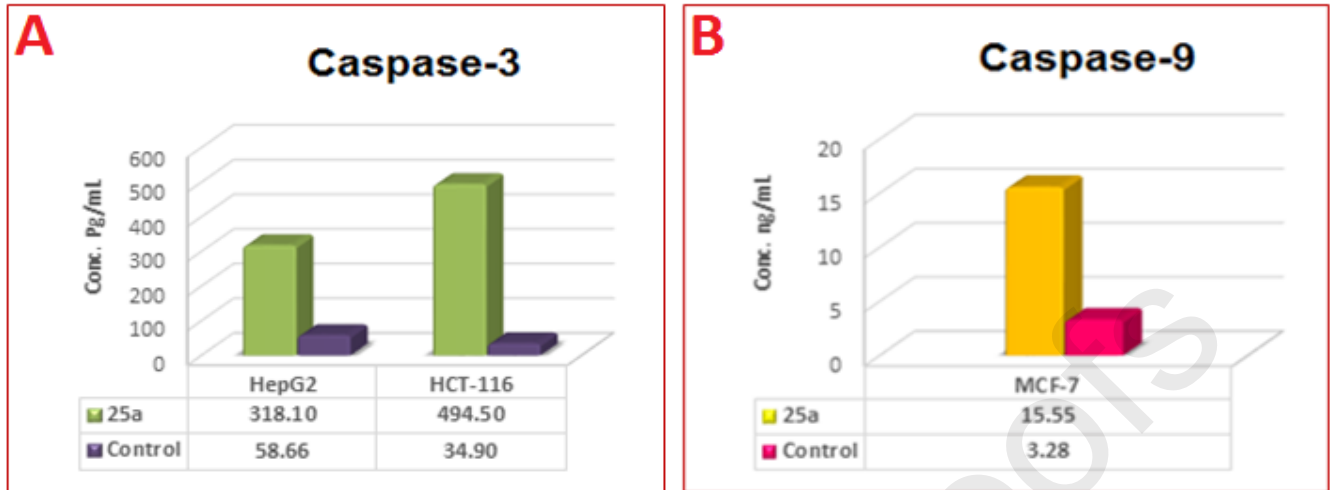


**Fig. 14. (A)** Level of caspase-3 in HepG2 and HCT-116 cells. **(B)** Level of caspase-9 in MCF-7 cells.

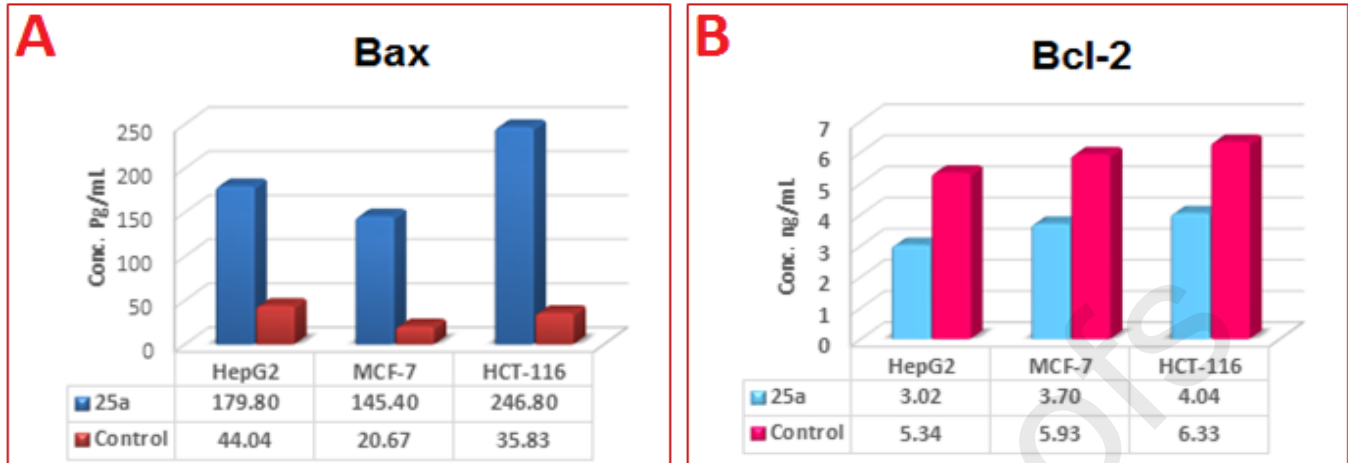


**Fig. 15. (A)** Level of Bax protein in HepG2, MCF-7 and HCT-116 cells. **(B)** Level of Bcl-2 protein in HepG2, MCF-7 and HCT-116 cells.

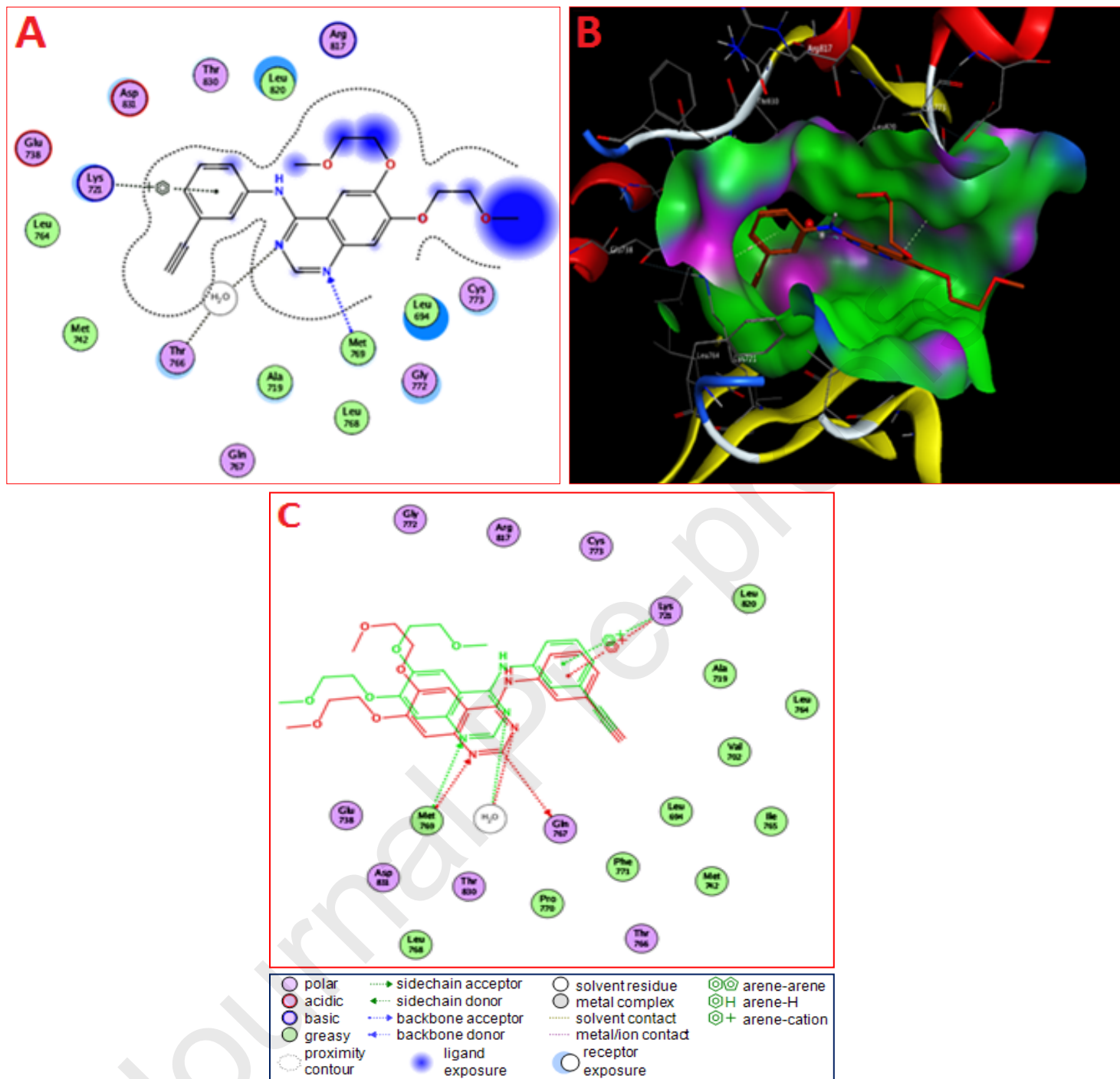


**Fig. 16.** (A) 2D Diagram illustrating erlotinib docking pose interactions with the hot spot amino acids in the active site of EGFR-TK. (B) 3D Diagram illustrating erlotinib docking pose interactions with the hot spot amino acids in the active site of EGFR-TK. Atoms are colored as following: carbon = orange, hydrogen = light gray, nitrogen = blue and oxygen = red. (C) 2D Representation of the superimposition of the co-crystallized erlotinib ligand (red) and the docking pose of erlotinib (green) in the active site of EGFR-TK. (PDB ID: 1M17).

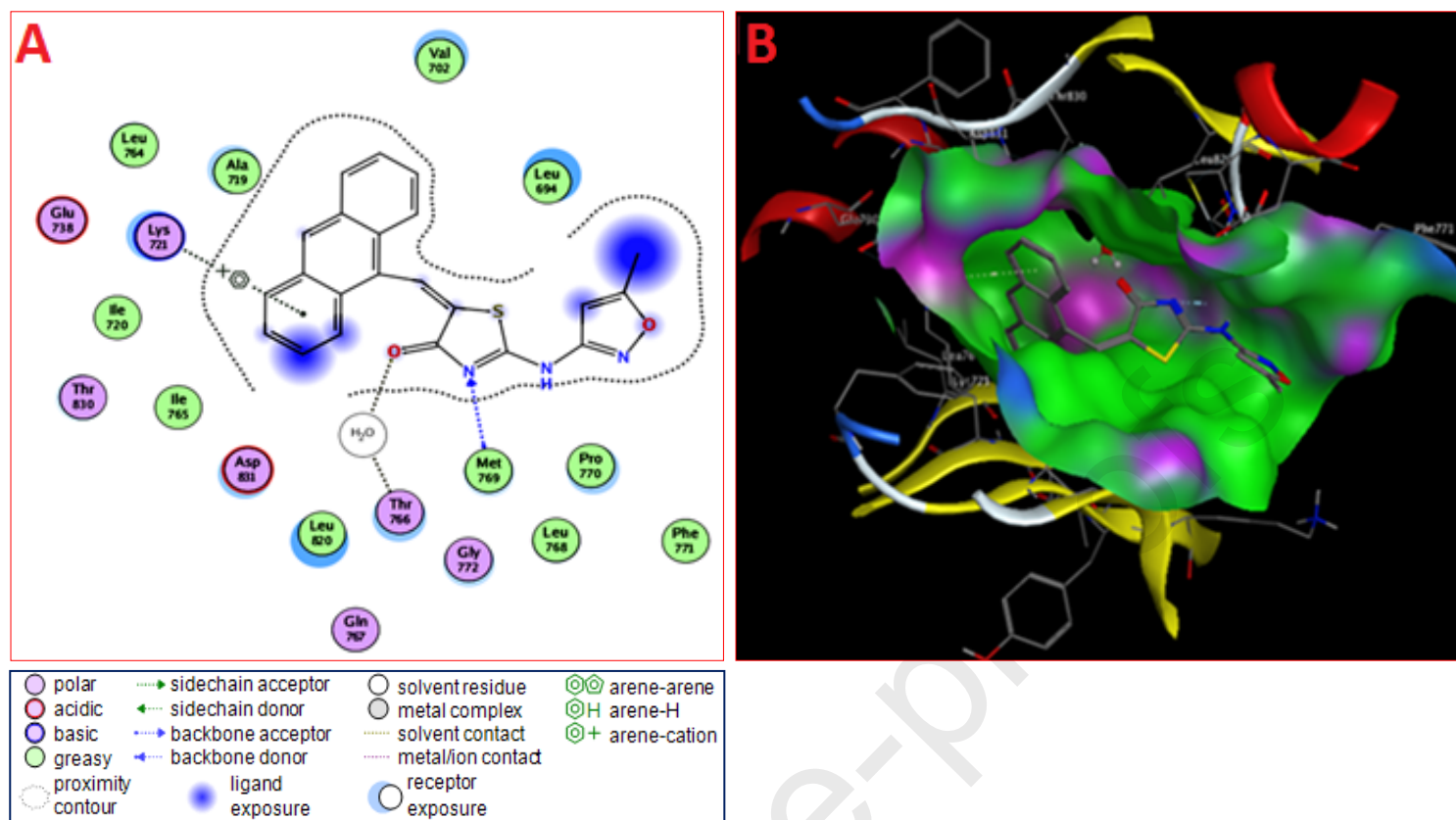


**Fig. 17.** (A) 2D Interaction of **25a** with the active site of EGFR-TK. (B) 3D Interaction of **25a** with the active site EGFR-TK. Atoms are colored as following: carbon = dark gray, hydrogen = light gray, nitrogen = blue, sulfur = yellow and oxygen = red. (PDB ID: 1M17).

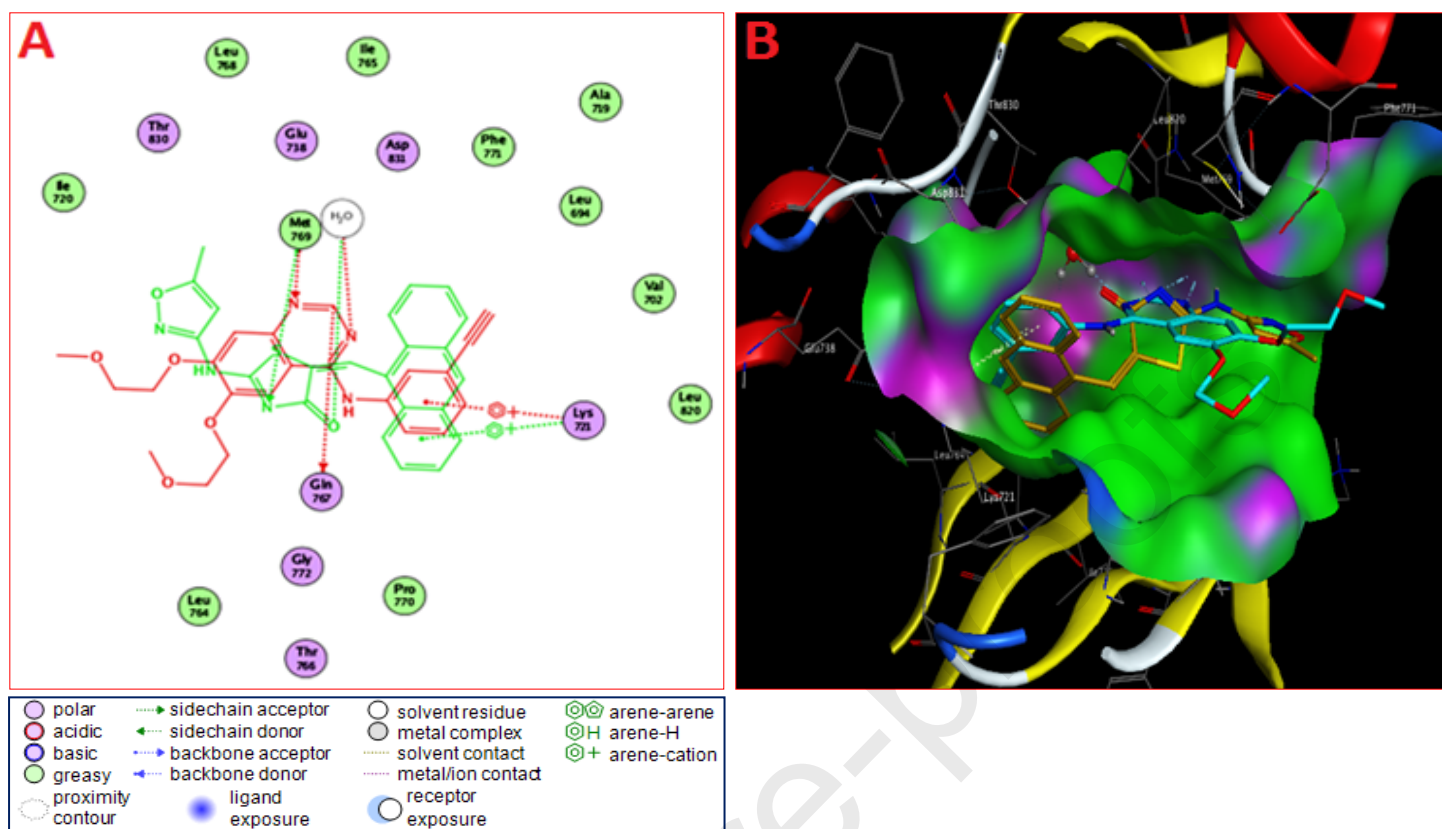


**Fig. 18.** (A) 2D Diagram of EGFR-TK-**25a** binding mode superposed on EGFR-TK-erlotinib complex. Erlotinib is colored red and **25a** is colored green. (B) 3D Diagram of EGFR-TK-**25a** binding mode superposed on EGFR-TK-erlotinib complex. Erlotinib is colored cyan and **25a** is colored yellow. (PDB ID: 1M17).

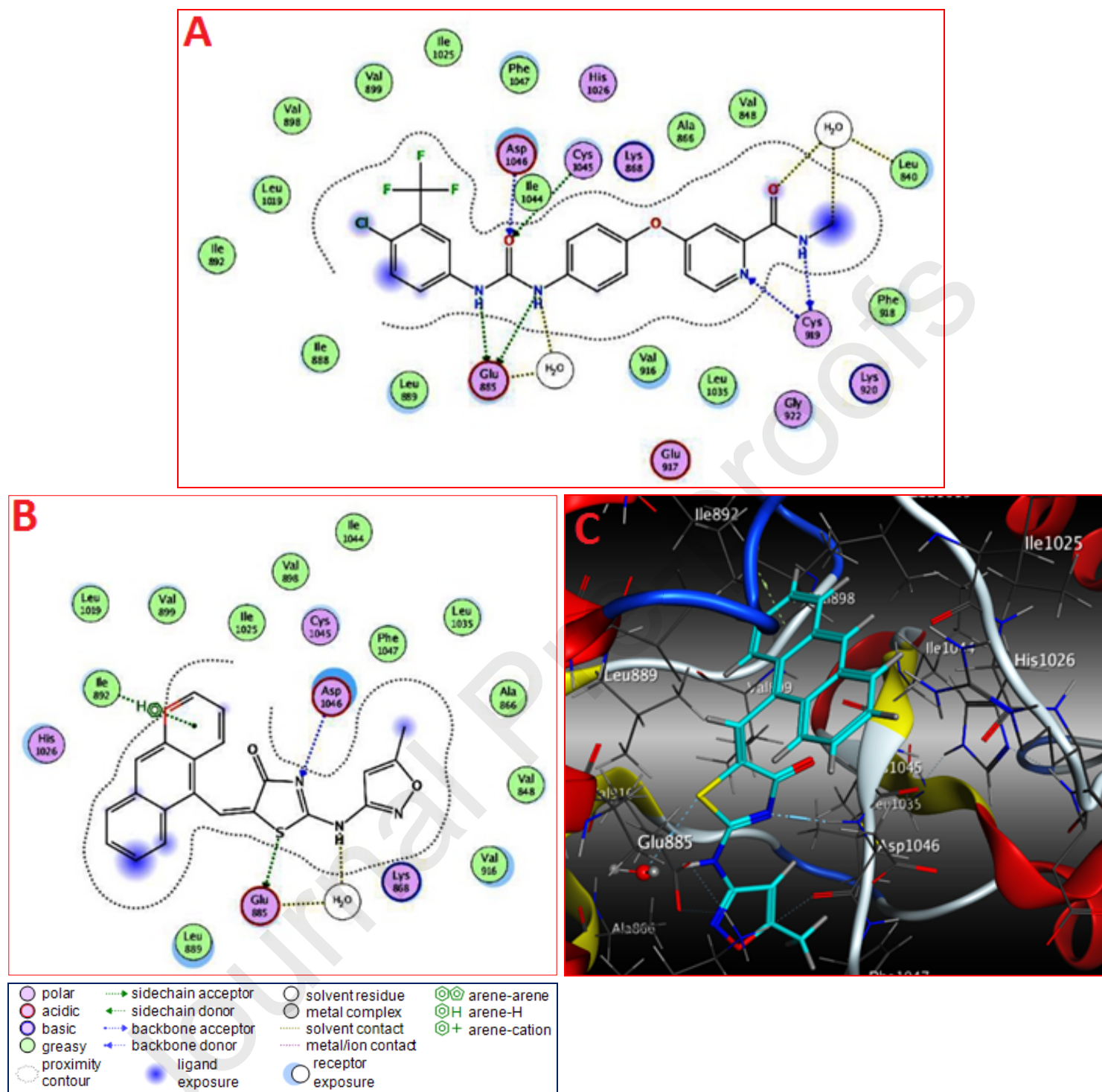


**Fig. 19.** (A) 2D Interaction of sorafenib with the active site of VEGFR-2. (B) 2D Interaction of **25a** with the active site of VEGFR-2. (C) 3D Interaction of **25a** with the active site of VEGFR-2. Atoms are colored as following: carbon = cyan, hydrogen = light gray, nitrogen = blue, sulfur = yellow and oxygen = red. (PDB ID: 4ASD).

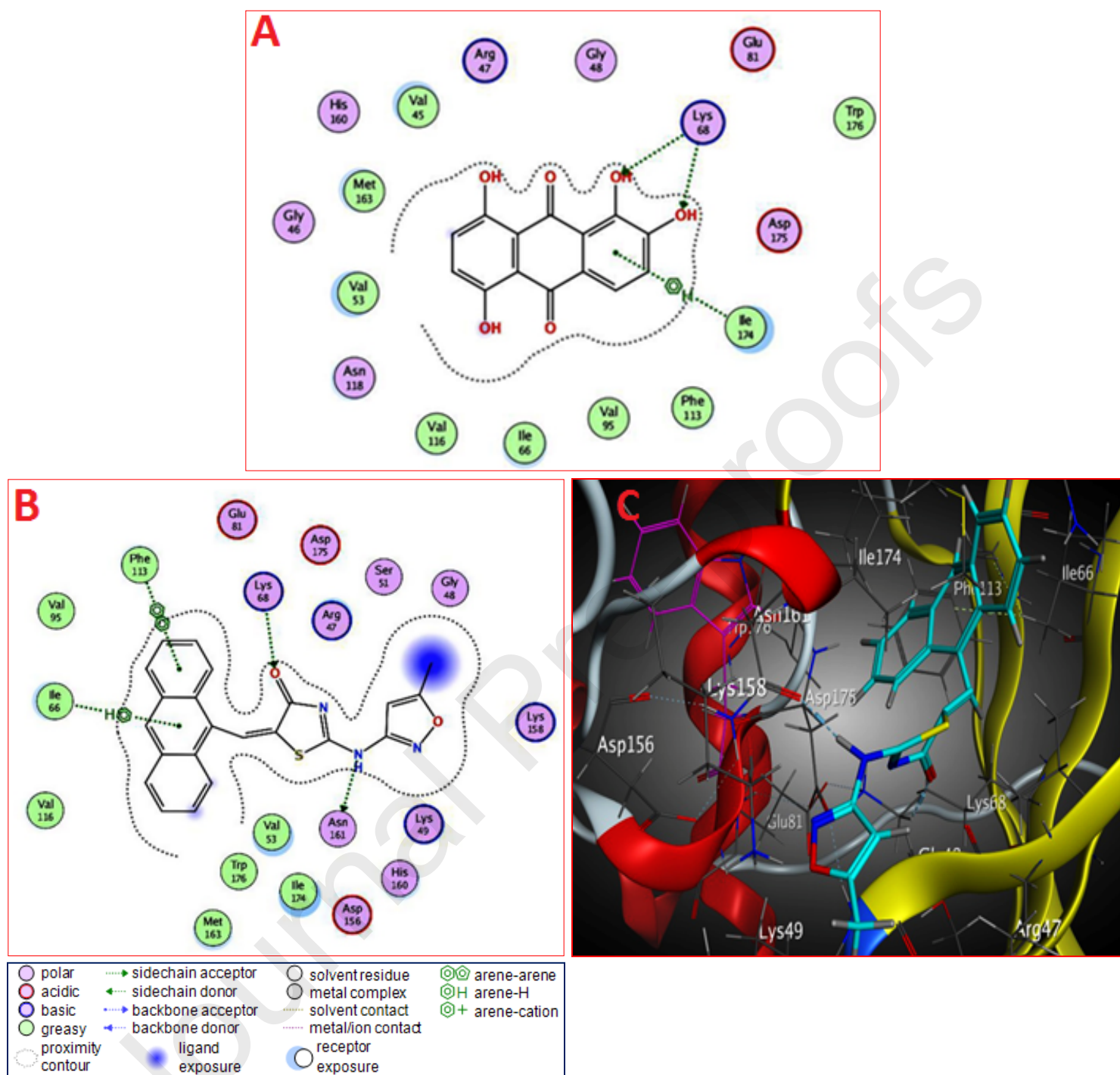
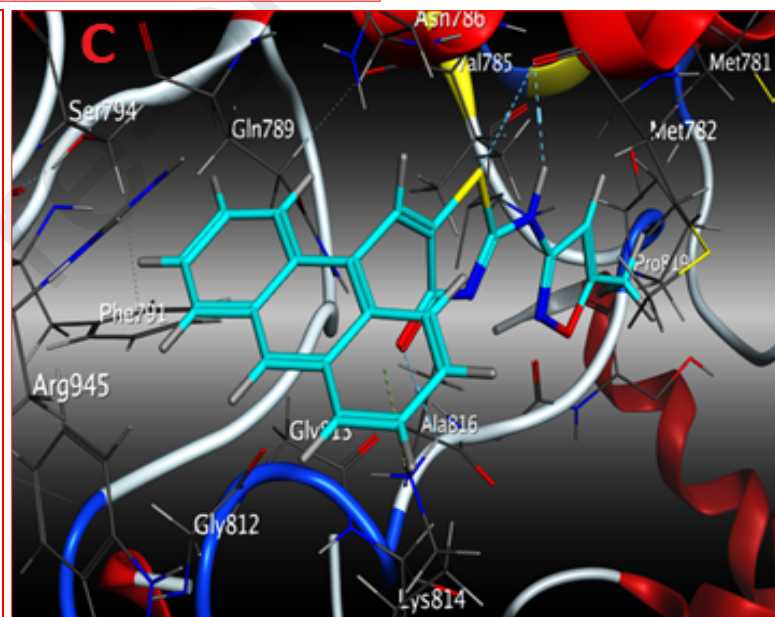
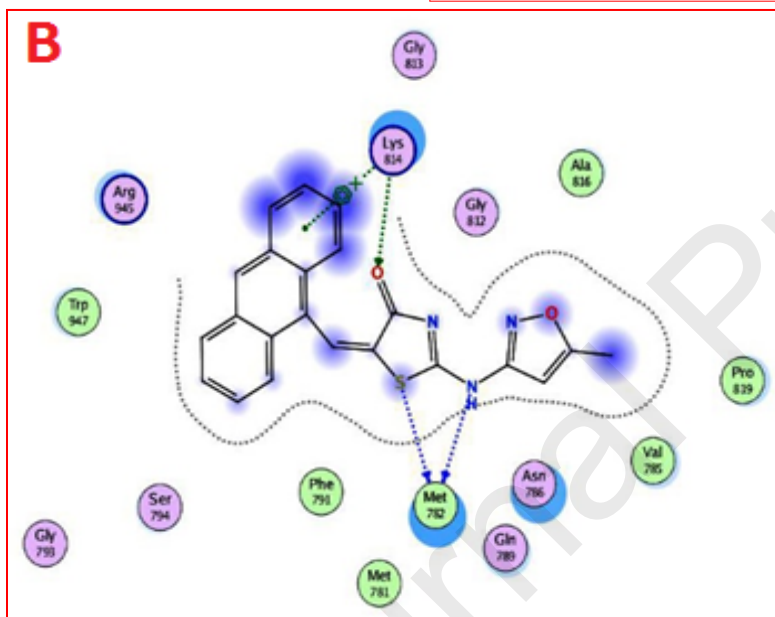
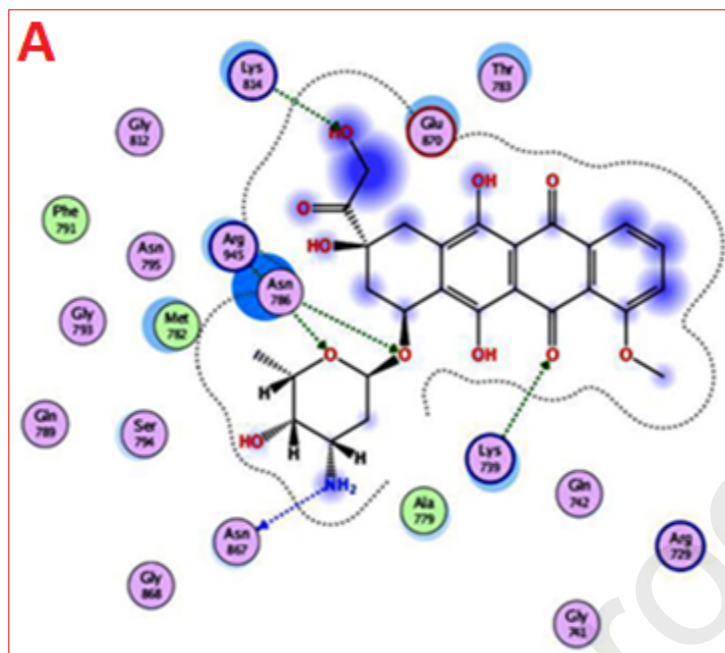


**Fig. 20.** (A) 2D Interaction of quinalizarin with the active site of CK2 $\alpha$ . (B) 2D Interaction of **25a** with the active site of CK2 $\alpha$ . (C) 3D Interaction of **25a** with the active site of CK2 $\alpha$ . Atoms are colored as following: carbon = cyan, hydrogen = light gray, nitrogen = blue, sulfur = yellow and oxygen = red. (PDB ID: 3FL5)



○ polar	→ sidechain acceptor	○ solvent residue	⊗⊗ arene-arene
○ acidic	← sidechain donor	○ metal complex	⊗H arene-H
○ basic	→ backbone acceptor	○ solvent contact	⊗+ arene-cation
○ greasy	← backbone donor	○ metal/ion contact	
○ proximity	○ ligand exposure	○ receptor	
○ contour		○ exposure	

**Fig. 21.** (A) 2D Interaction of doxorubicin with the active site of topoisomerase II $\beta$ . (B) 2D Interaction of **25a** with the active site of topoisomerase II $\beta$ . (C) 3D Interaction of **25a** with the active site of topoisomerase II $\beta$ . Atoms are colored as following: carbon = cyan, hydrogen = light gray, nitrogen = blue, sulfur = yellow and oxygen = red. (PDB ID: 3QX3).

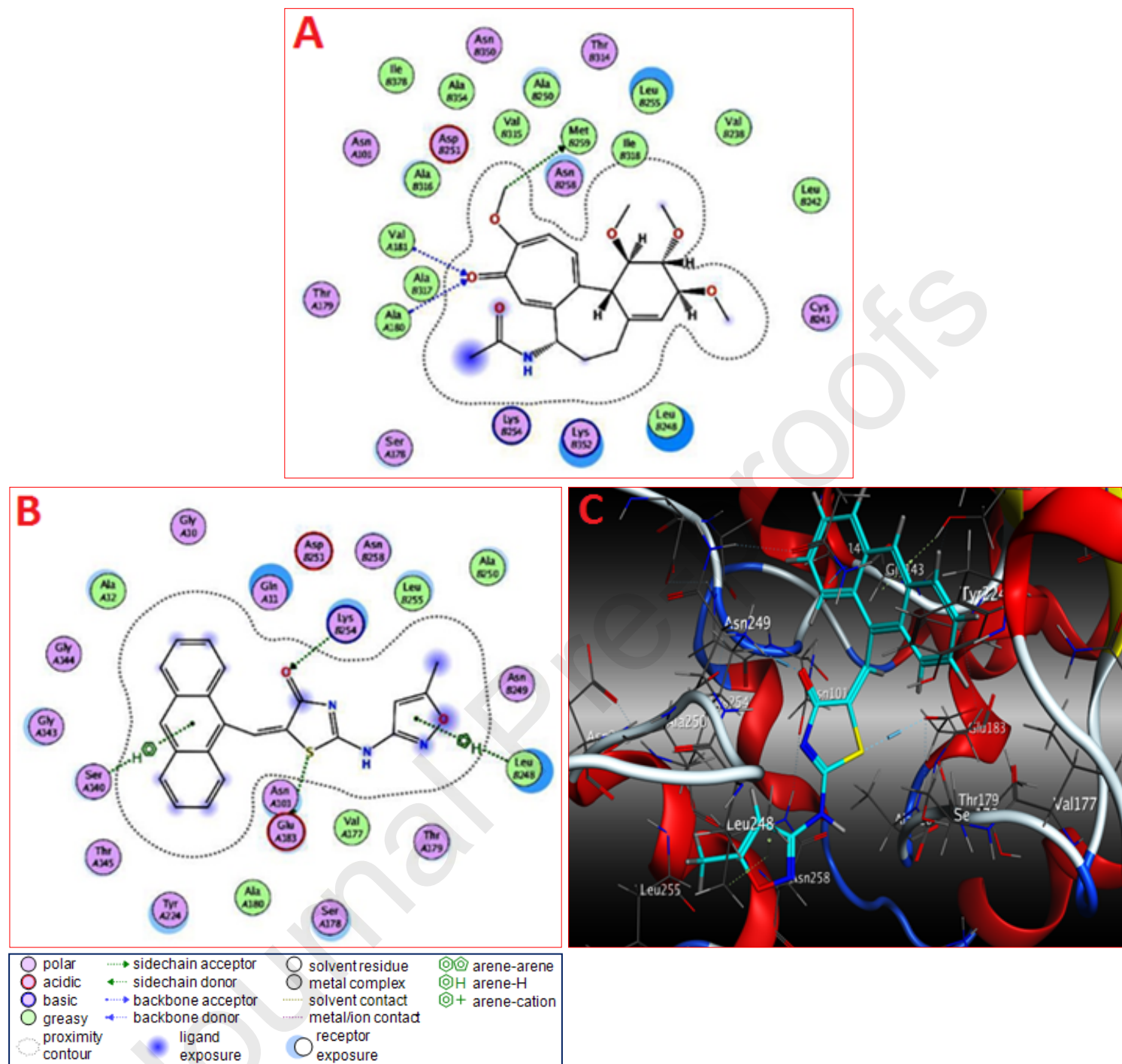


**Fig. 22.** (A) 2D Interaction of colchicine with colchicine binding site of tubulin. (B) 2D Interaction of **25a** with the colchicine binding site of tubulin. (C) 3D Interaction of **25a** with the colchicine binding site of tubulin. Atoms are colored as following: carbon = cyan, hydrogen = light gray, nitrogen = blue, sulfur = yellow and oxygen = red. (PDB code: 4O2B).

**Table 1.** *In vitro* antitumor activity of the new compounds.

Comp. No.	IC <sub>50</sub> (μM) <sup>a</sup>			Comp. No.	IC <sub>50</sub> (μM) <sup>a</sup>		
	HepG2	MCF-7	HCT-116		HepG2	MCF-7	HCT-116
<b>2a</b>	>100.00	>100.00	>100.00	<b>14b</b>	83.01±4.6	55.37±3.4	85.22±4.4
<b>2b</b>	>100.00	88.30±4.8	>100.00	<b>15a</b>	51.78±3.5	29.08±2.3	46.13±3.0
<b>3a</b>	>100.00	>100.00	>100.00	<b>15b</b>	37.15±2.6	22.96±1.7	33.59±2.4
<b>3b</b>	90.37±4.9	64.94±3.8	>100.00	<b>16a</b>	23.81±1.8	<b>14.81±1.2</b>	<b>20.81±1.6</b>
<b>4a</b>	<b>11.10±1.1</b>	<b>10.39±0.9</b>	<b>13.07±1.3</b>	<b>16b</b>	<b>18.27±1.4</b>	<b>9.42±0.8</b>	<b>11.48±1.0</b>
<b>4b</b>	<b>9.74±0.8</b>	<b>7.15±0.6</b>	<b>9.96±0.7</b>	<b>17a</b>	41.59±2.8	30.28±2.5	58.27±3.3
<b>5a</b>	61.95±3.8	48.87±3.3	75.32±4.0	<b>17b</b>	68.23±4.1	42.90±2.8	66.65±3.7
<b>5b</b>	74.79±4.4	59.81±3.7	92.59±5.1	<b>18a</b>	32.83±2.3	24.17±1.9	36.60±2.5
<b>6a</b>	>100.00	81.75±4.7	>100.00	<b>18b</b>	>100.00	>100.00	>100.00
<b>6b</b>	25.02±1.9	<b>19.63±1.5</b>	28.04±2.2	<b>19a</b>	>100.00	>100.00	>100.00
<b>7a</b>	63.48±3.9	65.07±3.9	88.16±4.7	<b>19b</b>	55.39±3.6	39.56±2.7	51.30±3.1
<b>7b</b>	65.27±4.0	56.16±3.5	80.11±4.3	<b>20a</b>	87.78±4.8	68.74±4.0	95.03±5.5
<b>8a</b>	<b>19.49±1.6</b>	<b>12.62±1.0</b>	<b>17.63±1.4</b>	<b>20b</b>	48.23±3.2	36.10±2.6	64.41±3.5
<b>8b</b>	39.14±2.6	27.05±2.1	38.38±2.7	<b>21a</b>	45.19±3.1	37.73±2.7	40.56±2.9
<b>9a</b>	50.27±3.4	44.83±2.9	73.15±3.9	<b>21b</b>	43.78±3.0	32.49±2.6	62.79±3.4
<b>9b</b>	57.11±3.8	47.85±3.2	78.37±4.1	<b>22a</b>	31.12±2.2	21.45±1.6	31.76±2.3
<b>10a</b>	35.04±2.4	<b>16.70±1.3</b>	26.24±2.0	<b>22b</b>	91.56±5.2	70.58±4.2	>100.00
<b>10b</b>	28.36±2.1	<b>17.16±1.4</b>	24.66±1.8	<b>23a</b>	>100.00	>100.00	>100.00
<b>11a</b>	71.54±4.3	51.92±3.2	89.61±4.9	<b>23b</b>	84.65±4.7	59.33±3.6	86.36±4.5
<b>11b</b>	93.46±5.3	78.16±4.5	>100.00	<b>24a</b>	>100.00	>100.00	>100.00
<b>12a</b>	56.72±3.5	44.16±3.0	75.81±4.2	<b>24b</b>	79.22±4.5	67.59±3.9	94.19±5.2
<b>12b</b>	>100.00	74.62±4.3	>100.00	<b>25a</b>	<b>6.86±0.5</b>	<b>6.38±0.4</b>	<b>7.72±0.5</b>
<b>13a</b>	52.20±3.4	45.68±3.0	69.01±3.7	<b>Doxorubicin</b>	4.50±0.2	4.17±0.2	5.23±0.3
<b>13b</b>	76.38±4.5	61.32±3.7	91.17±5.1	<b>Erlotinib</b>	8.19±0.4	4.16±0.2	11.21±0.6
<b>14a</b>	89.37±4.9	92.16±4.9	>100.00	----	----	----	----

<sup>a</sup>IC<sub>50</sub> (μM): 1-10 (very strong), 11-20 (strong), 21-50 (moderate), 51-100 (weak), > 100 (inactive).  
Bold values point to the best results.

**Table 2.** EGFR-TK inhibitory activity of the most active antitumor analogs.

Comp. No.	IC <sub>50</sub> (μM)
	EGFR-TK
<b>4a</b>	<b>0.106±0.002</b>
<b>4b</b>	0.124±0.004
<b>6b</b>	0.144±0.003
<b>8a</b>	<b>0.081±0.002</b>
<b>10a</b>	<b>0.064±0.001</b>
<b>10b</b>	<b>0.066±0.001</b>
<b>16a</b>	<b>0.081±0.002</b>
<b>16b</b>	0.150±0.003
<b>25a</b>	<b>0.054±0.001</b>
<b>Erlotinib</b>	0.067±0.001

Bold values point to the best results.

**Table 3.** VEGFR-2, CK2, topoisomerase II $\beta$  and tubulin polymerization inhibitory activities of compound **25a**.

Comp. No.	IC <sub>50</sub> ( $\mu$ M)			
	VEGFR-2	CK2	Topoisomerase II $\beta$	Tubulin
<b>25a</b>	<b>0.087<math>\pm</math>0.003</b>	0.171 $\pm$ 0.005	<b>0.13<math>\pm</math>0.001</b>	3.61 $\pm$ 0.06
<b>Quinalizarin</b>	-----	0.11 $\pm$ 0.003	-----	-----
<b>Sorafenib</b>	0.08 $\pm$ 0.002	-----	-----	-----
<b>Doxorubicin</b>	-----	-----	0.727 $\pm$ 0.005	-----
<b>Colchicine</b>	-----	-----	-----	1.28 $\pm$ 0.03

Bold values point to the best results.

**Table 4.** Summary of residues involved in arene-cation, arene-H and arene-arene interactions, number of hydrogen bonds, residues involved in hydrogen bonding interaction and docking energy score (kcal/mol) of compound **25a** with EGFR-TK, VEGFR-2, CK2, topoisomerase II $\beta$  and tubulin.

Biological target	Residues involved in arene-cation, arene-H and arene-arene interactions	No. of H-bonds	Residues involved in H-bonding interaction	Docking energy score (kcal/mol)
EGFR-TK	Lys721 <sup>a</sup>	2	Met769, Thr766	-10.80
VEGFR-2	Ile892 <sup>b</sup>	3	Asp1046, Glu885	-13.73
CK2	Ile66 <sup>b</sup> , Phe113 <sup>c</sup>	2	Asn161, Lys68	-6.21
Topoisomerase II $\beta$	Lys814 <sup>a</sup>	3	Met782, Lys814	-5.86
Tubulin	SerA140 <sup>b</sup> , LeuB248 <sup>b</sup>	2	LysB254, GluA183	-7.35

<sup>a</sup> arene-cation interaction.

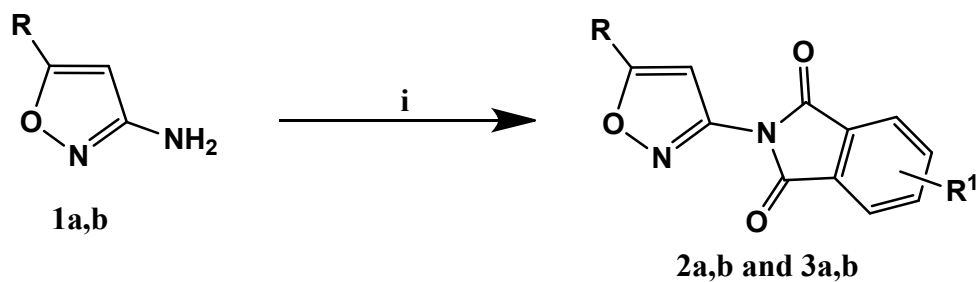
<sup>b</sup> arene-H interaction.

<sup>c</sup> arene-arene interaction.

**Table 5.** TPSA, Nrotb and calculated Lipinski's rule for compounds **2-25**.

Comp. No.	Molecular properties						No. of violations
	TPSA <sup>a</sup>	Nrotb <sup>b</sup>	miLogP <sup>c</sup>	nOH-NH <sup>d</sup>	nO-N <sup>e</sup>	M. wt.	
2a	65.11	1	3.90	0	5	365.99	0
2b	65.11	2	5.62	0	5	408.07	1
3a	65.11	1	4.42	0	5	543.79	1
3b	65.11	2	6.14	0	5	585.87	2
4a	55.13	2	0.55	1	4	174.59	0
4b	55.13	3	2.27	1	4	216.67	0
5a	55.13	3	0.82	1	4	188.61	0
5b	55.13	4	2.55	1	4	230.69	0
6a	67.60	3	0.19	1	6	225.25	0
6b	67.60	4	1.91	1	6	267.33	0
7a	61.61	3	0.23	1	6	238.29	0
7b	61.61	4	1.96	1	6	280.37	0
8a	61.61	4	0.61	1	6	252.32	0
8b	61.61	5	2.33	1	6	294.40	0
9a	61.61	5	1.63	1	6	314.39	0
9b	61.61	6	3.36	1	6	356.47	0
10a	61.61	4	1.93	1	6	300.36	0
10b	61.61	5	3.66	1	6	342.44	0
11a	67.60	4	0.09	1	6	239.28	0
11b	67.60	5	1.82	1	6	281.36	0
12a	61.61	4	0.14	1	6	252.32	0
12b	61.61	5	1.86	1	6	294.40	0
13a	61.61	5	0.51	1	6	266.35	0
13b	61.61	6	2.24	1	6	308.43	0
14a	61.61	6	1.54	1	6	328.42	0
14b	61.61	7	3.26	1	6	370.50	0
15a	61.61	5	1.83	1	6	314.39	0
15b	61.61	6	3.56	1	6	356.47	0
16a	67.49	2	0.24	1	5	197.22	0
16b	67.49	3	1.97	1	5	239.30	0
17a	81.16	3	2.24	1	6	275.29	0
17b	81.16	4	3.96	1	6	317.37	0
18a	68.02	3	3.81	1	5	370.25	0
18b	68.02	4	5.54	1	5	412.33	1
19a	68.02	3	3.43	1	5	299.36	0
19b	68.02	4	5.15	1	5	341.44	1
20a	68.02	3	3.79	1	5	364.22	0
20b	68.02	4	5.51	1	5	406.31	1
21a	68.02	3	4.26	1	5	354.22	0
21b	68.02	4	5.99	1	5	396.30	1
22a	68.02	3	3.73	1	5	337.76	0
22b	68.02	4	5.45	1	5	379.84	1
23a	68.02	4	4.78	1	5	361.43	0
23b	68.02	5	6.50	1	5	403.51	1
24a	68.02	3	4.16	1	5	335.39	0
24b	68.02	4	5.89	1	5	377.47	1
25a	68.02	3	5.28	1	5	385.45	1
<b>Doxorubicin</b>	206.08	5	0.57	7	12	543.52	3
<b>Erlotinib</b>	74.75	10	2.79	1	7	393.44	0

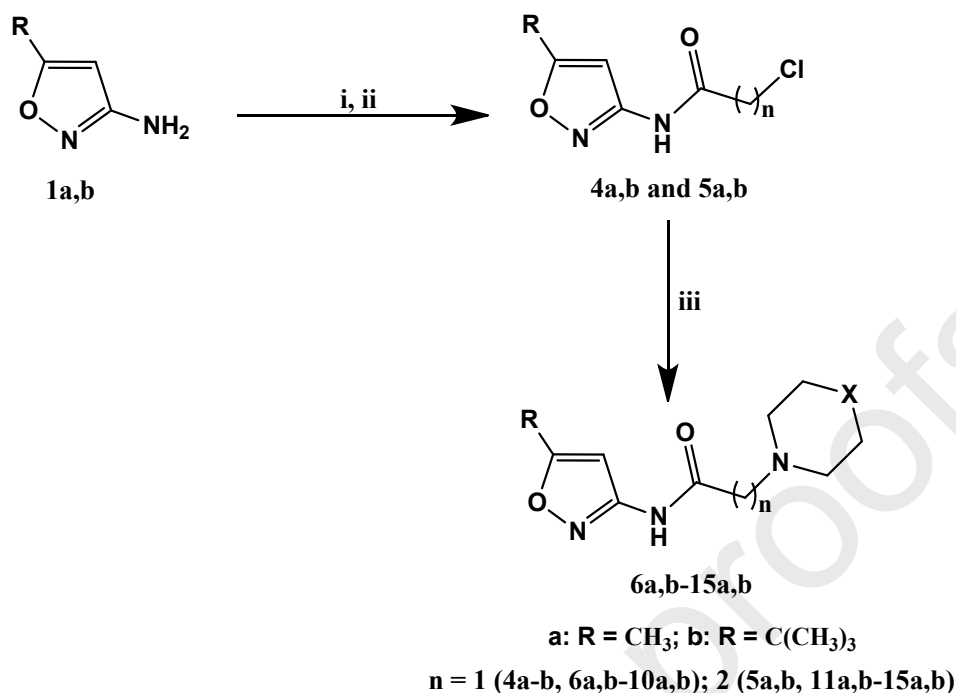
<sup>a</sup>TPSA: Topological polar surface area, <sup>b</sup>Nrotb: Number of rotatable bonds, <sup>c</sup>miLogP: Parameter of lipophilicity, <sup>d</sup>nOH-NH: Number of hydrogen bond donor sites, <sup>e</sup>nO-N: Number of hydrogen bond acceptor sites.



Comp. No.	R	R <sup>1</sup>
2a	CH <sub>3</sub>	4,5,6,7-(Cl) <sub>4</sub>
2b	C(CH <sub>3</sub> ) <sub>3</sub>	4,5,6,7-(Cl) <sub>4</sub>
3a	CH <sub>3</sub>	4,5,6,7-(Br) <sub>4</sub>
3b	C(CH <sub>3</sub> ) <sub>3</sub>	4,5,6,7-(Br) <sub>4</sub>

**Reagents, conditions and yields: i) 4,5,6,7-Tetrachloro/tetrabromophthalic anhydride, Glacial acetic acid, 100 °C, 20-30 min, 42-65%.**

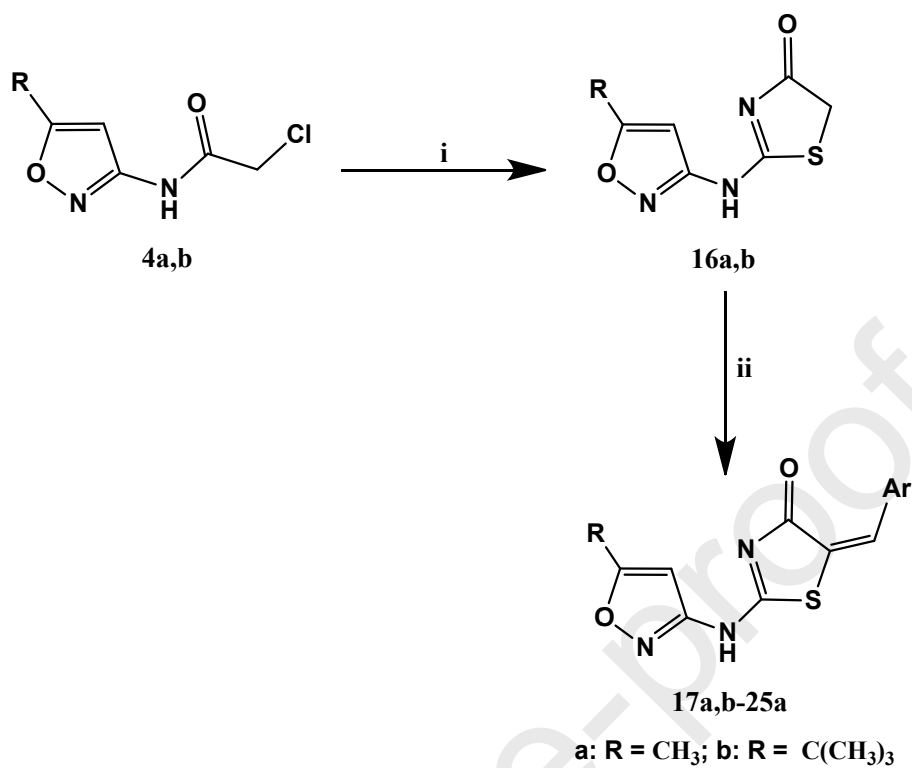
**Scheme 1. Synthesis of compounds 2a,b and 3a,b.**



Comp. No.	X	Comp. No.	X	Comp. No.	X
6a	O	9b		13a	
6b	O	10a		13b	
7a	N-CH <sub>3</sub>	10b		14a	
7b	N-CH <sub>3</sub>	11a	O	14b	
8a		11b	O	15a	
8b		12a	N-CH <sub>3</sub>	15b	
9a		12b	N-CH <sub>3</sub>	-----	-----

**Reagents, conditions and yields:** i) Chloroacetyl chloride, TEA, Chloroform, rt, 2-4 h, 60-65% (for **4a,b**), ii) Chloropropionyl chloride, anhydrous K<sub>2</sub>CO<sub>3</sub>, Toluene, rt, 2-4 h, 60-65% (for **5a,b**), iii) Morpholine or substituted piperazines, TEA, Toluene, reflux, 15-24 h, 40-75%.

**Scheme 2.** Synthesis of compounds **4a,b-15a,b**.



Comp. No.	Ar	Comp. No.	Ar	Comp. No.	Ar
17a		20a		23a	
17b		20b		23b	
18a		21a		24a	
18b		21b		24b	
19a		22a		25a	
19b		22b		-----	-----

**Reagents, conditions and yields:** i) Ammonium thiocyanate, Absolute ethanol, reflux, 3-5 h, 60-75%, ii) Araldehyde, Aqueous 10% NaOH, Absolute ethanol, rt, 24 h, 50-92%.

**Scheme 3.** Synthesis of compounds 16a,b-25a.

## References

- [1] T. Holbro, N.E. Hynes, ErbB receptors: Directing key signaling networks throughout life, *Annu Rev. Pharmacol. Toxicol.* 44 (2004) 195-217.
- [2] Y. Yarden, M.X. Sliwkowski, Untangling the ErbB signalling network, *Nat. Rev. Mol. Cell Biol.* 2 (2001) 127–137.
- [3] M. Höpfner, A.P. Sutter, A. Huether, D. Schuppan, M. Zeitz, H. Scherüb, Targeting the epidermal growth factor receptor by gefitinib for treatment of hepatocellular carcinoma, *J. Hepatol.* 41 (2005) 1008-1016.
- [4] D. Nguyen, S.X. Yang, Epidermal growth factor expression in breast cancer, *J. Clin. Oncol.* 23 (2005) 8118-8141.
- [5] J. Van der Veecken, S. Oliveira, R.M. Schiffelers, G. Storm, P.M. Henegouwen, R.C. Roovers, Crosstalk between epidermal growth factor receptor- and insulin-like growth factor-1 receptor signaling: Implications for cancer therapy, *Curr. Cancer Drug Targets* 9 (2009) 748-760.
- [6] R.I. Nicholson, J.M. Gee, M.E. Harper, EGFR and cancer prognosis, *Eur. J. Cancer* 37 (2001) S9–S15.
- [7] J. Mendelsohn, J. Baselga, Status of epidermal growth factor receptor antagonists in the biology and treatment of cancer, *J. Clin. Oncol.* 21 (2003) 2787–2799.
- [8] X.H. Ma, R. Wang, C.Y. Tan, Y. Jiang, T. Lu, H.B. Rao, X.Y. Li, M.L. Go, B.C. Low, Y.Z. Chen, Virtual screening of selective multitarget kinase inhibitors by combinatorial support vector machines, *Mol. Pharm.* 7 (2010) 1545-1560.
- [9] D.H. Boschelli, Small molecule inhibitors of receptor tyrosine kinases, *Drug Future* 24 (1999) 515-537.
- [10] S.L. Greig, Osimertinib: First Global Approval, *Drugs* 76 (2016) 263–273.
- [11] J.C. Chuang, A.A. Salahudeen, H.A. Wakelee, Rociletinib, a third generation EGFR tyrosine kinase inhibitor: Current data and future directions, *Expert Opin. Pharmacother.* 17 (2016) 989-993.
- [12] Y. Sakuma, Y. Yamazaki, Y. Nakamura, M. Yoshihara, S. Matsukuma, H. Nakayama, T. Yokose, Y. Kameda, S. Koizume, Y. Miyagi, WZ4002, a third-generation EGFR inhibitor, can overcome anoikis resistance in EGFR-mutant lung adenocarcinomas more efficiently than Src inhibitors, *Lab. Invest.* 92 (2012) 371-383.

- [13] J. Yong, C. Lu, X. Wu, Synthesis and preliminarily cytotoxicity to A549, HCT 116 and MCF-7 cell lines of thieno[2,3-*d*]pyrimidine derivatives containing isoxazole moiety, *Lett. Drug Des. Discov.* 15 (2018) 463-474.
- [14] D. Im, K. Jung, S. Yang, W. Aman, J. Hah, Discovery of 4-arylamido-3-methylisoxazole derivatives as novel FMS kinase inhibitors, *Eur. J. Med. Chem.* 102 (2015) 600-610.
- [15] J.N. Philoppes, P.F. Lamie, Design and synthesis of new benzoxazole/benzothiazole-phthalimide hybrids as antitumor-apoptotic agents, *Bioorg. Chem.* 89 (2019) 102978, DOI: [10.1016/j.bioorg.2019.102978](https://doi.org/10.1016/j.bioorg.2019.102978).
- [16] Y. Li, C. Gao, C. Zhang, X. Luan, X. Chen, H. Liu, Y. Chen, Y. Jiang, Discovery of benzimidazole derivatives as novel multi-target EGFR, VEGFR-2 and PDGFR kinase inhibitors, *Bioorg. Med. Chem.* 19 (2011) 4529-4535.
- [17] H.A. Abd El Razik, M. Mroueh, W.H. Faour, W.N. Shebaby, C.F. Daher, H.M.A. Ashour, H.M. Ragab, Synthesis of new pyrazolo[3,4-*d*]pyrimidine derivatives and evaluation of their anti-inflammatory and anticancer activities, *Chem. Biol. Drug Des.* 90 (2017) 83-96.
- [18] H.S. Abbas, S.S. Abd El-Karim, Design, synthesis and anticervical cancer activity of new benzofuran-pyrazol-hydrazono-thiazolidin-4-one hybrids as potential EGFR inhibitors and apoptosis inducing agents, *Bioorg. Chem.* 89 (2019) 103035, DOI: [10.1016/j.bioorg.2019.103035](https://doi.org/10.1016/j.bioorg.2019.103035).
- [19] K.R. Abdellatif, E.K.A. Abdelall, M.A. Abdelgawad, M.M. Abdelhakeem, H.A. Omar, Design and synthesis of certain novel arylidene thiazolidinone derivatives as anticancer agents, *Der Pharma Chem.* 7 (2015) 149-161.
- [20] D. Liang, Z. Su, W. Tian, J. Li, Z. Li, C. Wang, D. Li, H. Hou, Synthesis and screening of novel anthraquinone-quinazoline multitarget hybrids as promising anticancer candidates, *Future Med. Chem.* 12 (2020) 111-126.
- [21] B. Kolundzija, V. Markovic', T. Stanojkovic', L. Joksovic', I. Matic', N. Todorovic', M. Nikolic', M.D. Joksovic, Novel anthraquinone based chalcone analogues containing an imine fragment: Synthesis, cytotoxicity and anti-angiogenic activity, *Bioorg. Med. Chem. Lett.* 24 (2014) 65-71.
- [22] S. Haidar, A. Meyers, A. Bollacke, J. Jose, Synthesis and biological evaluation of 2,6-di(furan-3-yl)anthracene-9,10-dione as an inhibitor of human protein kinase CK2, *Pharmazie* 70 (2015) 772-776.

- [23] Y. Zhou, K. Li, S. Zhang, Q. Li, Z. Li, F. Zhou, X. Dong, L. Liu, G. Wu, R. Meng, Quinalizarin, a specific CK2 inhibitor, reduces cell viability and suppresses migration and accelerates apoptosis in different human lung cancer cell lines, *Indian J. Cancer* 52 (2015) 119-124.
- [24] P.J. Smith, N.J. Blunt, R. Desnoyers, Y. Giles, L.H. Patterson, DNA topoisomerase II-dependent cytotoxicity of alkylaminoanthraquinones and their *N*-oxides, *Cancer Chemother. Pharmacol.* 39 (1997) 455-461.
- [25] H. Prinz, P. Schmidt, K.J. Böhm, S. Baasner, K. Müller, M. Gerlach, E.G. Günther, E. Unger, Phenylimino-10*H*-anthracen-9-ones as novel antimicrotubule agents-synthesis, antiproliferative activity and inhibition of tubulin polymerization, *Bioorg. Med. Chem.* 19 (2011) 4183-4191.
- [26] H.C. Nickel, P. Schmidt, K.J. Böhm, S. Baasner, K. Müller, M. Gerlach, E. Unger, E.G. Günther, H. Prinz, Synthesis, antiproliferative activity and inhibition of tubulin polymerization by 1,5- and 1,8-disubstituted 10*H*-anthracen-9-ones bearing a 10-benzylidene or 10-(2-oxo-2-phenylethylidene) moiety, *Eur. J. Med. Chem.* 45 (2010) 3420-3438.
- [27] Q.P. Qin, Y.C. Liu, H.L. Wang, J.L. Qin, F.J. Cheng, S.F. Tang, H. Liang, Synthesis and antitumor mechanisms of a copper(II) complex of anthracene-9-imidazoline hydrazone (9-AIH), *Metallomics* 7 (2015) 1124-1136.
- [28] N.M. Ahmed, M. Youns, M.K. Soltan, A.M. Said, Design, synthesis, molecular modelling, and biological evaluation of novel substituted pyrimidine derivatives as potential anticancer agents for hepatocellular carcinoma, *J. Enzyme Inhib. Med. Chem.* 34 (2019) 1110-1120.
- [29] U. De, P. Chun, W.S. Choi, B.M. Lee, N.D. Kim, H.R. Moon, J.H. Jung, H.S. Kim, A novel anthracene derivative, MHY412, induces apoptosis in doxorubicin-resistant MCF-7/Adr human breast cancer cells through cell cycle arrest and downregulation of P-glycoprotein expression, *Int. J. Oncol.* 44 (2014) 167-176.
- [30] S.-Q. Xie, Z.-Q. Zhang, G.-Q. Hu, M. Xu, B.-S. Ji, HL-37, A novel anthracene derivative, induces Ca<sup>2+</sup>-mediated apoptosis in human breast cancer cells, *Toxicology* 254 (2008) 68-74.
- [31] D. Fabbro, S. Ruetz, E. Buchdunger, S.W. Cowan-Jacob, G. Fendrich, J. Liebetanz, T. O'Reilley, P. Traxler, B. Chaudhari, H. Fretz, J. Zimmermann, T. Meyer, G. Carvatti, P.

- Furet, P.W. Manley, Protein kinases as targets for anticancer agents: From inhibitors to useful drugs, *Pharmacol. Ther.* 93 (2002) 79-98.
- [32] J. Zhang, P.L. Yang, N.S. Gray, Targeting cancer with small molecule kinase inhibitors, *Nat. Rev. Cancer* 9 (2009) 28-39.
- [33] Z. Zhao, H. Wu, L. Wang, Y. Liu, S. Knapp, Q. Liu, N.S. Gray, Exploration of type II binding mode: A privileged approach for kinase inhibitor focused drug discovery?, *ACS Chem. Biol.* 9 (2014) 1230-1241.
- [34] S. Mowafy, A. Galanis, Z.M. Doctor, R.M. Paranal, D.S. Lasheen, N.A. Farag, P.A. Jänne, K.A. Abouzid, Toward discovery of mutant EGFR inhibitors; Design, synthesis and *in vitro* biological evaluation of potent 4-arylamino-6-ureido and thioureido-quinazoline derivatives, *Bioorg. Med. Chem.* 24 (2016) 3501–3512.
- [35] P. Furet, G. Caravatti, N. Lydon, J.P. Priestle, J.M. Sowadski, U. Trinks, P. Traxler, Modelling study of protein kinase inhibitors: Binding mode of staurosporine and origin of the selectivity of CGP 52411, *J. Comput. Aided Mol. Des.* 9 (1995) 465-472.
- [36] V. Gandin, A. Ferrarese, M. Dalla Via, C. Marzano, A. Chilin, G. Marzaro, Targeting kinases with anilino-pyrimidines: Discovery of *N*-phenyl-*N*'-[4-(pyrimidin-4-ylamino)phenyl]urea derivatives as selective inhibitors of class III receptor tyrosine kinase subfamily, *Sci. Rep.* 5 (2015) 16750, DOI: [10.1038/srep16750](https://doi.org/10.1038/srep16750).
- [37] L.K. Gediya, V.C. Njar, Promise and challenges in drug discovery and development of hybrid anticancer drugs, *Expert Opin. Drug Discov.* 4 (2009) 1099-1111.
- [38] C.V. Junior, A. Danuello, V.dS. Bolzani, E.J. Barreiro, C.A.M. Fraga, Molecular hybridization: A useful tool in the design of new drug prototypes, *Curr. Med. Chem.* 14 (2007) 1829-1852.
- [39] J. Domarkas, F. Dudouit, C. Williams, Q. Qiyu, R. Banerjee, F. Brahim, B.J. Jean-Claude, The combi-targeting concept: Synthesis of stable nitrosoureas designed to inhibit the epidermal growth factor receptor (EGFR), *J. Med. Chem.* 49 (2006) 3544-3552.
- [40] E. Proschak, H. Stark, D. Merk, Polypharmacology by design: A medicinal chemist's perspective on multitargeting compounds, *J. Med. Chem.* 62 (2019) 420–444.
- [41] D. Gerlier, T. Thomasset, Use of MTT colorimetric assay to measure cell activation, *J. Immunol. Methods* 94 (1986) 57-63.

- [42] F. Denizot, R. Lang, Rapid colorimetric assay for cell growth and survival. Modifications to the tetrazolium dye procedure giving improved sensitivity and reliability, *J. Immunol. Methods* 89 (1986) 271-277.
- [43] T. Mosmann, Rapid colorimetric assay for cellular growth and survival: Application to proliferation and cytotoxicity assays, *J. Immunol. Methods* 65 (1983) 55-63.
- [44] H. Ma, S. Deacon, K. Horiuchi, The challenge of selecting protein kinase assays for lead discovery optimization, *Expert Opin. Drug Discov.* 3 (2008) 607–621.
- [45] N.A. Smith, J.A. Byl, S.L. Mercer, J.E. Dewese, N. Osheroff, Etoposide quinone is a covalent poison of human topoisomerase II $\beta$ , *Biochemistry* 53 (2014) 3229-3236.
- [46] R.I. Ahmed, E.E.A. Osman, F.M. Awadallah, S.M. El-Moghazy, Design, synthesis and molecular docking of novel diarylcyclohexenone and diarylindazole derivatives as tubulin polymerization inhibitors, *J. Enzyme Inhib. Med. Chem.* 32 (2017) 176–188.
- [47] J.F. Díaz, J.M. Andreu, Assembly of purified GDP-tubulin into microtubules induced by taxol and taxotere: Reversibility, ligand stoichiometry, and competition, *Biochemistry* 32 (1993) 2747–2755.
- [48] M.A.I. Elbastawesy, A.A. Aly, M. Ramadan, Y.A.M.M. Elshaier, B.G.M. Youssif, A.B. Brown, G.E.D.A. Abuo-Rahma, Novel pyrazoloquinolin-2-ones: Design, synthesis, docking studies, and biological evaluation as antiproliferative EGFR-TK inhibitors, *Bioorg. Chem.* 90 (2019) 103045, DOI: [10.1016/j.bioorg.2019.103045](https://doi.org/10.1016/j.bioorg.2019.103045).
- [49] M.S. Abdelbaset, M. Abdel-Aziz, M. Ramadan, M.H. Abdelrahman, S.N.A. Bukhari, T.F.S. Ali, G.E.D.A. Abuo-Rahma, Discovery of novel thienoquinoline-2-carboxamide chalcone derivatives as antiproliferative EGFR tyrosine kinase inhibitors, *Bioorg. Med. Chem.* 27 (2019) 1076-1086.
- [50] H. Lei, S. Fan, H. Zhang, Y.J. Liu, Y.Y. Hei, J.J. Zhang, A.Q. Zheng, M. Xin, S.Q. Zhang, Discovery of novel 9-heterocyclyl substituted 9*H*-purines as L858R/T790M/C797S mutant EGFR tyrosine kinase inhibitors, *Eur. J. Med. Chem.* 186 (2019) 111888, DOI: [10.1016/j.ejmech.2019.111888](https://doi.org/10.1016/j.ejmech.2019.111888).
- [51] T.M. Thornton, M. Rincon, Non-classical P38 map kinase functions: Cell cycle checkpoints and survival, *Int. J. Biol. Sci.* 5 (2009) 44-52.
- [52] C.S. Devi, D.A. Kumar, S.S. Singh, N. Gabra, N. Deepika, Y.P. Kumar, S. Satyanarayana, Synthesis, interaction with DNA, cytotoxicity, cell cycle arrest and apoptotic inducing

- properties of ruthenium(II) molecular “light switch” complexes, *Eur. J. Med. Chem.* 64 (2013) 410–421.
- [53] Y.C. Li, Y.S. Tyan, H.M. Kuo, W.C. Chang, T.C. Hsia, J.G. Chung, Baicalein induced *in vitro* apoptosis undergo caspases activity in human promyelocytic leukemia HL-60 cells, *Food Chem. Toxicol.* 42 (2004) 37–43.
- [54] J. Singh, D.W. Park, D.H. Kim, N. Singh, S.C. Kang, K.W. Chi, Coordination-driven self-assembly of triazole-based apoptosis-inducible metallomacrocycles, *ACS Omega* 4 (2019) 10810-10817.
- [55] N.O. Donovan, J. Crown, H. Stunell, A.D.K. Hill, E. McDermott, N.O. Higgins, M.J. Duffy, Caspase 3 in breast cancer, *Clin. Cancer Res.* 9 (2003) 738-742.
- [56] M. Olsson, B. Zhivotovsky, Caspase and cancer, *Cell Death Differ.* 18 (2011) 1441–1449.
- [57] M. Zhou, X. Liu, Z. Li, Q. Huang, F. Li, C.Y. Li, Caspase-3 regulates the migration, invasion and metastasis of colon cancer cells, *Int. J. Cancer* 143 (2018) 921–930.
- [58] C. Tang, Y.H. Lu, J.H. Xie, F. Wang, J.N. Zou, J. S. Yang, Y.Y. Xing, T. Xi, Downregulation of survivin and activation of caspase-3 through the PI3K/Akt pathway in ursolic acid-induced HepG2 cell apoptosis, *Anticancer Drugs* 20 (2009) 249–258.
- [59] R.U. Jänicke, MCF-7 breast carcinoma cells do not express caspase-3, *Breast Cancer Res. Treat.* 117 (2009) 219–221.
- [60] S. Kagawa, J. Gu, T. Honda, T.J. McDonnell, S.G. Swisher, J.A. Roth, B. Fang, Deficiency of caspase-3 in MCF7 cells blocks Bax-mediated nuclear fragmentation but not cell death 1, *Clin. Cancer Res.* 7 (2001) 1474–1480.
- [61] H. Thomadaki, M. Talieri, A. Scorilas, Treatment of MCF-7 cells with taxol and etoposide induces distinct alterations in the expression of apoptosis-related genes BCL2, BCL2L12, BAX, CASPASE-9 and FAS, *Biol. Chem.* 387 (2006) 1081–1086.
- [62] Q. Cui, J.H. Yu, J.N. Wu, S.I. Tashiro, S. Onodera, M. Minami, T. Ikejima, P53-mediated cell cycle arrest and apoptosis through a caspase-3- independent, but caspase-9-dependent pathway in oridonin-treated MCF-7 human breast cancer cells, *Acta Pharmacol. Sin.* 28 (2007) 1057–1066.
- [63] P.D. Mace, S.J. Riedl, G.S. Salvesen, Caspase enzymology and activation mechanisms. In "Methods in Enzymology", A. Ashkenazi, J. Yuan, J. A. Wells (eds.), 1<sup>st</sup> Ed., Elsevier Inc., (2014) Chapter 7, 162-178.

- [64] U. De, P. Chun, W.S. Choi, B.M. Lee, N.D. Kim, H.R. Moon, J.H. Jung, H.S. Kim, A novel anthracene derivative, MHY 412, induces apoptosis in doxorubicin-resistant MCF-7/Adr human breast cancer cells through cell cycle arrest and downregulation of P-glycoprotein expression, *Int. J. Oncol.* 44 (2014) 167-176.
- [65] J.E. Chipuk, J.C. Fisher, C.P. Dillon, R.W. Kriwacki, T. Kuwana, D.R. Green, Mechanism of apoptosis induction by inhibition of the anti-apoptotic BCL-2 protein, *Proc. Natl. Acad. Sci. USA* 105 (2008) 20327-20332.
- [66] T. Moldoveanu, A.V. Follis, R.W. Kriwacki, D.R. Green, Many players in BCL-2 family affairs, *Trends Biochem. Sci.* 39 (2014) 101-111.
- [67] S. Cory, J.M. Adams, The Bcl2 family: Regulators of the cellular life-or-death switch, *Nat. Rev. Cancer* 2 (2002) 647-656.
- [68] K.J. Campbell, S.W.G. Tait, Targeting BCL-2 regulated apoptosis in cancer, *Open Biol.* 8 (2018) 180002, DOI: 10.1098/rsob.180002.
- [69] <https://www.rcsb.org/structure/1M17>.
- [70] <https://www.rcsb.org/structure/4ASD>.
- [71] <https://www.rcsb.org/structure/3FL5>.
- [72] <https://www.rcsb.org/structure/3QX3>.
- [73] <https://www.rcsb.org/structure/4O2B>.
- [74] MOE 2015.10 of Chemical Computing Group. Inc. <https://www.chemcomp.com/>.
- [75] R.U. Kadam, N. Roy, Recent trends in drug-likeness prediction: A comprehensive review of *in silico* methods, *Ind. J. Pharm. Sci.* 69 (2007) 609-615.
- [76] C.A. Lipinski, Lead- and drug-like compounds: The rule-of-five revolution, *Drug Discov. Today Technol.* 1 (2004) 337-341.
- [77] D.F. Veber, S.R. Johnson, H.Y. Cheng, B.R. Smith, K.W. Ward, K.D. Kopple, Molecular properties that influence the oral bioavailability of drug candidates, *J. Med. Chem.* 45 (2002) 2615-2623.
- [78] <https://www.molinspiration.com/cgi-bin/properties>.
- [79] U. Bhanushali, S. Rajendran, K. Sarma, P. Kulkarni, K. Chatti, S. Chatterjee, C.S. Ramaa, 5-Benzylidene-2,4-thiazolidenedione derivatives: Design, synthesis and evaluation as inhibitors of angiogenesis targeting VEGFR-2, *Bioorg. Chem.* 67 (2016) 139-147.

- [80] T.R.K. Reddy, C. Li, X. Guo, P.M. Fischer, L.V. Dekker, Design, synthesis and SAR exploration of tri-substituted 1,2,4-triazoles as inhibitors of the Annexin A2-S100A10 protein interaction, *Bioorg. Med. Chem.* 22 (2014) 5378-5391.
- [81] N. Singh, A.C. Tripathi, A. Tewari, R. Kumar, S.K. Saraf, Ulcerogenicity devoid novel non-steroidal anti-inflammatory agents (NSAIDs): Synthesis, computational studies and activity of 5-arylidene-2-imino-4-thiazolidinones, *Med. Chem. Res.* 24 (2015) 1927-1941.
- [82] P. Sharma, T.S. Reddy, D. Thummuri, K.R. Senwar, N.P. Kumar, V.G.M. Naidu, S.K. Bharghava, N. Shankaraiah, Synthesis and biological evaluation of new benzimidazole-thiazolidinedione hybrids as potential cytotoxic and apoptosis inducing agents, *Eur. J. Med. Chem.* 124 (2016) 608-621.
- [83] H.P. Buchstaller, M. Wiesner, O. Schadt, C. Amendt, F. Zenke, C. Sirrenberg, M. Grell, Glycinamide derivatives as RAF-kinase inhibitors, U.S. Patent (2006) WO 20060167261A1.
- [84] P.D. Cook, Escondido, Nucleobase heterocyclic combinatorialization, U.S. Patent (2002) WO 20020009748A1.

## Captions of Figures, Tables and Schemes

**Fig. 1.** Reported pyrimidine-based EGFR-TK inhibitors.

**Fig. 2.** Examples of isoxazoles **A,B**, isoindoline-1,3-diones **C**, chloroacetamides and chloropropionamides **D**, piperazinylacetamides and piperazinylpropionamides **E,F**, thiazolone **G** and arylidenethiazolones **H,I** with reported antitumor and EGFR-TK inhibitory activities.

**Fig. 3.** Examples of anthracene derivatives with reported EGFR-TK, VEGFR-2, CK2, topoisomerase II $\beta$  and tubulin polymerization inhibitory activities.

**Fig. 4.** The pharmacophore model of the ATP-binding site of EGFR-TK.

**Fig. 5.** Summary of the possible modifications carried out for design of the new compounds with expected EGFR-TK inhibitory activity.

**Fig. 6.** The designed new hybrids **2a,b** and **3a,b** as potential antitumor agents and EGFR-TKIs.

**Fig. 7.** The designed new hybrids **4a,b**, **5a,b**, **6a,b-15a,b**, **16a,b** and **17a,b-25a** as potential antitumor agents and EGFR-TKIs.

**Fig. 8.** Percentage inhibition of EGFR-TK by compounds **4a**, **4b**, **6b**, **8a**, **10a**, **10b**, **16a**, **16b** and **25a** at concentration of 10  $\mu$ M.

**Fig. 9.** Percentage inhibition of VEGFR-2, CK2, topoisomerase II $\beta$  and tubulin polymerization by compound **25a** at concentration of 10  $\mu$ M.

**Fig. 10.** Cell cycle distribution for HepG2, MCF-7 and HCT-116 cells treated with vehicle control and **25a** (at the IC<sub>50</sub> of the corresponding cell line) for 24 h.

**Fig. 11.** Flow cytometry analysis of cell cycle distribution in HepG2, MCF-7 and HCT-116 cells after treatment with **25a** (at the IC<sub>50</sub> of the corresponding cell line) for 24 h.

**Fig. 12.** Annexin V-FITC/PI double staining for analysis of apoptosis in HepG2, MCF-7 and HCT-116 cells after treatment with **25a** (at the IC<sub>50</sub> of the corresponding cell line) for 24 h. Q1 quadrant refers to necrotic cells; Q2 quadrant refers to late apoptosis; Q3 quadrant refers to live cells; Q4 quadrant refers to early apoptosis. Total apoptosis is the summation of early and late apoptosis.

**Fig. 13.** Percentage apoptosis in HepG2, MCF-7 and HCT-116 cells after treatment with vehicle control and **25a** (at the IC<sub>50</sub> of the corresponding cell line) for 24 h.

**Fig. 14.** (A) Level of caspase-3 in HepG2 and HCT-116 cells. (B) Level of caspase-9 in MCF-7 cells.

**Fig. 15.** (A) Level of Bax protein in HepG2, MCF-7 and HCT-116 cells. (B) Level of Bcl-2 protein in HepG2, MCF-7 and HCT-116 cells.

**Fig. 16.** (A) 2D Diagram illustrating erlotinib docking pose interactions with the hot spot amino acids in EGFR-TK binding site. (B) 3D Diagram illustrating erlotinib docking pose interactions with the hot spot amino acids in EGFR-TK binding site. Atoms are colored as following: carbon = orange, hydrogen = light gray, nitrogen = blue and oxygen = red. (C) 2D representation of the superimposition of the co-crystallized erlotinib ligand (red) and the docking pose of erlotinib (green) in the EGFR-TK binding site.

**Fig. 17.** (A) 2D Interaction of **25a** with EGFR-TK binding site. (B) 3D Interaction of **25a** with EGFR-TK binding site. Atoms are colored as following: carbon = dark gray, hydrogen = light gray, nitrogen = blue, sulfur = yellow and oxygen = red.

**Fig. 18.** (A) 2D Diagram of EGFR-TK-**25a** binding mode superposed on EGFR-TK-erlotinib complex. Erlotinib is colored red and **25a** is colored green. (B) 3D Diagram of EGFR-TK-**25a** binding mode superposed on EGFR-TK-erlotinib complex. Erlotinib is colored cyan and **25a** is colored yellow.

**Fig. 19.** (A) 2D Interaction of sorafenib with the active site of VEGFR-2. (B) 2D Interaction of **25a** with the active site of VEGFR-2. (C) 3D Interaction of **25a** with the active site of VEGFR-2. Atoms are colored as following: carbon = cyan, hydrogen = light gray, nitrogen = blue, sulfur = yellow and oxygen = red. (PDB ID: 4ASD).

**Fig. 20.** (A) 2D Interaction of quinalizarin with the active site of CK2 $\alpha$ . (B) 2D Interaction of **25a** with the active site of CK2 $\alpha$ . (C) 3D Interaction of **25a** with the active site of CK2 $\alpha$ . Atoms are colored as following: carbon = cyan, hydrogen = light gray, nitrogen = blue, sulfur = yellow and oxygen = red. (PDB ID: 3FL5)

**Fig. 21.** (A) 2D Interaction of doxorubicin with the active site of topoisomerase II $\beta$ . (B) 2D Interaction of **25a** with the active site of topoisomerase II $\beta$ . (C) 3D Interaction of **25a** with the active site of topoisomerase II $\beta$ . Atoms are colored as following: carbon = cyan, hydrogen = light gray, nitrogen = blue, sulfur = yellow and oxygen = red. (PDB ID: 3QX3).

**Fig. 22.** (A) 2D Interaction of colchicine with colchicine binding site of tubulin. (B) 2D Interaction of **25a** with the colchicine binding site of tubulin. (C) 3D Interaction of **25a** with the colchicine binding site of tubulin. Atoms are colored as following: carbon = cyan, hydrogen = light gray, nitrogen = blue, sulfur = yellow and oxygen = red. (PDB code: 4O2B).

**Table 1.** *In vitro* antitumor activity of the new compounds.

**Table 2.** EGFR-TK inhibitory activity of the most active antitumor analogs.

**Table 3.** VEGFR-2, CK2, topoisomerase II $\beta$  and tubulin polymerization inhibitory activities of compound **25a**.

**Table 4.** Summary of residues involved in arene-cation, arene-H and arene-arene interactions, number of hydrogen bonds, residues involved in hydrogen bonding interaction and docking energy score (kcal/mol) of compound **25a** with EGFR-TK, VEGFR-2, CK2, topoisomerase II $\beta$  and tubulin.

**Table 5.** TPSA, Nrotb and calculated Lipinski's rule for compounds **2-25**.

**Scheme 1.** Synthesis of compounds **2a,b** and **3a,b**.

**Scheme 2.** Synthesis of compounds **4a,b-15a,b**.

**Scheme 3.** Synthesis of compounds **16a,b-25a**.